MASSIVE MIMO WIRELESS SYSTEMS

UNDER AN RF CHAINS CONSTRAINT

by

Zeeshan Azmat Shaikh
B.Sc. Electrical Engineering
M.Sc. Electrical Engineering

Dissertation submitted in fulfilment of the requirements

for the degree of

DOCTOR OF PHILOSOPHY

Department of Engineering
Faculty of Science and Engineering
Macquarie University
Sydney, Australia

12th of August 2016

ABSTRACT

Massive MIMO is an exciting new technology which is revolutionizing the wireless community. Massive MIMO serves multiple users with increased data rates using a massively large number of antenna elements at the base station using simple beamforming techniques. In digital beamforming, each antenna element is connected to a dedicated radio-frequency (RF) chain. With so many antenna elements, it is not practical to have a dedicated RF chain for each antenna element due to high fabrication cost and power consumption.

We start by considering the pilot contamination problem in which inter-cell interference occurs because the channel estimate of a user sending a particular training sequence in one cell is corrupted by the transmissions of the users using the same training sequence in other cells. To mitigate pilot contamination, we consider an adaptive least-squares algorithm in massive MIMO which employs bi-directional training to optimize precoders and receive filters without doing channel estimation. We characterize the impact of using different types of training sequences on sum-rate performance of a multi-cell system. We demonstrate analytically that usage of random training sequences across cells, offers better performance than usage of identical training sequences for a fixed number of interferers which is critical because it avoids having to synchronize the users across cells.

The thesis next considers the challenges arising from the the limited number of RF chains. There are a variety of approaches to tackle the problem of RF

chains constraint. The first approach is to study generalized spatial modulation (GSM) in which RF chains are connected to a subset of antennas. We propose novel compressive sensing (CS) aided detection algorithm which offers superior performance to existing algorithms. For imperfect channel state information, we use CS in conjunction with total least-squares to mitigate the effect of contaminated channel estimates. Our CS framework is premised on the assumption of frequency-selective fading for GSM to account for high data-rate applications. We derive the achievable rates for GSM and provide closed-form expressions for upper and lower bounds of the achievable rates to investigate the capacity gains offered by GSM under finite alphabet constraint. The second approach we take is to investigate the antenna selection for massive MIMO whereby the limited number of RF chains are connected to the best subset of antennas. We derive a theorem which provides a concise formula for the limiting normalized channel power gain in the large system dimensions.

Finally, the application of massive MIMO in millimeter-wave (mmWave) band under RF chains constraint is analysed. The performance bottleneck in mmWave massive MIMO is beam-alignment due to narrow beams. We propose beam-alignment algorithms under RF chains constraint to improve upon existing schemes. We derive theorems which provide closed-form expressions for probability of beam-misalignment of energy and Bayesian detectors for analogue beam-steering. Moreover, we perform asymptotic analysis for Bayesian detector and demonstrate that probability of beam misalignment tends to zero in the limit of infinite number of BTS antennas under RF chains constraint. The results demonstrate that Bayesian detection offers superior performance over energy detection in terms of mmWave beam-alignment which is imperative because it minimizes beam pointing losses.

STATEMENT OF CANDIDATE

I certify that the work in this thesis has not previously been submitted for a degree nor has it been submitted as part of the requirements for a degree to any other university or institution other than Macquarie University.

I also certify that the thesis is an original piece of research and it has been written by me.

In addition, I certify that all information sources and literature used are indicated in the thesis.

.....

Zeeshan Azmat Shaikh

ACKNOWLEDGMENTS

I would like to thank to my supervisor, Professor Stephen Hanly for his valuable support and supervision. His advice, motivation, ideas, and intuitions have been invaluable during the course of my PhD. I admire his critical eye for important research avenues. He always keeps an open mind in all academic discussions.

I would like to extend my thanks to Prof. Iain Collings for his ideas, practical insights and for giving me an opportunity to join his research group as a visiting postgraduate student while he was at CSIRO. Further, I would like to take this opportunity to warmly thank to Dr. Philip Whitings for encouragement and stimulating discussions.

My sincere thanks go to Macquarie Univerity and Society for Industrial and Endowment Fund (SIEF) for providing me generous scholarship without which this research work could not have been possible.

In the name of love to which it is all about.

Contents

List of Figures

List of Algorithms

Chapter 1

Introduction

1.1 Background

Over the past few years with the advent of smart phones and tablets, we have observed a phenomenal growth in the number of wireless devices connected across the globe. Owing to bandwidth-hungry real-time videos, online gaming, high-definition movies and other multi-media applications, each wireless user demands more bits-per-second of data at the same time. This data deluge seems to be never ending and it is expected that the growth of mobile data traffic will be approximately ten-fold globally between 2016 and 2019, reaching 24.3 exabytes per month worldwide in 2019 [1]. Consequently, next generation wireless system designers have to satisfy three requirements: i) delivering massive throughputs to a multitude of users simultaneously, ii) ensuring reliable transmission of data, iii) designing cost-effective devices within the budget of a customer.

Multiple-input multiple-output (MIMO) technology has been thoroughly investigated over the last two decades and adopted by many wireless standard bodies as it can significantly enhance the capacity and reliability of a wireless link. The initial research on MIMO systems concentrated on point-to-point MIMO systems, where two devices trans-

mit and receive data to each other via multiple antennas at both sides. An excellent overview of information theoretic results for single-user MIMO is given in [2]. It is well known that for a point-to-point link with N_T transmit antennas and N_R receive antennas, capacity increases linearly with $\min\{N_T, N_R\}$ [3]. However, in the recent past, researchers have focused on point-to-multipoint MIMO or multi-user MIMO (MU-MIMO) systems when in [4], it was demonstrated analytically that similar capacity scaling is applicable when a base-transceiver station (BTS) equipped with N_T antenna elements exchanges data with N_R single-antenna user terminals.

In MU-MIMO, a single BTS communicates with single-antenna terminals at the same time while not requiring rich scattering environment due to multi-user diversity. It carries many advantages over point-to-point links. For instance, the costly equipment is required at the BTS only and single antennas can be used at user terminals. Moreover, resource allocation is simplified : every active user shares all the time-frequency slots because the users can be separated using different spatial signatures. Therefore, MU-MIMO is also called space-division multiple access (SDMA) at times. To reap these benefits of MU-MIMO, it has been applied in wireless standards including 802.11 (WiFi), 802.l6 (WiMAX), and long-term evolution (LTE) [5].

The information theoretic achievable throughput and the capacity region of vector Gaussian broadcast channel, which represents MU-MIMO downlink scenario, have been investigated in [6, 7]. Moreover, a lot of effort has been devoted towards the performance evaluation of MU-MIMO under practical constraints such as imperfect channel state information at the transmitter (CSIT) [8], the overhead occuring due to downlink channel estimation and CSIT feedback [9] and the extension to joint precoding over clusters of multiple BTSs [10–12]. Theoretical results on scaling of sum capacity of cellular networks with MIMO links have been reported in [13]. However in practice, MU-MIMO with frequency-divison duplex (FDD) mode and roughly equal number of BTS terminals

and user terminals is not a scalable technology. For example, the LTE standard can accommodate only up to eight antenna elements at the BTS.

Massive MIMO (a.k.a. large MIMO, full dimensional MIMO, hyper MIMO) technology is an upcoming paradigm that offers capacity scaling by possibly orders of magnitude in comparison to existing technologies [14]. In massive MIMO, a massive array of antenna elements is mounted on a BTS. A BTS antenna array equipped with potentially hundreds of elements can serve tens of users in the same time-frequency resource with simple signal processing techniques. Asymptotic random matrix theory results kick in to prove that in massive MIMO the propagation channel vectors become pairwise asymptotically orthogonal which in turn shows that the effect of uncorrelated noise are negligible and the required transmitted energy per bit approaches zero in the limit of infinite number of BTS antenna elements [15]. Additionally, linear signal processing schemes such as matched-filtering detection and precoding become near-optimal thereby reducing the complexity and energy consumption of signal processing.

In massive MIMO, time-division duplexing (TDD) mode is adopted which relies on reciprocity between forward and reverse links and uplink training is performed, although FDD mode may be feasible in some cases [16]. Massive MIMO relies on the channel-state information (CSI) on both the reverse and forward links in order to do matched filtering/combining at the BTS. In reverse link, it is straightforward to obtain the channel estimates by sending training sequences from all the user terminals and performing channel estimation at the BTS. The number of time-frequency resources required to do this estimation is proportional to number of user terminals, thus, number of user terminals is limited by the coherence interval. However, in the forward link it is quite difficult to do channel estimation as the number of time-frequency resources required scales with the number of BTS antenna elements which grows without bound in massive MIMO.

In addition to massive MIMO systems operating at microwave frequencies, millimeter-

wave (mmWave) communication system has been envisaged as a key component of next-generation wireless networks. Owing to the scarcity of spectrum in microwave bands, researchers aim at exploring the previously untapped higher frequency bands in 30 to 300 GHz range which is termed mmWave band because the operating wavelength in the mmWave realm is on the order of millimeters. The mmWave communications and massive MIMO systems need not have to be two competing wireless communication systems. Interestingly, both of them can be used in tandem to get the best of both worlds. For instance, in the mmWave realm, high path loss occurs due to energy absorption from the surrounding medium. It has been shown in [14] that massive MIMO can achieve high signal-to-interference-plus-noise ratio (SINR) by concentrating the signal energy into narrow areas, therefore, mmWave massive MIMO systems can compensate for high path loss via focusing energy into ever-smaller regions of space to bring tremendous improvements in throughput and radiated energy efficiency. Thus, massive MIMO is *favourable* for centimetre-wave frequencies but is *essential* for mmWave frequencies. On the other hand, large physical aperture due to huge array of antennas is an issue for massive MIMO systems operating at microwave frequencies because inter-element spacing should be no less than half the wavelength to circumvent spatial correlation. Due to wavelengths in millimeter-wave range in mmWave regime, a large number of antenna elements can be packed in small phsyical aperture thereby achieving huge array gains in limited physical space. Thus, both the wireless communication technologies complement each other and can improve each other's limitations.

1.2 Key Challenges

In this section, we highlight the challenges encountered in massive MIMO systems operating in TDD mode under the constraint of limited radio-frequency (RF) chains. Fur-

thermore, we illustrate the challenge of performing beam alignment in mmWave massive MIMO systems. In subsection 1.2.1, we explain the pilot contamination problem which occurs due to reuse of pilots across cells in massive MIMO systems. In subsection 1.2.2, we illustrate the issue of limited number of RF chains because massive MIMO is premised on the assumption that each antenna element is connected to a dedicated RF chain. In subsection 1.2.3, we highlight the problem of doing beam alignment which is necessary to establish link in mmWave massive MIMO system.

1.2.1 Pilot Contamination

The pilot contamination problem arises when the BTS adopts TDD mode which does not vanish as the number of antenna elements at the BTS is increased. The user terminals transmit pairwise orthogonal training sequences in reverse link in order to acquire perfect CSI at BTS under TDD mode. The maximum number of orthogonal sequences in reverse link is limited by coherence interval which is the product of coherence time and coherence bandwidth. Ideally, the training sequences of users within one cell should not only be pairwise orthogonal but also be pairwise orthogonal with the training sequences of other cells. However, given a finite amount of coherence time and bandwidth, the number of orthogonal sequences is limited which in turn sets a limit on the number of user terminals served by the whole system. In an attempt to accommodate more users, the training sequences in one cell are chosen to be orthogonal and the same set of training sequences are reused in the neighbouring cells. This 'pilot reuse' scheme enables a maximum number of terminals in each cell. Now, identical training sequences assigned to user terminals in neighbouring cells will interfere with each other during the estimation phase which is termed "pilot contamination".

Simply put, when the BTS correlates the received signal in training phase with the training sequence associated with a particular user, its channel estimate is corrupted

by all the channels associated with users in neighbouring cells having sent the same training sequence. During the course of downlink data transmission, the BTS beamforms signals not only towards its own users but also towards users in other cells which is termed 'directed interference'. The directed interference continues to exist in uplink data transmission [17]. The directed interference and the desired signal increase with the number of antenna elements at the BTS at the same rate. Thus, pilot contamination leads to reduction in data rates despite the large number of antenna elements yielding huge array gains in massive MIMO systems.

1.2.2 RF Chains Constraint

A key challenge in massive MIMO is to harness the large spatial degrees-of-freedom (DOF) under the constraint of limited RF chains. The DOF is defined as the rank of the MIMO channel matrix in the angular domain [18]. The huge DOF can be exploited to significantly enhance the spatial multiplexing/beamforming gain leveraging digital precoding after acquiring the CSI at BTS. However, in digital precoding/combining the amplitudes and phases of complex modulation symbols are modified at the baseband and then up-converted to operating frequency after processing through digital-to-analogue converters (DACs)/analogue-to-digital converters (ADCs), mixers, and power amplifiers (PAs)/low-noise amplifiers (LNAs). The assembly of DAC/ADC, mixer, and the PA/LNA is termed the 'RF chain' [19, 20]. At the BTS, each antenna element is fed with the output port of a dedicated RF chain. RF chain is the most expensive component due to high fabrication cost and power consumption of mixed signal components like high-resolution ADCs and DACs. The cost of RF chains is an economic problem as one RF chain per antenna element is employed in massive MIMO due to baseband processing. Additionally, it is an overhead to physically install extra RF chains in existing LTE system to upgrade them to massive MIMO. Thus, it is challenging to maintain high data rates and low probability

of error in massive MIMO system under the constraint of limited RF chains.

1.2.3 Beam Alignment

MmWave massive MIMO systems require a huge array of antennas to provide large array gain in order to overcome tiny antenna apertures. However, due to practical limitations on cost, complexity and power consumption, it impossible in practice to use a dedicated RF chain for each antenna in mmWave realm. Thus, the constraint of limited RF chains becomes more significant in mmWave massive MIMO systems due to requirement of hundreds of antenna elements. Due to the same reason, systems like IEEE 802.11ad support single-stream transmission only and employ analogue beamforming which requires only one RF chain. Moreover, entrywise channel estimation in mmWave massive MIMO systems is cumbersome due to a large number of antenna elements and low signal-to-noise ratio (SNR) before beamforming. In order to achieve huge beamforming gain, the beam sent by the BTS must be steered and aligned. Under the constraint of limited RF chains, recent works on hybrid analogue and digital precoding have been overviewed in [21]. Another viable approach for beam alignment is beam training which has been developed in [22, 23]. In this approach, instead of performing explicit channel estimation, the direction in which beam has to be transmitted, is estimated via sending training signals. Thus, the channel vector is characterized by a single parameter which is direction-of-arrival. As the beams are narrow due to huge array of antennas, so if the beam points in undesired direction, it leads to huge loss in data rates. Thus, the beam alignment is an issue of paramount importance in mmWave massive MIMO systems.

1.3 Contributions

This thesis addresses the challenges associated with massive MIMO which is anticipated to be an integral part of fifth generation (5G) wireless systems because massive MIMO arguably will be ultimate embodiment of MIMO technology. In this thesis, we assume perfect synchrnonization between transmitter and receiver(s). Furthermore, we assume that the channel linking the transmitter and receiver suffers from small-scale Rayeligh fading (complex-Gaussian distributed channel). The large-scale fading which includes path-loss and shadowing are not assumed in the channel model in this thesis. The large-scale fading is generally used to estimate the coverage area and outage [24] which are not the main challenges addressed in this thesis. Large-scale fading is generally mitigated using *macroscopic diversity* whereby a mobile station can substantially improve the SNR on the forward link by selecting a base station which is not shadowed when others are [24, p. 381].

1.3.1 Mitigation of Pilot Contamination

Pilot contamination is considered to be performance bottleneck in TDD massive MIMO systems. The earlier solution to pilot contamination in [25] is premised on the exchange of second-order statistics among interfering base stations which necessitates the backhaul links among base stations across all cells. Our main contribution concerning pilot contamination is the use of random training sequences across different cells in an adaptive beamforming framework which do not estimate the channels explicitly. Our proposed random training sequences do not need any exchange of statistical channel knowledge across cells thereby eliminating the need of backhaul during the estimation phase. The proposed training sequences offer better data rates than the training sequences employed in massive MIMO wherein same set of pairwise orthogonal sequences are reused in all cells.

Furthermore, we analysed the impact of structure of training sequences on the design of base stations' beamformers using random matrix theoretic results.

1.3.2 Solutions for Limited RF chains

The key challenge in massive MIMO systems is to maintain system's performance under the constraint of limited RF chains. Generalized spatial modulation (GSM) can be used in conjuction with massive MIMO systems under an RF chains' constraint to improve the spectral efficiency. For GSM massive MIMO system, we propose a novel compressive sensing aided detection algorithm for frequency-selective channel to cope with the increased data rate requirements in 5G systems. Our proposed algrithm outperforms the existing compressive sensing based detection techniques in terms of mean-square error and probability of error. Our proposed algorithm takes into account the noisy channel estimates occuring due to pilot contamination which has not been considered in literature to the best of our knowledge. Additionally, we proposed a compressive sensing (CS) recovery scheme for a precoded multi-user GSM massive MIMO system.

Antenna selection is capable of harnessing the spatial degrees of freedom offered by the large number of antennas in massive MIMO under RF chains' constraint. Our key contribution is large system analysis of massive MIMO under RF chains' constraint using antenna selection technique. Our proposed capacity scaling law provides insights into the system's behavior. The required number of RF chains to achieve a target capacity for a given number of transmit antennas can be calculated using our proposed capacity deterministic equivalent. Moreover, extensive Monte Carlo simulations are not required to simulate the system's behavior while using our large system analysis. For fixed number of RF chains, the antenna selection provides more capacity gain in comparison to GSM system, however, this comes at the cost of having CSI at transmitter in antenna selection which is not required in GSM systems.

1.3.3 Novel Beam Alignment Schemes

In mmWave massive MIMO systems, beam alignment needs to be performed prior to data transmission to avoid beam-mismatch losses. Under single-path channel in mmWave realm, we provide two algorithms for beam alignment. Our proposed algorithms offer superior performance than the optimal exhaustive search in terms of mean-square error (MSE) and probability of beam misalignment. In contrast to conventional energy detection, we proposed Bayesian approach for beam detection which beats the peformance of energy detection in terms of beam-misalignment probability. Analytical expression for probability of beam misalignment for exhaustive search and Bayesian detection are derived. Mathematical expressions are verified via extensive numerical simulations and numerical results verify the accuracy of mathematical results.

1.3.4 Contributions Outline

- In Chapter 3, we quantify the impact of pilot contamination under adaptive beamforming using different structures of training sequences.
- In Chapter 3, Fig. 3.3 shows that for 30 antennas at BTS and SNR of 30 dB, random training sequences across cells offer 4.62 % improvement over identical training sequences across cells in terms of network capacity of a multi-cell system under pilot contamination problem.
- In Chapter 4, Algorithm 1 is a novel CS aided detection algorithm which offers 14 dB performance improvement over conventional CS algorithm as shown in Fig. 4.1.
- The algorithm 1 in Chapter 4 offers an error rate of 4×10^{-3} which is less than error rate of 2×10^{-2} offered by conventional CS algorithm as shown in Fig. 4.2.

- In Section 4.3 of Chapter 4, we offer a novel recovery scheme for precoded multi-user GSM system based on precoding and compressive sensing which offers comparable performance to interference-free single-user GSM system.

- Figure 4.5 shows that for $N_T = 20, N_c = 2$, single-user GSM system offers a BER of 9×10^{-4} whereas multi-user GSM using proposed CS recovery offers BER of 0.5×10^{-3}. For $N_T = 40, N_c = 2$, single-user GSM offers 3×10^{-3} whereas multi-user GSM using proposed CS recovery offers very close BER of 4×10^{-3}.

- In Chapter 5, we derive the achievable information rate of the GSM system under finite alphabet constraint which is given in Eq. (5.27).

- In Chapter 5, we derive Proposition 1 which provides the closed-form expression for a lower bound on the achievable rate of GSM system under finite alphabet constraint.

- In Chapter 5, we derive Proposition 2 which provides the closed-form expression for an upper bound on the achievable rate of GSM system under finite alphabet constraint.

- Fig. 5.1 reveals that the GSM system can offer the same achievable rate as the SM system but using less transmit antennas and with a lower channel estimation burden.

- Fig. 5.2 demonstrates that the Monte Carlo average of the derived achievable rate in Eq. (5.27) is approximated reasonably tightly in low and high SNR regimes.

- Fig. 5.4 shows that GSM system with the proposed precoding scheme offers better performance than the un-precoded GSM system in the medium SNR regime (0-15 dB).

- In Chapter 6, we derive Theorem 3 which provides a scaling capacity law using a law of large numbers for single-user massive multiple-input single-output (MISO) systems under RF chains constraint when antenna selection is employed.

- In Chapter 6, the upper and lower bounds of the deterministic equivalent of the capacity of the massive MISO systems under RF chains constraint are derived and the result is given in Eq. (6.41).

- In Chapter 6, Figs. 6.2 and 6.3 show that random capacity realizations fluctuate around the derived capacity approximation and fluctuations become less when we increase the transmit antennas from $N_T = 50$ to $N_T = 500$ for fixed $\beta = \frac{1}{5}$.

- In Chapter 7, the novel Algorithms 2 and 3 are proposed which outperform the existing hierarchical search and exhaustive search techniques for mmWave beam-alignment.

- In Chapter 7, we derive Theorem 4 which provides the probability of beam-misalignment under energy detection criterion in a mmWave system.

- In Chapter 7, we derive Theorem 5 which provides the probability of beam-misalignment under a Bayesian detection criterion in a mmWave system.

- Fig. 7.11 in Chapter 7 shows that our proposed Algorithm 3, which is premised on a refined hierarchical search, offers 10 dB less mean-square error than exhaustive search at SNR of 0 dB.

- Fig. 7.12 in Chapter 7 demonstrates that our proposed Algorithm 3 offers an error-rate of 4×10^{-3} whereas exhaustive search offers an error rate of 2×10^{-3} at SNR of 0 dB.

- Fig. 7.13 reveals that simulation results verify the Theorems 4 and 5 which provide the probability of beam-misalignment under energy and Bayesian detection.

1.4 Thesis Organization

In Chapter 3, we consider an adaptive beamforming scheme for multi-cell massive MIMO in order to mitigate the "pilot contamination" problem. The considered scheme has been previously applied in [26, 27] for MIMO interference networks. Specifically, we focus on studying the impact of different types of training sequences on "pilot contamination" in multi-cell massive MIMO. The considered scheme uses bi-directional training in which training sequences are transmitted in forward link from beamformers at BTS to adapt the user terminals' receive filters and then the training sequences using terminals' filters acting as beamformers, are transmitted in reverse link to adapt the beamformers at the BTSs' side. The adaptation of both the transmitters and receivers sides is performed using the least-squares objective function. The adaptive beamforming scheme shows improvement in terms of average sum rate if the random training sequences are transmitted from users in different cells. We corroborate our mathematical analysis via numerical results which demonstrate the superiority of using random training sequences over identical training sequences across different cells.

In Chapter 4, GSM is studied in order to investigate massive MIMO under limited RF chains without sacrificing spectral efficiency. In GSM, a subset of antennas is chosen at every signalling instant based on incoming data and coupled with output ports of limited RF chains [28]. The choice of subset of antennas is governed by the incoming data pattern. At the receiver, by decoding the choice of subset of antennas, the encoded information is decoded which will be large for massive MIMO system. To account for high data-rate applications, we adopted MIMO inter-symbol interference (ISI) channel which

leads to a block Toeplitz channel matrix. Specifically, we use CS for detecting the indices of activated antennas and subsequently we employ linear zero-forcing (ZF) receiver for demodulation. To account for imperfect CSI at receiver due to "pilot contamination", we propose to attempt total-least squares (TLS) for demodulation. Under perfect and imperfect CSI, our proposed algorithm offers better performance than existing CS based detection schemes for GSM. Further, we propose a CS recovery scheme for a precoded multi-user GSM system. The ZF based precoding scheme decouples the multi-user wireless channel into several single-user systems by leveraging the CSIT. Numerical results are shown to verify the mathematical analysis.

In Chapter 5, we provide an information theoretic treatment of a GSM based MIMO system in order to evaluate the achievable information rates of GSM under finite alphabet constraint (QPSK,QAM etc). First, we develop an analytical framework in which the input-output relationship of a GSM system has been cast in terms of binary-input single-output random variables. Under the developed framework, we investigate the achievable information rates for GSM as a function of SNR. Additionally, we derive the closed-form expressions for lower and upper bounds of achievable rate. Furthermore, we provide achievable information rate for a precoded GSM based on CSIT. It is observed that by leveraging the sparse information encoding in GSM, high achievable rates are possible for large MIMO under limited number of RF chains.

In Chapter 6, we focus on further application of antenna selection techniques to massive MIMO system under RF chains constraints. Antenna Selection is a promising signal processing technique which reduces the number of required RF chains while keeping the system's performance at a certain minimum level. We provide a large systems analysis of antenna selection aided downlink beamforming in massive multiple-input single-output (MISO) under RF chains constraint using the strong law of large numbers. Specifically, we investigate the capacity performance of an antenna selection scheme employed in a

massive MISO system in large system dimensions. Numerical experiments corroborate that the proposed deterministic equivalents are accurate even for relatively small N_c, N_T where N_c is the number of RF chains.

In Chapter 7, we focus on beam-alignment schemes for mmWave massive MIMO techniques under the constraint of RF chains limitation. Owing to scarcity of bandwidth at microwave frequencies, there has been a flurry of recent interest in the wireless research community in the area of mmWave frequencies. A mmWave massive MIMO system is a strong candidate for delivering gigabit-per-second throughputs due to abundant unlicensed spectrum in mmWave bands. mmWave massive MIMO systems will deploy high-gain electronically steerable directional antennas to cope with the incurred path loss at mmWave frequencies. The beam alignment problem becomes much more crucial due to pencil-sharp narrow beams produced by high-gain antennas. Moreover, the issue of RF chains constraint becomes crucial at mmWave frequencies due to the huge cost of high speed ADCs and DACs as the bandwidth of the signal to be processed is very high. We investigate the case of analogue beamforming for one user which uses only one RF chain and propose algorithms to improve upon existing schemes for beam-alignment.

Chapter 2

Mathematical Tools and Preliminaries

Some of the mathematical tools and preliminaries which will be used in rest of thesis are described here for interested reader.

2.1 Random Matrix Theory

Here we provide a useful lemma about long random vectors [29] which will be used in Chapter 3.

Lemma 1. *Let* $\boldsymbol{x} = [x_1 \cdots x_n]^T$ *and* $\boldsymbol{y} = [y_1 \cdots y_n]^T$ *be* $N \times 1$ *vectors whose elements are independent-and-identically distributed (i.i.d.) random variables (RVs) with* $\mathbb{E}[x_i] = \mathbb{E}[y_i] = 0$, $\mathbb{E}[|x_i|^2] = \sigma_x^2$, *and* $\mathbb{E}[|y_i|^2] = \sigma_y^2$, $i = 1, 2, ..., n$. *Assume that* $\boldsymbol{x}$ *and* $\boldsymbol{y}$ *are independent. Applying the law of large numbers, we obtain*

$$\frac{1}{n}\boldsymbol{x}^H\boldsymbol{x} \xrightarrow{a.s.} \sigma_x^2 \; as \; n \uparrow \infty \tag{2.1}$$

$$\frac{1}{n}\boldsymbol{x}^H\boldsymbol{y} \xrightarrow{a.s.} 0 \; as \; n \uparrow \infty \tag{2.2}$$

where $\xrightarrow{a.s.}$ *denotes almost sure convergence.*

2.2 Information Theory

In order to obtain a tool for performance evaluation of digital communication systems, the term information must be mathematically defined. The concept of information is too wide to be summarized completely by one definition. However, for a given probability distribution a quantity entropy is defined in literature which has several properties conforming with the intuitive notion of measure of amount of information. This concept is complemented with the notion of mutual information which quantifies the amount of information which one random variable contains about a correlated random variable. In fact, mutual information is a special case of a more general quantity called relative entropy. Relative entropy is a measure of the distance between two probability distributions. All these measures share a range of properties and are interrelated. After defining entropy and mutual information, we present the relation between these measures and some of their properties without proofs which are necessary for the derivations in the subsequent sections. For proofs, the interested reader is referred to [30]. The definitions, properties and relationships presented in next section will be used in Chapter 5 for calculations involving entropies and mutual informations.

2.2.1 Measures of Quantifying information

Entropy and Mutual Information

Let X be a discrete random variable which can take on values from a finite alphabet $\mathcal{X} = \{x_1, \cdots, x_M\}$ and the associated probability mass function be $p_X(x) = Pr\{X = x\}, x \in \mathcal{X}$,i.e., $X \sim p_X(x)$. One particular example of this discrete random variable is a digital memoryless source which emits symbols $x_1, \cdots, x_M$ with probabilities $Pr\{X = x_1\}, \cdots, Pr\{X = x_M\}$ respectively. Memoryless property simply means that the current symbol emitted is independent of the previous symbol. Thus all the symbols are statistically

independent. Here, we introduce notion of entropy which is a measure of uncertainty of a random variable.

Entropy

The entropy $H(X)$ of a discrete random variable X is defined by

$$H(X) := -\sum_{x \in \mathcal{X}} p_X(x) \log p_X(x) \tag{2.3}$$

The logarithm is to the base two and the units of entropy are bits unless stated otherwise. For instance, the entropy of a fair coin is 1 bit. In calculations of above expression, we will use the convention $0 \log 0$ which may be easily justified by continuity as $x \log x \to 0$ as $x \to 0$. Recall that the expected value of a function $g(X)$ of a random variable X can be expressed as

$$\mathbb{E}_X \left[g(X) \right] = \sum_{x \in \mathcal{X}} g(x) p_X(x) \tag{2.4}$$

Thus entropy may be compactly expressed in terms of statistical expectation operator,

$$H(X) := \mathbb{E}_X \left[\log \frac{1}{p_X(X)} \right] \tag{2.5}$$

In the example of discrete memoryless source, the entropy of the source is a function of symbol probabilities instead of their values because entropy quantifies the amount of uncertainty on the average. It is interesting here to indicate the probability distribution for symbols that yield maximum entropy. Entropy being a measure of uncertainty will be maximized if symbols' probability distribution generates maximum uncertainty. On qualitative grounds, the entropy will be maximum for discrete uniform distribution, i.e., when the source emits all the symbols with equal probabilities.

Joint Entropy and Conditional Entropy

Since the scope of transmission is communication between two or more subscribers, at least two information sources X and Y communicating symbols $x \in \mathcal{X}$ and $y \in \mathcal{Y}$ respectively need to be considered so that we can quantify the amount of information communicated by two sources jointly on the average. Thus (X, Y) may be considered to be a single vector-valued information source characterized by a random vector and its associated joint probability distribution $(X, Y) \sim p_{X,Y}(X, Y)$. The joint entropy $H(X, Y)$ of a pair of discrete random variables (X, Y) with a joint distribution $p_{X,Y}(X, Y)$ may be defined as

$$H(X, Y) := -\sum_{x \in \mathcal{X}} \sum_{y \in \mathcal{Y}} p_{X,Y}(x, y) \log p_{X,Y}(x, y) \tag{2.6}$$

Like entropy, joint entropy can be expressed in terms of statistical expectation operator,

$$H(X, Y) := \mathbb{E}_{X,Y}\left[\log \frac{1}{p_{X,Y}(X, Y)}\right] \tag{2.7}$$

In digital communication systems, y_μ is known at the receiver where μ is an index into the alphabet of channel outputs. If the channel is noiseless, then the knowledge of y_μ completely determines the transmitted symbol under the assumption of additive-white-Gaussian noise (AWGN) channel. Owing to noise disturbances, there is certain degree of uncertainty concerning the transmitted symbol upon reception of y_μ. If $Pr(x_\nu|y_\mu)$ characterizes the conditional probability that x_ν would have been transmitted when y_μ is received, then $\log[1/Pr(x_\nu|y_\mu)]$ is the uncertainty about x_ν when y_μ is received. If this uncertainty is averaged out over all x_ν and y_μ, then we obtain $H(X|Y)$, which is the average uncertainty about the transmitted symbol x when a symbol y is received. Thus,

the conditional entropy of X given the Y may be defined as

$$\begin{aligned} H(X|Y) &:= -\mathbb{E}_{X,Y}\left[\log p_{Y|X}(Y|X)\right] && (2.8)\\ &= -\sum_{x\in\mathcal{X}}\sum_{y\in\mathcal{Y}} p_{X,Y}(x,y)\log p_{X|Y}(x|y) && (2.9)\\ &= -\sum_{y\in\mathcal{Y}} p_Y(y)\sum_{x\in\mathcal{X}} p_{X|Y}(x|y)\log p_{X|Y}(x|y) && (2.10)\\ &= -\sum_{y\in\mathcal{Y}} p_Y(y)H(X|Y=y) && (2.11) \end{aligned}$$

Thus, the conditional entropy of a random variable given another is the expected value of the entropies of the conditional distributions, averaged over the conditioning random variable. The units of conditional entropy is bits per symbol. Specifically, $H(X|Y)$ is the average loss of information about a transmitted symbol when a symbol is received. Naturally, the average information of a random variable X is decreased by the knowledge of correlated random variable Y so that

$$H(X|Y) \leq H(X) \tag{2.12}$$

holds. The equality holds only for the case when X and Y are independent random variables.

Mutual information

The most important measure of information is mutual information which describes the average amount of information common to both random variables. Specifically, it measures how much knowledge of one random variable reduces uncertainty about the other. For instance, if two random variables X and Y are independent, then knowledge of X does not yield any information about Y and the other way around. Thus, mutual information in this case is zero. On the other hand, if X is a deterministic function of Y, then the knowledge of X determines the value of Y and vice versa because all the information contained in X is shared with Y. Consequently, in this case mutual information is

equal to entropy of Y (*or* X). For a noiseless channel, the average amount of information received would be $H(X)$ bits per received symbol which is nothing but the entropy of the source. However, for noisy channels, there will be loss of information $H(X|Y)$ about the transmitted symbol per received symbol. As a result, the amount of information the receiver receives on the average, $I(X;Y)$ bits per received symbol would be

$$\mathcal{I}(X;Y) := H(X) - H(X|Y) \quad \text{bits per symbol} \tag{2.13}$$

Simply put, mutual information is a measure of amount of information that one random variable contains about the another correlated random variable. Effectively, it is the reduction in uncertainty of one random variable due to knowledge of the correlated random variable. In terms of probability distributions, Eq. (2.13) may be expressed as follows

$$\mathcal{I}(X;Y) = \mathbb{E}_{X,Y} \log \frac{p_{X,Y}(x,y)}{p_X(X)p_Y(Y)} \tag{2.14}$$

$$= \sum_{x\in\mathcal{X}} \sum_{y\in\mathcal{Y}} \log \frac{p_{X,Y}(x,y)}{p_X(x)p_Y(y)} \tag{2.15}$$

Thus, mutual information may also be interpreted as the relative entropy or Kullback Leibler distance between the joint distribution and the product of marginal distributions. It may also also be interpreted as the expected value of the log-likelihood ratio of joint and product of marginal distributions. Relative entropy is well known to be a measure of distance between two probability distributions. For definition of relative entropy or Kullback Leibler distance, the interested reader is referred to [30].

Chain Rules for Entropy and Mutual information

It is straightforward to prove that the entropy of a collection of random variables is the sum of collection of the conditional entropies.

$$H(X_1, X_2, \cdots, X_M) = \sum_{\nu=1}^{M} H(X_\nu | X_1, \cdots, X_{\nu-1}) \tag{2.16}$$

$$\leq \sum_{\nu=1}^{M} H(X_\nu) \tag{2.17}$$

where the equality holds only for the case when the random variables are statistically independent. Since mutual information is a difference of entropy and conditional entropy and both of them satisfy chain rule, therefore, mutual information also satisfies chain rule.

$$\mathcal{I}(X_1, X_2, \cdots, X_M; Y) = \sum_{\nu=1}^{M} \mathcal{I}(X_\nu; Y | X_1, \cdots, X_{\nu-1}) \tag{2.18}$$

$$\leq \sum_{\nu=1}^{M} \mathcal{I}(X_\nu; Y) \tag{2.19}$$

where the equality holds only for the case when the random variables are statistically independent. It is instructive here to define the conditional mutual information for derivations in the upcoming sections.

Definition

The conditional mutual information of random variables X and Y given Z can be defined as the expected value of the mutual information of X and Y given the value of Z. In terms of entropies, it can be expressed as follows.

$$\mathcal{I}(X; Y|Z) := H(X|Z) - H(X|Y, Z) \tag{2.20}$$

$$= \mathbb{E}_{X,Y,Z}\left[\log \frac{p_{X,Y|Z}(X, Y|Z)}{p_{X|Z}(X|Z) p_{Y|Z}(Y|Z)}\right] \tag{2.21}$$

Jensen's Inequality

If f is a convex function and X is a random variable, then Jensen's inequality reads

$$\mathbb{E}[f(X)] \geq f(\mathbb{E}[X]) \tag{2.22}$$

Moreover, if f is strictly convex, then the equality in (2.22) implies that $X = \mathbb{E}[X]$ with probability one (i.e., X is a constant).

Shannon (Ergodic) Capacity

When CSIT is not available, then data is transmitted at fixed rate from the source. Since data transmission is performed during all fading states, the effective capacity is reduced due to presence of deep fades. Shannon (Ergodic) capacity of a wireless fading channel with receiver CSI and an average power constraint can be defined as follows [31].

$$C = \int_0^\infty \log_2(1+\gamma) p_\Gamma(\gamma) d\gamma \tag{2.23}$$

It is noteworthy that Shannon capacity is a statistical average. In other words, it is equal to channel capacity of an AWGN channel with SNR γ, given by $B\log_2(1+\gamma)$, averaged over the distribution of γ.

2.3 Compressive Sensing

Computers have become omnipresent in our daily life in offices, industries and homes for personal use. They operate on bits of zeros and ones rendering digital operations necessary. Moreover, majority of electronic devices used now a days for important purposes such as telecommunication, surveillance, and remote sensing etc execute digital operations. Owing to invention of ADC, digital devices have become part and parcel of the so-called digital age.

Most of the naturally occuring signals are analogue in nature. Analogue signals are sampled and quantized by ADCs to generate digital signals. Nyquist sampling theorem has been accepted worldwide as doctrine of discrete-time signal processing and signal acquisition. This celebrated theorem was implied by the work of Nyquist in 1928 [32] and later proved by Shannon in 1949 [33]. The theorem states that in order to reconstruct an arbitrary bandlimited signal perfectly from its samples, it is essential that sampling rate should be greater than twice the highest frequency present in the signal (the Nyquist rate).

The resultant samples generated by sampling process are given as input to sophisticated signal processing algorithms to produce desirable outputs. The sampling circuits in ADCs sample the incoming analogue signal at proportionately higher rates as the bandwidth of incoming signal increases. Consequently, high speed ADCs are required which are expensive. Moreover, the computational complexity increases which in turn burdens the battery and data storage requirements. For applications requiring extremely high resolution, this process can be prohibitively complex rendering it infeasible.

The data storage requirement can be alleviated by incorporating advanced compression algorithms in ADCs. The compression algorithms minimize the storage issue by transforming the huge amount of data into relatively smaller set of samples. In applications such as digital images and video cameras, the Nyquist rate is so high that compression becomes necessary due to large number of samples prior to storage or transmission. However, this solution is not viable for applications that need higher sampling rates because the samples must be stored before performing compression. Additionally, the process of compression discards most of the information content obtained after sampling. Thus, enhancing the sampling rate is not a feasible solution for applications requiring high resolution because in compression, most of the information content is discarded. In some applications including medical scanners and radars, either the sensor is expensive or the

measurement process is costly. In such cases, we are not able to collect sufficient measurements to satisfy the Nyquist rate.

2.3.1 Compressive Sensing Framework

The compressive sensing is a paradigm shift in statistical signal processing. It is a relatively new technology which lies in the overlapping area of statistics, optimization, and signal processing. This technique enables us to reduce the sampling rate to cope with the demands of sophisticated digital signal processing algorithms. Intuitively, this scheme aims at doing sampling in a smart fashion such that information content of the siganl remains unaltered. This aim is achieved by performing the sampling based on the actual information content and the structure of the signals and not the maximum frequency content.

Interestingly, most signals we are dealing with, are highly compressible because they can be represented by a set of sparse or nearly sparse coefficients. CS is capable of acquiring a signal from a small set of incoherent measurements with a sampling rate which is less than Nyquist rate provided the signal is sparse or compressible in some transform domain. In essence, sampling is performed in such a way that results in compressed data. Many signals encountered in wireless communications are sparse which makes the CS an integral part of the design and analysis of 5G wireless communication systems.

In the next subsections, we discuss the important conditions to be satisfied by CS in order to recover the sparse signal from measurements which are far fewer than the Nyquist rate. Furthermore, we discuss the measurement process and the reconstruction algorithms to recover the sparse signal from measurements.

Sparsity

Compressive sesning (a.k.a. compressed sampling) was coined by Donoho [34] and Candes et al [35]. This is based on the principle that the sparsity of the signal can be exploited to recover it from small set of its linear measurements. A sparse signal is defined as the signal which contains very few significant components and the rest of the components are zero. It is interesting to mention here that a compressible signal has a small number of active components but the rest of enrties are not necessarily zero. It has been shown in [34, 35] that a signal which is not compressible/sparse in its original domain can also recovered from a small set of incoherent measurements provided it has a sparse representation in some underlying domain.

Sparsity is exhibited by both man-made and naturally occuring signals. Examples of sparse signals include video/image signals, speech signals, siganls obtained from biometric algorithms and signals sensed from galaxies etc. Such abundant existence of sparse signals render the CS an attractive scheme to devise simple and low-complexity signal processing algorithms for the purpose of reconstruction. Some examples in which a priori knowledge of sparsity is exploited include but are not limited to magnetic resonance imaging (MRI), network tomography and magnetoencephalography (MEG) etc.

Measurement Process

In CS, the sparse signal is not sampled in conventional manner. Instead, the measurements of sparse signal are acquired as linear combinations of its components. Let $\boldsymbol{x} \in \mathbb{R}^N$ be the K-sparse signal where K is sparsity and let $\boldsymbol{y} \in \mathbb{R}^M$ represent the acquired measurement vector with $M < N$. Now, the measurement process reads

$$\boldsymbol{y} = \boldsymbol{\Psi x} + \boldsymbol{n} \tag{2.24}$$

where $\boldsymbol{n} \sim \mathcal{N}(\mathbf{0}, \sigma_w^2 \boldsymbol{I})$ is the white Gaussian noise and $\boldsymbol{\Psi}$ is the $M \times N$ sensing matrix generating the desired linear combinations of components of $\boldsymbol{x}$. The sensing matrix should be designed in such a manner so as to retain the information content present in the signal. A matrix having this desired property can be designed with high probability if its elements are chosen to be independent and identically distributed random variables characterized by zero-mean Gaussian distribution [34, 35].

It has been demonstrated in [34,35] that for the aforementioned setup, a sparse signal $\boldsymbol{x}$ having $K << N$ non-zero components can be reconstructed from just $M \geq cK \log(\frac{N}{K})$ measurements with c a small constant. To date, several algorithms have been proposed for CS recovering using very few measurements. Here, we will discuss most important CS reconstruction algorithms.

Reconstruction Algorithms

Since the nullspace of $\boldsymbol{\Psi}$ is non-empty for underdetermined setup, so Eq. (2.24) has infinite many solutions. However, if the desired signal $\boldsymbol{x}$ is known to be sparse, then the most straightforward solution will be minimization of l_0 norm. The l_0 norm minimization solution can be setup as follows.

$$\hat{\boldsymbol{x}} = \arg\min \|\boldsymbol{x}\|_0 \quad \text{s.t.} \quad \|\boldsymbol{y} - \boldsymbol{\Psi}\boldsymbol{x}\|_2 \leq \epsilon \tag{2.25}$$

This solution in fact determines the sparsity level of the $\boldsymbol{x}$. Simply put, it counts the non-zero entries of $\boldsymbol{x}$. In essence, this optimization program attempts to minimize the total number of active components in $\boldsymbol{x}$ and consequently, it achieves the sparset solution. In practice, this solution amounts to searching over all the support sets via an exhautive search which becomes prohibitively complex for signals of large dimensions and therefore, it is an NP-hard problem.

Convex Relaxation

It has been demonstrated in [34, 35] that the program in (2.25) can be solved via convex relaxation and $\boldsymbol{x}$ would be recovered with high probability by solving the following l_1 optimization problem,

$$\hat{\boldsymbol{x}} = \arg\min \|\boldsymbol{x}\|_1 \; s.t. \; \|\boldsymbol{y} - \boldsymbol{\Psi}\boldsymbol{x}\|_2 \leq \epsilon \tag{2.26}$$

The above setup is a convex optimization problem that easily boils down to a linear program known as basis-pursuit denoising (BPDN) [36] which can be solved via interior-point methods. These methods possess polynomial complexity, i.e. $\mathcal{O}(N^3)$. More efficient greedy pursuit algorithms have been proposed which are faster but they offer less accurate solutions than convex relaxation.

Restricted Isometry Property

In CS, the signal $\boldsymbol{x}$ could be recovered from knowledge of $\boldsymbol{y}$ if $\boldsymbol{\Psi}$ had full column rank. In this case, $\boldsymbol{x}$ would be the unique solution of

$$\min \|\boldsymbol{y} - \boldsymbol{\Psi}\boldsymbol{x}\|_2^2 \tag{2.27}$$

or $\hat{\boldsymbol{x}} = (\boldsymbol{\Psi}^T\boldsymbol{\Psi})^{-1}\boldsymbol{\Psi}^T\boldsymbol{y}$. However, CS employs underdetermined system, i.e., $\boldsymbol{\Psi}$ has fewer rows than columns because the information signal is downsampled. It is well-known that such a matrix cannot have full column rank and consequently, underdetermined systems have multiple solutions. Recall that $\boldsymbol{x}$ is sparse or nearly sparse and prior to CS recovery, the support of active components is not known. Thus, given merely that $\boldsymbol{x}$ is sparse, CS recovery depends solely on type of matrix $\boldsymbol{\Psi}$.

The restricted isometry property (RIP) proposed by Candes and Tao [37] is a fundamental condition for CS recovery of sparse signals. If a matrix $\boldsymbol{\Psi}$ satisfies RIP, then it is guaranteed that solution to l_1-minimization problem becomes equivalent to the solution of l_0-minimization problem. Here we provide a useful definition of RIP.

Definition

The matrix $\boldsymbol{Psi} \in \mathbb{R}^{M\times N}$ has the RIP of order K if $\exists$ a constant $\epsilon_K \in (0,1) \ni$

$$(1-\epsilon_K) \leq \frac{\|\boldsymbol{\Psi x}\|_2^2}{\|\boldsymbol{x}\|_2^2} \leq (1+\epsilon_K) \tag{2.28}$$

holds $\forall$ $K-$ sparse signals $\boldsymbol{x} \in \mathbb{R}^N$ ($\forall \boldsymbol{x}$ with $\|\boldsymbol{x}\|_0 \leq K$). The RIP condition can be interpreted in terms of singular values. If all the eigenvalues of all the submatrices $\boldsymbol{\Psi}_S^T \boldsymbol{\Psi}_S$ are restricted to the interval $(1-\epsilon_K, 1+\epsilon_K)$, then it is equivalent to the statement that the matrix $\boldsymbol{\Psi}$ satisfies RIP of order K with isometry constant ϵ_K. Here $\boldsymbol{\Psi}_S$ is an $M \times K$ submatrix of $\boldsymbol{\Psi}$ indexed by the set S with cardinality $|S| \leq K$. It should be noticed that by definition of RIP, the matrix $\boldsymbol{\Psi}$ needs to satisfy this condition for all the $\binom{N}{K}$ submatrices $\boldsymbol{\Psi}_S^T \boldsymbol{\Psi}_S$ [38]. Given a matrix $\boldsymbol{\Psi}$, the task of establishing the RIP is a combinatorial problem which becomes prohibitively complex for large N. Fortunately, it has been found out that matrix ensembles satisfy the RIP. For instance, Baraniuk et al. [38] demonstrated that a random $M \times N$ matrix with i.i.d. Gaussian entries distributed according to $\mathcal{N}(0, \frac{1}{M})$ will satisfy RIP of order K with high probability if $M = \mathcal{O}(K \log(\frac{N}{K}))$. For the l_1-minimization problem (2.26), establishing the RIP of order $2K$ with constant $\epsilon_{2K} < 0.4652$ for a given $\boldsymbol{\Psi}$ guarantees exact recovery of any $K-$sparse signal $\boldsymbol{x} \in \mathbb{R}^N$ [39].

2.4 Total-Least-Squares Estimation

Most of the linear problems in communications, control and signal processing can be modelled via following matrix-vector relationship,

$$\boldsymbol{y} = \boldsymbol{\Psi x} + \boldsymbol{n}. \tag{2.29}$$

Here $\boldsymbol{y}$ is received/measurement signal, $\boldsymbol{x}$ is the signal of interest to be estimated and $\boldsymbol{\Psi}$ is the measurement/sensing matrix. In most of applications, it is reasonable to assume

that noise is AWGN, i.e., the power spectral density of noise is flat and its probability distribution is Gaussian ($\boldsymbol{n} \sim \mathcal{N}(\mathbf{0}, \sigma_n^2 \boldsymbol{I})$).

For the linear data model in Eq. (2.4), the ordinary least-squares (OLS) attempts to minimize the error in the measurement process which amounts to minimizing the following objective function :

$$\min \quad \|\boldsymbol{y} - \boldsymbol{y}^{'}\|_2 \quad \text{s.t.} \quad \boldsymbol{y}^{'} \in \mathcal{C}(\boldsymbol{\Psi}) \tag{2.30}$$

$$\textit{or} \quad \min \quad \|\boldsymbol{y} - \boldsymbol{\Psi}\boldsymbol{x}\|_2 \tag{2.31}$$

Once a minimzer $\boldsymbol{y}^{'}$ is calculated, then any $\boldsymbol{x}$ satisfying $\boldsymbol{y}^{'} = \boldsymbol{\Psi}\boldsymbol{x}$ is termed OLS solution and $\triangle\boldsymbol{y}^{'} = \boldsymbol{y} - \boldsymbol{y}^{'}$ the corresponding OLS correction. One such OLS solution is shown here [40],

$$\boldsymbol{x}_{ols} = (\boldsymbol{\Psi}^T\boldsymbol{\Psi})^{-1}\boldsymbol{\Psi}^T\boldsymbol{y}. \tag{2.32}$$

For AWGN channel model, Eq. (2.32) is also termed the best-linear-unbiased estimator (BLUE) [40]. The OLS estimation is premised on the underlying assumption that the measurement matrix is known perfectly and errors are present only in $\boldsymbol{y}$. This is not a realistic assumption because the measurement matrix is not known perfectly due to sampling or modeling errors in $\boldsymbol{\Psi}$. For instance, in wireless channel the estimated channel matrix contains estimation noise. So, the more appropriate data model is as follows.

$$\boldsymbol{y} = (\boldsymbol{\Psi} + \boldsymbol{\Psi}_e)\boldsymbol{x} + \boldsymbol{n}. \tag{2.33}$$

where $\boldsymbol{\Psi}_e$ is the noise in $\boldsymbol{\Psi}$. Golub proposed to use TLS estimation in [41] which takes into account the noise in the measurement matrix. In order to accout for errors in the measurement matrix, TLS attempts to minimize not only the noise in received vector but also in the measurement matrix. Let $\widehat{\boldsymbol{\Psi}}_{ls} = \boldsymbol{\Psi} + \boldsymbol{\Psi}_e$, then the TLS objective function can be expressed as follows.

$$\min_{\hat{\boldsymbol{\Psi}}_{tls}, \hat{y} \in \mathcal{C}(\hat{\boldsymbol{\Psi}}_{tls})} \| \; vec[\hat{\boldsymbol{\Psi}}_{ls} \quad \boldsymbol{y}] - vec[\hat{\boldsymbol{\Psi}}_{tls} \quad \hat{\boldsymbol{y}}] \; \|^2 \tag{2.34}$$

The following theorem is derived in [41,42] and is presented here for illustrative purposes.

Theorem 1. *Let* $\boldsymbol{U}\acute{\boldsymbol{\Sigma}}\boldsymbol{V}^T$ *be the Singular-Value Decomposition (SVD) of* $\hat{\boldsymbol{\Psi}}_{tls}$ *and* $\boldsymbol{U}\boldsymbol{\Sigma}\boldsymbol{V}^T$ *be the SVD of* $\left[\hat{\boldsymbol{\Psi}}_{ls} \mid \boldsymbol{y}\right]$*.If* $\hat{\sigma}_n \geq \sigma_{n+1}$ *then the signal estimate for total-least-squares estimation exists and is unique and it can be expressed as follows.*

$$\hat{\boldsymbol{x}}_{tls} = \left(\langle \hat{\boldsymbol{\Psi}}_{ls}, \hat{\boldsymbol{\Psi}}_{ls} \rangle - \sigma_{N+1}^2 \boldsymbol{I}_{N+1}\right)^{-1} \langle \hat{\boldsymbol{\Psi}}_{ls}, \boldsymbol{y} \rangle \tag{2.35}$$

Proof.

SVD can be used to find a closed-form expression for TLS solution. It is constructive here to write $\boldsymbol{y} \approx \hat{\boldsymbol{\Psi}}_{ls}\boldsymbol{x}$ in the following form

$$\left[\hat{\boldsymbol{\Psi}}_{ls} \mid \boldsymbol{y}\right] \left[\boldsymbol{x}^T \mid -1\right]^T \approx 0 \tag{2.36}$$

Let the SVD of $\left[\hat{\boldsymbol{\Psi}}_{ls} \mid \boldsymbol{y}\right]$ be $\boldsymbol{U}\boldsymbol{\Sigma}\boldsymbol{V}^T$. Here $\boldsymbol{U}$ and $\boldsymbol{V}$ represents the left and right singular matrices respectively. Singular Values are contained in $\boldsymbol{\Sigma} = diag[\sigma_1, \cdots, \sigma_{n+1}]$. If $\sigma_{n+1} \neq 0$ then the rank of $\left[\hat{\boldsymbol{\Psi}}_{ls} \mid \boldsymbol{y}\right]$ is $n+1$ and the corresponding row space $\mathcal{R}\left[\hat{\boldsymbol{\Psi}}_{ls} \mid \boldsymbol{y}\right] \in \mathbb{R}^{n+1}$. Consequently the null space, which is orthogonal complement of row space, will be empty and Eq. (2.36) will be inconsistent. In order to make it consistent, the rank of $\left[\hat{\boldsymbol{\Psi}}_{ls} \mid \boldsymbol{y}\right]$ should be reduced to n. Here we invoke Eckart-Young-Mirsky (EVM) theorem which provides us with best rank n TLS approximation $\left[\hat{\boldsymbol{\Psi}}_{tls} \mid \hat{\boldsymbol{y}}\right]$ of $\left[\hat{\boldsymbol{\Psi}}_{ls} \mid \boldsymbol{y}\right]$. Thus TLS approximation may be expressed as

$$\left[\hat{\boldsymbol{\Psi}}_{tls} \mid \hat{\boldsymbol{y}}\right] = \boldsymbol{U}\hat{\boldsymbol{\Sigma}}\boldsymbol{V}^T \quad with \quad \hat{\boldsymbol{\Sigma}} = diag[\sigma_1, \cdots, \sigma_{n+1}, 0].$$

The above approximation is best in the sense that it minimized the deviations in variance. The minimal TLS correction from EVM theorem can be expressed as

$$\sigma_{n+1} = \min_{rank([\hat{\boldsymbol{\Psi}}_{ls}|\boldsymbol{y}])=n} \| \, vec[\hat{\boldsymbol{\Psi}}_{ls} \mid \boldsymbol{y}] - vec[\hat{\boldsymbol{\Psi}}_{tls} \mid \hat{\boldsymbol{y}}] \, \|_2 \, . \tag{2.37}$$

and this TLS correction matrix can be attained for

$$\left[\hat{\boldsymbol{\Psi}}_{ls} \mid \boldsymbol{y}\right] - \left[\hat{\boldsymbol{\Psi}}_{tls} \mid \hat{\boldsymbol{y}}\right] = \left[\triangle\hat{\boldsymbol{\Psi}}_{tls} \mid \triangle\hat{\boldsymbol{y}}\right] = \sigma_{n+1}\boldsymbol{u}_{n+1}\boldsymbol{v}_{n+1}^T$$

Now this correction matrix has rank one and following set of equations is consistent.

$$\left[\hat{\boldsymbol{\Psi}}_{tls} \mid \hat{\boldsymbol{y}}\right]\left[\boldsymbol{x}^T \mid -1\right]^T = 0 \tag{2.38}$$

The solution set of this system of equations comprises of one vector only $\boldsymbol{v}_{n+1}$ which is the last column of $\boldsymbol{V}$. This right-most singular vector belongs to null-space, i.e., $\boldsymbol{v}_{n+1} \in \aleph(\left[\hat{\boldsymbol{\Psi}}_{tls} \mid \hat{\boldsymbol{y}}\right])$. We can normalize $\boldsymbol{v}_{n+1}$ by its last component $\boldsymbol{v}_{n+1}(n+1)$ to obtain the following TLS solution.

$$\left[\frac{\hat{\boldsymbol{x}}_{tls}}{-1}\right] = \frac{-1}{\boldsymbol{v}_{n+1}(n+1)}\boldsymbol{v}_{n+1} \tag{2.39}$$

If $\boldsymbol{v}_{n+1}(n+1) \neq 0$, then

$$\begin{aligned} \hat{\boldsymbol{y}} &= \hat{\boldsymbol{\Psi}}_{tls}\hat{\boldsymbol{x}}_{tls} \\ &= \frac{-1}{\boldsymbol{v}_{n+1}(n+1)}[\boldsymbol{v}_{n+1}(1), \cdots, \boldsymbol{v}_{n+1}(n)]^T \in \mathcal{C}(\hat{\boldsymbol{\Psi}}_{tls}), \end{aligned} \tag{2.40}$$

i.e., $\hat{\boldsymbol{y}} \in \mathcal{C}(\hat{\boldsymbol{\Psi}}_{tls})$ is satisfied and consequently TLS problem is solved for the considered assumptions. The interlacing theorem for singular values leads to following chain of inequalities,

$$\sigma_1 \geq \acute{\sigma}_1 \geq \cdots \geq \sigma_n \geq \acute{\sigma}_n \geq \sigma_{n+1} \tag{2.41}$$

If we assume $\hat{\sigma}_n \geq \sigma_{n+1}$ then it prevents σ_{n+1} from becoming repeated singular value of $\left[\hat{\boldsymbol{\Psi}}_{ls} \mid \boldsymbol{y}\right]$. If

$$\left[\hat{\boldsymbol{\Psi}}_{ls} \mid \boldsymbol{y}\right]^T \left[\hat{\boldsymbol{\Psi}}_{ls} \mid \boldsymbol{y}\right] \left[\frac{\boldsymbol{z}}{0}\right] = \sigma_{n+1}^2 \left[\frac{\boldsymbol{z}}{0}\right], \tag{2.42}$$

and $0 \neq \boldsymbol{z} \in \mathbb{R}^n$ then this implies $\hat{\boldsymbol{\Psi}}_{ls}^T \hat{\boldsymbol{\Psi}}_{ls} \boldsymbol{z} = \sigma_{n+1}^2 \boldsymbol{z}$ which is a contradiction because $\hat{\sigma}^2$ is smallest eigenvalue of $\hat{\boldsymbol{\Psi}}_{ls}^T \hat{\boldsymbol{\Psi}}_{ls}$. Consequently, there must be a vector in $\aleph(\left[\hat{\boldsymbol{\Psi}}_{tls} \mid \hat{\boldsymbol{y}}\right])$ whose last component is non-zero. This implies that there exists a solution for TLS problem. Since the nullity of $\left[\hat{\boldsymbol{\Psi}}_{tls} \mid \hat{\boldsymbol{y}}\right]$ is unity so the TLS solution must be unique. The condition that $\hat{\sigma}_n \geq \sigma_{n+1}$ ensures that $\hat{\boldsymbol{x}}_{tls}$ exists and is unique. As $\boldsymbol{v}_i$ are right singular vectors so they are eigenvectors of $\left[\hat{\boldsymbol{\Psi}}_{ls} \mid \boldsymbol{y}\right]^T \left[\hat{\boldsymbol{\Psi}}_{ls} \mid \boldsymbol{y}\right]$ therefore they satisfy the following eigenvector equations:

$$\left[\hat{\boldsymbol{\Psi}}_{ls} \mid \boldsymbol{y}\right]^T \left[\hat{\boldsymbol{\Psi}}_{ls} \mid \boldsymbol{y}\right] \left[\begin{array}{c} \hat{\boldsymbol{x}}_{tls} \\ \hline -1 \end{array}\right] = \sigma_{n+1}^2 \left[\begin{array}{c} \hat{\boldsymbol{x}}_{tls} \\ \hline -1 \end{array}\right]$$

$$\left[\begin{array}{c|c} \langle \hat{\boldsymbol{\Psi}}_{ls}, \hat{\boldsymbol{\Psi}}_{ls} \rangle & \langle \hat{\boldsymbol{\Psi}}_{ls}, \boldsymbol{y} \rangle \\ \hline \langle \boldsymbol{y}, \hat{\boldsymbol{\Psi}}_{ls} \rangle & \|\boldsymbol{y}\|^2 \end{array}\right] \left[\begin{array}{c} \hat{\boldsymbol{x}}_{tls} \\ \hline -1 \end{array}\right] = \sigma_{n+1}^2 \left[\begin{array}{c} \hat{\boldsymbol{x}}_{tls} \\ \hline -1 \end{array}\right]$$

If we simplify the top block of the above matrix-vector relation, then we will end up with following TLS solution.

$$\hat{\boldsymbol{x}}_{tls} = \left(\langle \hat{\boldsymbol{\Psi}}_{ls}, \hat{\boldsymbol{\Psi}}_{ls} \rangle - \sigma_{N+1}^2 \boldsymbol{I}_{N+1} \right)^{-1} \langle \hat{\boldsymbol{\Psi}}_{ls}, \boldsymbol{y} \rangle \tag{2.43}$$

where σ_{N+1} is the smallest singular value of the augmented matrix $\left[\hat{\boldsymbol{\Psi}}_{ls} | \boldsymbol{y}\right]$.

Chapter 3

Analysis of Adaptive Least Squares Filtering in Massive MIMO

In this chapter, we analyse the adaptive least-squares filtering in massive MIMO in order to study the effect of pilot contamination in adaptive beamforming scenario where instead of performing channel estimation, training sequences are used to train the precoders and decoders. Section 3.1 provides the motivation and related work of adaptive beamforming in massive MIMO. Section 3.2 gives the system model of a multi-cell scenario for pilot and data transmission. In Section 3.3, we perform the pilot contamination analysis in which orthogonal, identical and random pilots are treated separately. In Section 3.4, we provide simulation results to verify the mathematical analysis. Section 3.5 concludes the chapter 3.

3.1 Motivation and Related Work

In traditional cellular systems, frequency reuse was employed to enhance the system capacity. The universal frequency reuse among neighbouring cells leads to severe inter-cell interference which causes degradation of SINR especially for cell edge users. Several al-

gorithms were designed to mitigate this SINR deterioration by exploiting the additional degrees of freedom offered by the use of antenna arrays at BTS. In coordinated beamforming, all the BTSs share their CSI and beamforming vectors are designed jointly [43]. The authors in [43] reveal ways to design a downlink beamformer in a truly distributed manner. In their approach, they do not assume any central processing unit. Instead they use message passing between neighbouring BTSs for downlink beamforming to accomplish macrodiversity. Specifically, the global beamforming computation is distributed among BTSs and only local communication is established between adjacent BTSs. In network MIMO, BTSs share the message data over the backhaul link in addition to CSI exchange [13]. In Network MIMO (a.k.a. multicell MIMO), multicell processing is implemented in the form of joint precoding. However, complete data sharing incurs high capacity backhaul links which are not feasible in certain applications.

Though coordinated beamforming does not entail exchange of user data, the exchange of CSI across the BTSs on a fast time scale and low latency basis is challenging when it comes to implementation. A noncooperative scheme termed as "Massive MIMO" is introduced in [15] which relaxes the requirement of CSI exchange. This scheme suggests that as we increase the number of antenna elements N_T at base station, the channel from BTS to desired user will become orthogonal to that of interfering users. Thus low-complexity signal processing scheme maximum-ratio combining or spatial matched filtering is possible at the BTS side by simply aligning the beamforming vector with the desired channel. The capacity performance of this scheme is plagued by "pilot contamination" effect which is in fact inter-cell interference.

In pilot contamination, the channel estimate of desired user in its own cell is contaminated by the channels of users in other cells which are using same pilot sequence as that of desired user. The pilot contamination problem is shown in the Fig. 3.1 for illustrative purposes. The authors in [25] suggest that if the users are scheduled in terms of pilot

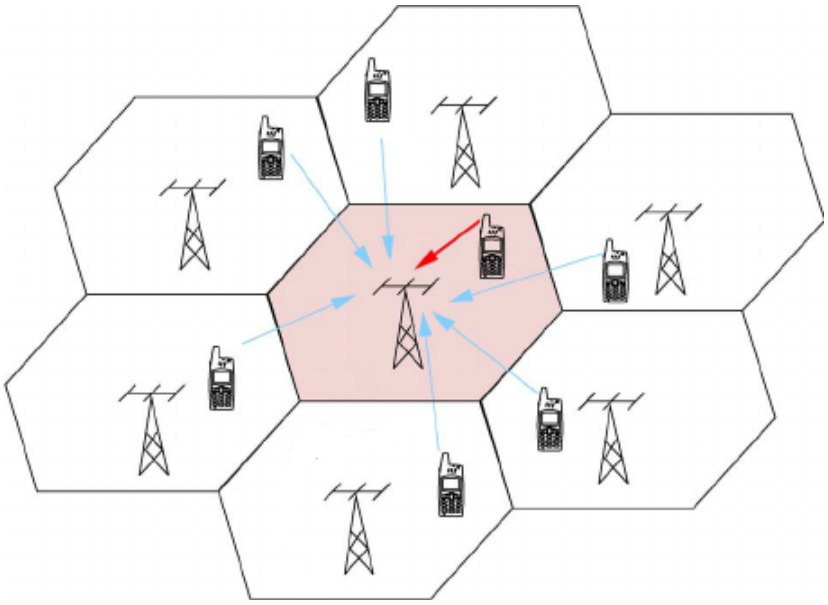

Figure 3.1: Pilot Contamination in Massive MIMO [44]

sequence allocation intelligently then this effect can be minimized. This idea is based on the premise that all the pilot sequences in one cell are mutually orthogonal however the other cells are also using the same set of pilot sequences due to limited coherence time. The authors demonstrate that as the number of base station antennas increases, the pilot contamination effect vanishes under certain conditions on subspaces of channel covariance matrices of desired and interfering users. The suggested scheme exploits the dormant side-information lying in second-order statistics of desired and interfering users' channels. The minimum-mean-square error (MMSE) estimator of the desired channel depends upon the covariance matrices of the interfering users' channels owing to pilot contamination. In [25], a coordination algorithm for pilot sequences assignment to users in the L cells was proposed. This algorithm assigns a given training sequence to a user in one cell whose spatial characteristics are maximally different from those of interfering users having assigned identical pilot sequences in other cells. Consequently, the MMSE estimator of desired user's channel has no more residuals of contaminating channel covariance matrices of interfering users. This algorithm requires coordination among neighbouring

base stations for scheduling of training sequences across cells.

The use of a large number of antennas at BTS enables us to achieve higher spectral efficiencies owing to beamforming/array gains. In coordinated beamforming, all the BTSs must have CSI of channels between neighbouring BTSs and their users. In [26], the overhead for having CSI at transmitters or receivers has been alleviated. An adaptive distributed algorithm is designed for updating the precoders and receiver filters iteratively to optimize the sum rate. The proposed algorithm is a variant of max-SINR algorithm and was analyzed under MIMO interference network assumption. The max-SINR algorithm also iterates back and forth between transmitter and receiver assuming perfect CSI [45]. Max-SINR is a celebrated algorithm which attempts to maximize the SINR on a stream-by-stream basis instead of explicitly minimizing the leaked interference. It has been established that max-SINR is optimal within the family of linear beamformers at high SNRs. It has also been shown that it achieves better throughput than sum-rate gradient algorithms in the medium SNR regime.

With perfect CSI, similar iterative algorithms are proposed in [46]. The authors in [46] adopted a joint MMSE design approach that jointly optimizes the transmit precoders and receive spatial filters. Moreover, their proposed SINR algorithm is proven to converge in contrast to previous max-SINR algorithms. Similarly, bidirectional training schemes are used to do channel estimation in [47]. Particularly, they focus on the optimal power allocation between reverse training, forward training and data transmission. They provide closed-form solutions for power allocation using high SNR approximations. Under proposed power allocation scheme, they achieve near-optimal performance in terms of symbol-error rate (SER) for different modulation schemes over a wide range of SNRs. Bidirectional training without channel estimation has been employed for adaptive beamforming in [26] but that paper does not consider the impact of "pilot contamination" and is restricted to single cell MIMO interference network and i.i.d. training sequences.

In this chapter, we consider a multi-cell setting in which each cell has one BTS and one user or mobile station (MS). We have chosen one MS in each cell for adaptive beamforming as the same approach of having one user in each cell for a multi-cell system has been adopted in [25]. The authors in [25] have adopted one user per cell because in massive MIMO, the channel of a desired user in one cell is contaminated by only one user per neighbouring cell. In this chapter, we assume that the users are using random sequences which are random across cells but are orthogonal within the same cell, so it is reasonable to assume one user per cell since the amount of collective interference from a set of random training sequences will be less than the interference of an identical training sequence due to tiny side lobes. The authors in [25] are analysing pilot contamination during channel estimation and we focus on training precoders and decoders directly without doing channel estimation.

In this chapter, the BTS is equipped with an array of N_T antenna elements and MS is equipped with single antenna. Initially, all the BTSs transmit their training sequences to the MSs synchronously and MSs update their receive filters. In the next phase, all the users transmit their training sequences synchronously to the BTSs which update their beamforming filters. After the filters are optimized, data is transmitted. The receive filters are assumed to be linear with intereference considered as noise. Consequently, the information rate is determined by the received SINR. Our objective is to analyse the impact of "pilot contamination" in adaptive beamforming scheme under different structures of training sequences. Specifically, we employ orthogonal, identical and random pilot sequences in both directions and study their effect on the average sum rate where sum rate is the sum of information rates of MSs in different cells.

Our approach is based on multi-cell TDD systems and we analyse that as the number of BTS antenna elements increases, the sum rates achieved by the adaptive least-squares based filtering under random training sequences is higher than that achieved under iden-

tical training sequences. The approach in [25] is premised on coordination across cells to schedule training sequences in intelligent way so that interfering users across cells do not interfere but this comes at the cost of coordination across cells for training sequence scheduling which on a fast time scale and low latency basis is challenging when it comes to implementation. We propose random training sequence so that overhead introduced by control channel or backhaul is eliminated.

3.2 System Model

Consider a cellular network with L time-synchronised cells. Each cell has one BTS which is equipped with N_T antenna elements. The mobile station (MS) has one antenna. The channel between j-th BTS and k-th MS is denoted by a complex vector $\boldsymbol{h}_{kj} \sim \mathcal{CN}(\mathbf{0}, \mathbf{R})$, where $\mathbf{R}$ is the $N_T \times N_T$ covariance matrix of the channel gains. It is assumed that transmitters and receivers have no explicit knowledge of the CSI. All the transmissions are assumed to be synchronous and channel is assumed to be TDD to exploit channel reciprocity. In downlink, the k-th BTS beamforms the transmitted symbol with a rank one precoding matrix $\boldsymbol{v}_k \in \mathbb{C}^{N_T}$ and MS processes the received signal with a receive filter $\boldsymbol{g}_k \in \mathbb{C}$. The received signal at k-th MS contains inter-cell interference owing to synchronous transmissions from all BTSs. For instance, the k-th MS receives the following signal at i-th time instant.

$$z_k(i) = \langle \boldsymbol{h}_{kk}, \boldsymbol{v}_k \rangle x_k(i) + \underbrace{\sum_{j \neq k} \langle \boldsymbol{h}_{kj}, \boldsymbol{v}_j \rangle x_j(i)}_{ISI} + n_k(i)$$

where $n_k(i)$ is zero mean complex Gaussian noise with variance σ_o^2. Let $\boldsymbol{x}_k = [x_k(1) \cdots x_k(\tau)]$ be a $1 \times N_T$ sequence of symbols transmitted over the channel then the received

sequence of symbols at k-th MS can be expressed as

$$\boldsymbol{z}_k = \sum_{j=1}^{L} \langle \boldsymbol{h}_{kj}, \boldsymbol{v}_j \rangle \boldsymbol{x}_j + \boldsymbol{n}_k \tag{3.1}$$

$$= [\langle \boldsymbol{h}_{k1}, \boldsymbol{v}_1 \rangle \cdots \langle \boldsymbol{h}_{kL}, \boldsymbol{v}_L \rangle] \underbrace{\begin{pmatrix} \text{——}\boldsymbol{x}_1\text{——} \\ \cdot \\ \cdot \\ \cdot \\ \text{——}\boldsymbol{x}_L\text{——} \end{pmatrix}}_{=\boldsymbol{X}} + \boldsymbol{n}_k$$

$$= \left[\tilde{h}_{k1} \cdots \tilde{h}_{kL}\right] \boldsymbol{X} + \boldsymbol{n}_k \tag{3.2}$$

$$\boldsymbol{z}_k = \tilde{\boldsymbol{h}}_k^T \boldsymbol{X} + \boldsymbol{n}_k \tag{3.3}$$

where $\boldsymbol{z}_k = [z_k(1) \cdots z_k(\tau)]$ is the $1 \times \tau$ received sequence at the MS and the measurement noise is a $1 \times \tau$ sequence of independent Gaussian random variables $\boldsymbol{n}_k = [n_k(1) \cdots n_k(\tau)]$. Here $\tilde{\boldsymbol{h}}_k = \left[\tilde{h}_{k1} \cdots \tilde{h}_{kL}\right]^T = [\langle \boldsymbol{h}_{k1}, \boldsymbol{v}_1 \rangle \cdots \langle \boldsymbol{h}_{kL}, \boldsymbol{v}_L \rangle]^T$ is the beamforming gain vector for k-th user from different BTSs. $\boldsymbol{X}$ is the data matrix whose rows represent the data sequences of different transmitters. During the training phase, the rows of $\boldsymbol{X}$ are training sequences, and τ is the length of the training sequence (see below).

This compact system model facilitates analysis in the upcoming section. It is assumed that CSI is not known at BTSs or MSs. The adaptive least squares filtering scheme described here is inspired by the adaptive beamforming scheme presented in [26]. In this scheme, beams and receive filters are jointly optimized iteratively. This scheme comprises of iterating a forward optimization in which MSs' receive filters are optimized with fixed beams, with a backward optimization in which beams are optimized via transmission of data in uplink. In backward direction, receive filters are fixed and act as beamformers. Initially, a pilot sequence $\boldsymbol{x}_k = \boldsymbol{b}_k$ is transmitted by the k-th BTS in forward direction

and receive filter at k-th MS is optimized as follows:

$$\hat{g}_k = \arg\min_{g_k} \|\boldsymbol{b}_k - g_k^* \boldsymbol{z}_k\|^2 \tag{3.4}$$

$$= (\boldsymbol{z}_k \boldsymbol{z}_k^H)^{-1} \boldsymbol{z}_k \boldsymbol{b}_k^H \tag{3.5}$$

This is referred to as *forward training*. All the BTSs transmit pilot sequences synchronously and MSs update their receive filters. In the training phase, $\boldsymbol{X} = \boldsymbol{B}$ is the pilot matrix whose rows contain the pilot sequences of L BTSs. Once the receive filters at MSs have been optimized, we fix them and transmit the training sequences $\{\boldsymbol{s}_i\}_{i=1}^L$ in the reverse direction from MSs to BTSs. The sequence of receive signals at k-th BTS can be expressed as

$$\boldsymbol{Y}_k = \sum_{j=1}^{L} \boldsymbol{h}_{jk} g_j^* \boldsymbol{s}_j + \mathbf{N_k} \tag{3.6}$$

Here $\boldsymbol{Y}_k = [\boldsymbol{y}_k(1) \cdots \boldsymbol{y}_k(\tau)]$ is received signal matrix which contains a sequence of τ independent receive signals at the k-th BTS and $\boldsymbol{y}_k(i) \in \mathbb{C}^{N_T}$ and $\mathbf{N_k} = [\mathbf{n_k}(\mathbf{1}) \cdots \mathbf{n_k}(\tau)]$ is the $N_T \times \tau$ uplink noise matrix at k-th BTS. $\boldsymbol{s}_j$ is the $1 \times \tau$ uplink training sequence. In matrix form, the above equation can be expressed as follows:

$$\boldsymbol{Y}_k = \boldsymbol{H}_k \boldsymbol{D}_{\boldsymbol{g}^*} \boldsymbol{S} + \mathbf{N_k} \tag{3.7}$$

where $\boldsymbol{S}$ is a pilot matrix whose rows contain pilot sequences sent by MSs of different cells. $\boldsymbol{D}_{\boldsymbol{g}^*} = \mathsf{diag}[g_i^*]_{i=1\cdots L}$ and $\boldsymbol{H}_k = [\boldsymbol{h}_{1k} \cdots \boldsymbol{h}_{Lk}]$ is a matrix whose columns represent the channels between MSs of different cells and k-th BTS. The k-th BTS updates its beamformer according to following least-squares cost function:

$$\hat{\boldsymbol{v}}_k = \arg\min_{\boldsymbol{v}_k} \|\boldsymbol{s}_k - \boldsymbol{v}_k^H \boldsymbol{Y}_k\|^2$$

$$= (\boldsymbol{Y}_k \boldsymbol{Y}_k^H)^\dagger \boldsymbol{Y}_k \boldsymbol{s}_k^H \tag{3.8}$$

These iterations are performed back and forth once. Once the filters are optimized, data is sent in forward direction. For a given set of optimized beamformers $\{g_k\}_{k=1}^L$ and $\{\boldsymbol{v}_k\}_{k=1}^L$,

the SINR at the k-th MS can be expressed as

$$\gamma_k = \frac{|g_k^* \langle \boldsymbol{h}_{kk}, \boldsymbol{v}_k \rangle|^2}{\sum_{j \neq k} |g_k^* \langle \boldsymbol{h}_{kj}, \boldsymbol{v}_j \rangle|^2 + \sigma_o^2 |g_k|^2} \tag{3.9}$$

Consequently, the sum rate $\sum_{k=1}^{K} \log(1 + \gamma_k)$ is calculated. We attempt to choose the optimal precoders and receive filters in such a way so as to maximize the average sum rate. It is well known that MMSE estimator maximizes the SINR but it needs perfect CSI. We rely on adaptive least squares filtering which does not need CSI. However, its performance approaches that of MMSE estimator as the length of training sequence increases.

3.3 Pilot Contamination Analysis

In Eq. (3.8), the BTS precoder filter comprises of two terms. One is sample covariance matrix of the received sequence at BTS and the second term is the cross-correlation between received sequence and the transmitted training sequence. The second term is acting as a steering vector [48]. This steering vector steers the beam of antenna array at BTS depending upon the structure of transmitted training sequences from MSs in L cells. We analyse the impact of structure of training sequences on the steering vector and the resulting "pilot contamination" in the following subsections. As our aim is to analyse the effect of "pilot contamination", we assume that there is no uncorrelated Gaussian noise in the precoder estimate.

3.3.1 Orthogonal Pilots

If pilots are orthogonal in time domain, then $\boldsymbol{S}\boldsymbol{S}^H = \tau \mathbf{I}$ where $\boldsymbol{s}_k \boldsymbol{s}_k^H = \tau$ is pilot sequence power, and $\mathbf{I}$ is the $L \times L$ identity matrix. Here all the pilot sequences are equal in power but mutually orthogonal. Assuming the noise to be negligible for analysis, we analyse the

pilot contamination in k-th precoding filter as follows:

$$\begin{aligned} \boldsymbol{Y}_k\boldsymbol{Y}_k^H &= (\boldsymbol{H}_k\boldsymbol{D}_{\boldsymbol{g}^*}\boldsymbol{S})(\boldsymbol{H}_k\boldsymbol{D}_{\boldsymbol{g}^*}\boldsymbol{S})^H && (3.10)\\ &= \boldsymbol{H}_k\boldsymbol{D}_{\boldsymbol{g}^*}\boldsymbol{S}\boldsymbol{S}^H\boldsymbol{D}_{\boldsymbol{g}^*}^H\boldsymbol{H}_k^H && (3.11)\\ &= \tau\boldsymbol{H}_k\boldsymbol{D}_{\boldsymbol{g}^*}\boldsymbol{D}_{\boldsymbol{g}^*}^H\boldsymbol{H}_k^H && (3.12)\\ &= \tau\sum_{i=1}^{L}|g_i|^2\boldsymbol{h}_{ik}\boldsymbol{h}_{ik}^H && (3.13) \end{aligned}$$

The above term is a normalization factor. But the crucial role is played by the projection of received sequence onto the transmitted pilot sequence in the BTS precoder estimator.

$$\begin{aligned} \boldsymbol{Y}_k\boldsymbol{s}_k^H &= \boldsymbol{H}_k\boldsymbol{D}_{\boldsymbol{g}^*}\boldsymbol{S}\boldsymbol{s}_k^H && (3.14)\\ &= \begin{pmatrix} | & & | \\ g_1^*\boldsymbol{h}_{1k} & \cdots & g_L^*\boldsymbol{h}_{Lk} \\ | & & | \end{pmatrix} \begin{pmatrix} \text{——}\boldsymbol{s}_1\text{——} \\ \cdot \\ \cdot \\ \cdot \\ \text{——}\boldsymbol{s}_L\text{——} \end{pmatrix} \boldsymbol{s}_k^H \\ &= \tau g_k^*\boldsymbol{h}_{kk} && (3.15) \end{aligned}$$

The above projection is free of pilot contamination, due to the orthogonality of the training sequence. The BTS precoding filter in terms of channel vectors and MSs's filters can be expressed as:

$$\begin{aligned} \hat{v}_k &= \left(\tau\sum_{i=1}^{L}|g_i|^2\boldsymbol{h}_{ik}\boldsymbol{h}_{ik}^H\right)^{\dagger}(\tau g_k^*\boldsymbol{h}_{kk}) && (3.16)\\ &= \left(\sum_{i=1}^{L}|g_i|^2\boldsymbol{h}_{ik}\boldsymbol{h}_{ik}^H\right)^{\dagger}(g_k^*\boldsymbol{h}_{kk}) && (3.17) \end{aligned}$$

Thus, the precoder filter estimation is independent of pilot sequence power in the aforementioned scenario and zero noise conditions.

3.3.2 Identical Pilots

If all the MSs are transmitting same training sequences, then $\boldsymbol{S}\boldsymbol{S}^H = \tau \mathbf{J}_L$ where $\mathbf{J}_L$ is an $L \times L$ matrix of all ones. Now the normalization term can be simplified as follows:

$$\begin{aligned} \boldsymbol{Y}_k \boldsymbol{Y}_k^H &= \left(\boldsymbol{H}_k \boldsymbol{D}_{\boldsymbol{g}^*} \boldsymbol{S}\right) \left(\boldsymbol{H}_k \boldsymbol{D}_{\boldsymbol{g}^*} \boldsymbol{S}\right)^H && (3.18) \\ &= \tau \boldsymbol{H}_k \boldsymbol{D}_{\boldsymbol{g}^*} \mathbf{J}_L \boldsymbol{D}_{\boldsymbol{g}^*}^H \boldsymbol{H}_k^H && (3.19) \\ &= \tau \sum_{i=1}^{L} \sum_{j=1}^{L} g_i^* g_j \boldsymbol{h}_{ik} \boldsymbol{h}_{jk}^H && (3.20) \end{aligned}$$

Similarly, the projection of received sequence onto pilot sequence can be expressed as follows:

$$\begin{aligned} \boldsymbol{Y}_k \boldsymbol{s}^H &= \boldsymbol{H}_k \boldsymbol{D}_{\boldsymbol{g}^*} \boldsymbol{S} \boldsymbol{s}^H && (3.21) \\ &= \tau \boldsymbol{H}_k \boldsymbol{D}_{\boldsymbol{g}^*} [1 \cdots 1]^T && (3.22) \\ &= \tau \sum_{l=1}^{L} g_l^* \boldsymbol{h}_{lk} && (3.23) \end{aligned}$$

This projection contains all the interfering channels and is highly contaminated. This implies that the usage of identical pilots in different cells leads to pilot contamination. Regardless of the fact that we are not estimating channels, pilot contamination is occuring in BTS's precoding filter's estimate. In nutshell, the BTS's precoding filter's estimate can be expressed as

$$\begin{aligned} \hat{\boldsymbol{v}}_k &= \left(\tau \sum_{i=1}^{L} \sum_{j=1}^{L} g_i^* g_j \boldsymbol{h}_{ik} \boldsymbol{h}_{jk}^H\right)^{\dagger} \left(\tau \sum_{l=1}^{L} g_l^* \boldsymbol{h}_{lk}\right) && (3.24) \\ &= \left(\sum_{i=1}^{L} \sum_{j=1}^{L} g_i^* g_j \boldsymbol{h}_{ik} \boldsymbol{h}_{jk}^H\right)^{\dagger} \left(\sum_{l=1}^{L} g_l^* \boldsymbol{h}_{lk}\right) && (3.25) \end{aligned}$$

The above expression holds as the effect of noise is dominated by the beamforming gains.

3.3.3 Random Pilots

We want to quantify the impact of random pilot sequences on our adaptive beamformer at BTS. Specifically, we choose random training sequences of zero mean and variance c for the performance evaluation in terms of average sum rate. We use the Lemma 1 from Chapter 2 for analysis of asymptotic behaviour of different random pilots.

The application of Lemma 1 implies that with random pilot sequences, always of energy c, then as τ tends to infinity, we have $\boldsymbol{S}\boldsymbol{S}^H$ tending to $c\mathbf{I}$, where $\mathbf{I}$ is the $L \times L$ identity matrix. Now the normalization term can be expressed as follows:

$$\begin{aligned}
\lim_{\tau\to\infty} \boldsymbol{Y}_k\boldsymbol{Y}_k^H &= (\boldsymbol{H}_k\boldsymbol{D}_{\boldsymbol{g}^*}\boldsymbol{S})(\boldsymbol{H}_k\boldsymbol{D}_{\boldsymbol{g}^*}\boldsymbol{S})^H && (3.26)\\
&= \boldsymbol{H}_k\boldsymbol{D}_{\boldsymbol{g}^*}\boldsymbol{S}\boldsymbol{S}^H\boldsymbol{D}_{\boldsymbol{g}^*}^H\boldsymbol{H}_k^H && (3.27)\\
&\overset{a.s.}{\to} c\boldsymbol{H}_k\boldsymbol{D}_{\boldsymbol{g}^*}\boldsymbol{D}_{\boldsymbol{g}^*}^H\boldsymbol{H}_k^H && (3.28)\\
&= c\sum_{l=1}^{L}|g_l|^2\boldsymbol{h}_{lk}\boldsymbol{h}_{lk}^H && (3.29)
\end{aligned}$$

where c is the energy of the random training sequence. On the other hand, the steering vector can be expressed as follows:

$$\begin{aligned}
\lim_{\tau\to\infty} \boldsymbol{Y}_k\boldsymbol{s}_k^H &= \boldsymbol{H}_k\boldsymbol{D}_{\boldsymbol{g}^*}\boldsymbol{S}\boldsymbol{s}_k^H && (3.30)\\
&= \begin{pmatrix} | & & | \\ g_1^*\boldsymbol{h}_{1k} & \cdots & g_L^*\boldsymbol{h}_{Lk} \\ | & & | \end{pmatrix} \begin{pmatrix} \text{——}\boldsymbol{s}_1\text{——} \\ \cdot \\ \cdot \\ \cdot \\ \text{——}\boldsymbol{s}_L\text{——} \end{pmatrix} \boldsymbol{s}_k^H && (3.31)\\
\lim_{\tau\to\infty} \boldsymbol{Y}_k\boldsymbol{s}_k^H &\overset{a.s.}{\to} cg_k^*\boldsymbol{h}_{kk} && (3.32)
\end{aligned}$$

The k-th BTS filter in terms of channel vectors and MSs's filters can be expressed as:

$$\lim_{\tau\to\infty} \hat{v}_k \overset{a.s.}{\to} \left(c\sum_{i=1}^{L} |g_i|^2 \boldsymbol{h}_{ik}\boldsymbol{h}_{ik}^H \right)^{\dagger} (cg_k^*\boldsymbol{h}_{kk}) \tag{3.33}$$

$$= \left(\sum_{i=1}^{L} |g_i|^2 \boldsymbol{h}_{ik}\boldsymbol{h}_{ik}^H \right)^{\dagger} (g_k^*\boldsymbol{h}_{kk}) \tag{3.34}$$

Remark. *Thus, as the length of random training sequence is increased, the performance of adaptive least squares filtering using random training sequences approaches the performance of adaptive least squares using orthogonal training sequences asymptotically with the number of interferers remaining fixed. However, in practice the training sequence length is finite and limited by coherence time of the channel.*

3.4 Simulation

In this section, numerical results are presented to corroborate the mathematical analysis in the previous section. All the measurement noises are assumed to be AWGN with variance σ_o^2. The data symbols are assumed to be unit variance and SNR is taken to be equal to $\frac{1}{\sigma_o^2}$. The channel vector covariance matrix is assumed to be equal to identity matrix, i.e., $\mathbf{R} = \mathbf{I}$. All the results are averaged over 1000 Monte Carlo runs. Here we consider three cells each having one MS and one BTS with an antenna array of N_T antenna elements.

Fig. 3.2 shows the average sum rate of this cellular network versus training sequence length. It is evident from the graph that as the training sequence length increases, the average sum rate increases for all the structures of training sequences. However, the performance of adaptive least-squares filtering at BTS with random training sequences is better than the performance of the same filtering scheme with identical training sequences as long as the number of interferers is fixed. This is because the cross-correlation term in the filter at BTS is acting as beamformer and it steers the beam of antenna array in the direction of the intended training sequence. For orthogonal training sequences, it is

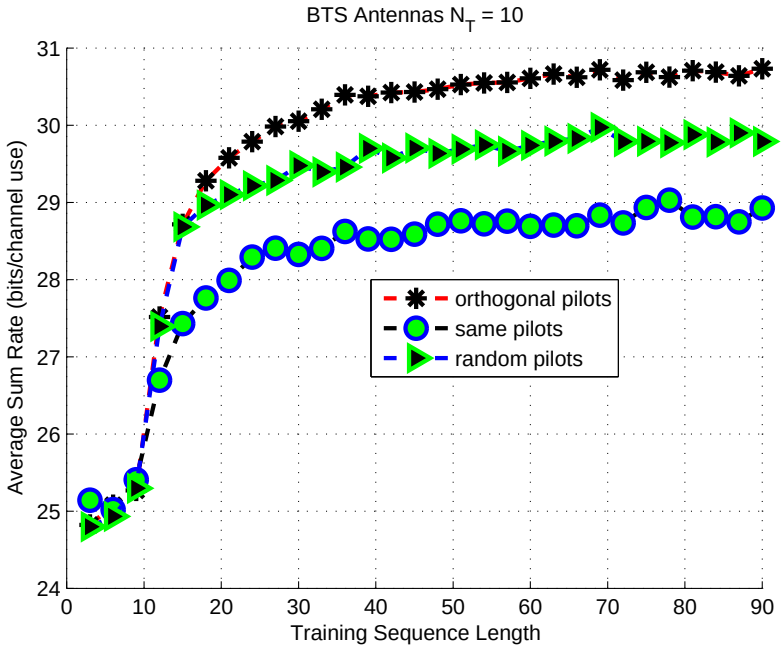

Figure 3.2: Average Sum Rate versus Training Sequence Length, SNR = 30 dB

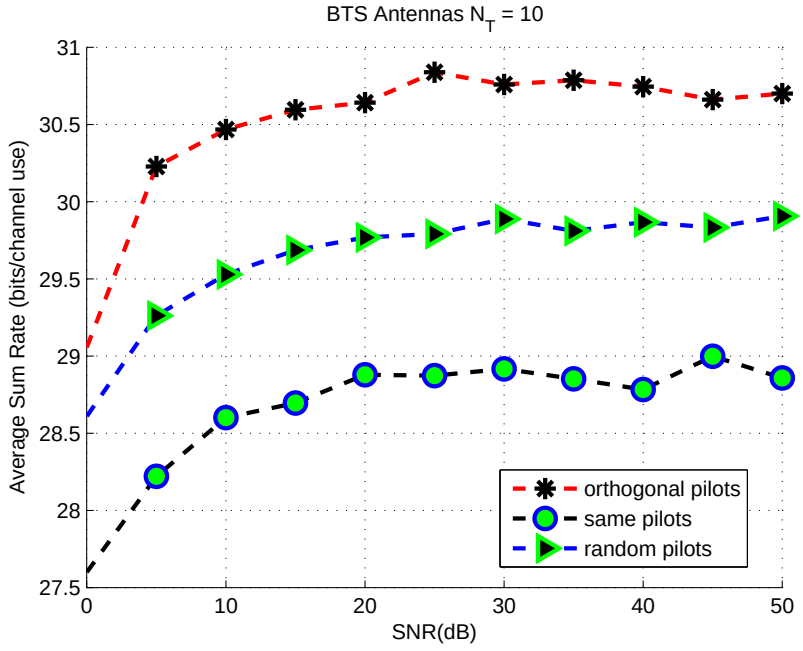

Figure 3.3: Average Sum Rate versus SNR

.

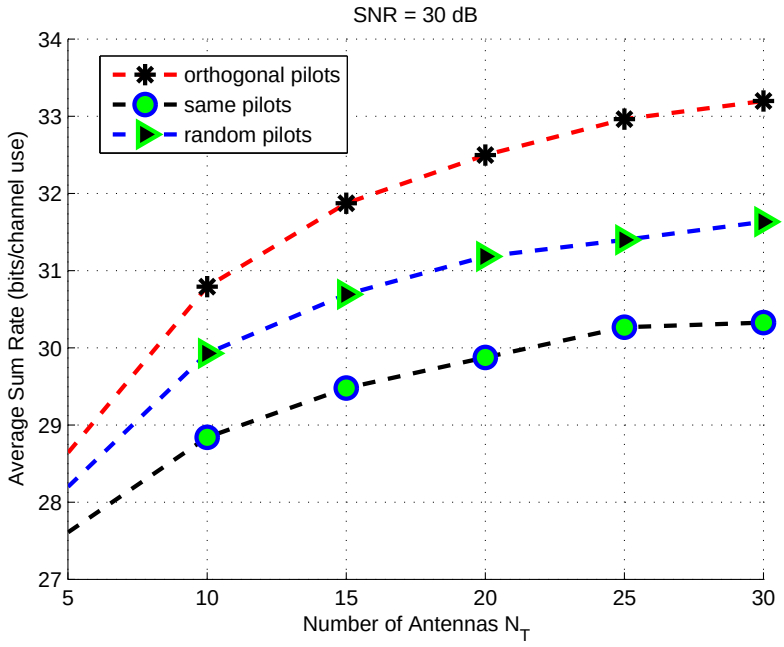

Figure 3.4: Average Sum Rate versus Number of Antennas N_T

steering a null towards orthogonal sequences and in case of identical pilot sequences it is steering the sidelobes towards users which are in other cells. It is apparent that the sidelobes towards other users have low energy in case of random training sequences and hence "pilot contamination" effect is considerably less than in the case in which identical training sequences are transmitted by users in different cells. In Fig. 3.2, the SNR is fixed at 30 dB. This value of high SNR is chosen to satisfy the requirements of low bit error rate (BER) for applications requiring high reliability.

Now, we fix the training sequence length and see the variations in average sum rate with respect to changes in SNR under different training sequence structures. Fig. 3.3 shows the plot of average sum rate versus SNR. SNR is varied from 0 to 50 dB and training sequence length is kept at 90. The gap between the sum rate of random training sequences and that of identical training sequences is 1 bits/channel use at 50 dB. Thus, the random training sequences are offering better performance than identical training

sequences in terms of average sum rate as in this case, the steering vector in the BTS precoding filter has reasonably less contamination.

Now, we fix the SNR at 30 dB and vary the number of antenna elements at the BTS. In Fig. 3.4, the average sum rate is plotted versus number of antenna elements N_T. It is obvious from the figure that as we increase the number of antennas, the average sum rate increases. This is due to additional spatial links created by the use of more antenna elements at the BTS array. Here again the performance of random training sequences is in between identical training sequences and orthogonal training sequences. The random training sequences offer atleast 1 bits/channel use better performance than identical training sequences when the number of antennas at base station is greater than ten.

3.5 Conclusion

We have considered an adaptive least squares filtering in large scale antenna systems under bidirectional training scheme which operates without the knowledge of CSI. The presented algorithm jointly optimized the transmit precoders and receive filters without any coordination among base stations. The impact of properties of training sequences on sum rate performance of cellular system has been quantified. It has been shown through mathematical analysis and numerical results that the random training sequences offer better performance than identical training sequences in terms of sum rate when the number of interferers is fixed. Moreover, it has been quantified that random training sequences start becoming orthogonal as the length of training sequences grow which is approachable in low mobility scenarios.

In case of multiple users per cell, random training sequences will interfere with each other for short coherence intervals. However, if we reuse the same set of orthogonal train-

ing sequences across cells, the amount of correlation with an identical training sequence will be higher than the sum of individual tiny correlations of a set of random training sequences from an adjacent cell due to tiny sidelobes. This chapter offers a preliminary work on pilot contamination analysis under adaptive beamforming in massive MIMO. The future work is directed towards quantifying the impact of multiple users using random training sequences across different cells for pilot contamination analysis.

Chapter 4

Compressive-Sensing-Aided Detection for Generalized-Spatial-Modulation Massive-MIMO Systems

Spatial Modulation (SM), a novel modulation format, has the potential to relax the constraint of one RF chain per antenna element at the BTS in massive MIMO without compromising on spectral efficiency. GSM is an extension of SM which uses more than one but less than N_T RF chains and provides higher spectral efficiency. In this chapter, we focus on receiver design for data detection in massive MIMO exploiting the sparse structure of the transmit vector of the GSM systems.

This chapter is organized as follows. Section 4.1 highlights the motivation and related work. Section 4.2 provides CS aided data detection for GSM systems in MIMO ISI wireless channels in which we provide the system modeling and problem formulation, CS framework, and an algorithm to perform CS aided sparse data detection under perfect and

imperfect CSI. Section 4.3 discusses sparse recovery for Multi-user GSM system in which we start with multi-user GSM modeling, then after discussing the precoding scheme, we provide a CS framework for multi-user GSM data detection.

4.1 Motivation and Related Work

SM is a modulation technique which only uses one RF chain for all the antenna elements, thereby entirely avoiding inter-channel interference (ICI) and requiring no synchronization between the transmitting antennas while maintaining high spectral efficiency [49]. The principle of spatial modulation is quite simple: a block of information bits is mapped onto a constellation point in the signal and spatial domain which includes the selection of a particular antenna. Thus, part of the information is encoded into the selection of the transmit antenna. The receiver estimates the transmitted signal and the transmit antenna number and uses both of these to decode the block of information bits. This detection is achieved via iterative maximum-ratio combining (i-MRC). Spatial modulation is currently attracting attention due to its reduced receiver complexity as compared to conventional MIMO . Additionally, its BER and achieved spectral efficiency are comparable to V-BLAST but using less complexity.

GSM is an extension of SM in which the same symbol is transmitted from more than one transmit antennas [28]. In GSM, information is conveyed through the selection of multiple antennas unlike SM, where one antenna is activated. Nevertheless, the number of activated antennas, which is equal to the number of available RF chains, is much less than the total number of antenna elements. This scheme not only avoids ICI but also takes advantage of transmit diversity gains. As the number of combinations of transmit antennas is much higher than the actual number of transmit antennas, GSM systems have higher spectral efficiency in comparison to SM systems.

In massive MIMO, the BTS possesses a large number of antenna elements and limited RF chains which make the GSM an attractive modulation format to tackle the problem of limited RF chains. In GSM, the receiver has to detect not only the information symbol transmitted but also the specific subset of antennas. The maximum-likelihood (ML) detector has been investigated for GSM [50]. CS techniques which exploit the sparse structure of transmit data for GSM has been proposed in [51].

CS has been studied extensively in statistical signal processing, optimization and statistics [52]. CS extracts a signal, which is sparse in some underlying basis, from a small set of measurements with a sampling rate much lower than the Nyquist rate. If the measurement/sensing matrix satisfies the RIP, then the sparse support of such signals can be estimated [37]. Owing to the fact that most naturally occurring signals can be approximated to be sparse in some basis, CS can be employed for their reconstruction with high probability given sufficient measurements of the signal [53]. The applications of CS recovery can be found in the one-pixel camera, channel estimation in MIMO broadcast channel [54], multi-antenna downlink broadcasting [55], cellular downlink resource sharing [56], and mmWave systems etc.

This design criterion of having fewer RF chains than antenna elements induces a high degree of sparsity in the transmit symbol vector. The authors in [57] exploited this fact and presented a normalized CS based detection algorithm for space-shift keying (SSK) systems whose performance is comparable to maximum-likelihood (ML) algorithms. Particularly, their proposed detector is premised on formulating the SSK-type detection criterion as a convex optimization program. This approach provides significant speedup by leveraging the intrinsic sparsity of SSK-type schemes which is beneficial to cope with prohibitively high detection overhead in a massive MIMO system. However, as in SSK systems, incoming bits only modulate the antenna indices, so their proposed solution is limited to antenna index detection only. Recently a CS algorithm basis-pursuit denoising

(BPDN) has been applied by [51] to perform joint detection of indices of activated RF chains and data symbols emitted over the transmission channel in GSM systems. They show via numerical results that their proposed algorithm can not only demonstrate better performance than those of ZF and MMSE detectors but can also work well in the underdetermined systems. However, the authors use a simplified frequency-flat channel model which does not suffice for high data rate applications. Moreover, their proposed algorithm is limited to the scenario in which receiver has perfect knowledge of CSI which is not a realistic constraint particularly in the context of massive MIMO systems.

The performance of SM in the context of a multi-user scenario has been studied recently in [58]. In [58], a precoding scheme for downlink multi-user SM system is put forward which reduces the inter-user interference. The authors demonstrate via numerical results that their proposed scheme offers reduced BER in comparison to conventional ZF precoding. For fixed N_T and single-antenna MSs, the proposed technique achieves higher sum rate than ZF precoding. Since the precoder matrix is a function of channel indices, therefore, in each signalling interval, the precoder matrix is calculated online and consequently the computational complexity is high. In [59], a precoding scheme for downlink multi-user SM is proposed which minimizes the multi-user interference. Specifically, their proposed precoding scheme allows the users to use a single-user ML detector whose computational complexity grows exponentially with the increase of number of transmit antennas and modulation order. Since, the precoder matrix is a function of the data symbols so in each signalling interval new precoder matrix has to be calculated which is computationally expensive.

Our contributions are threefold. Our proposed algorithm is applicable even in the case of channel estimation errors and demonstrates very good detection accuracy under imperfect channel knowledge in contrast to the prior applications of CS algorithms to sparse-modulation systems. To the best of our knowledge, this is the first time that CS

techniques have been applied in conjunction with a TLS filtering approach to handle imperfect CSI. Further, it is the first extension of GSM to frequency-selective channels. Finally, we propose a novel sparse recovery scheme for multi-user precoded GSM system.

4.2 Compressive Sensing aided Data Detection for GSM Systems in MIMO ISI Wireless Channels

4.2.1 System Modeling and Problem Formulation

Suppose we have a point-to-point MIMO *inter-symbol interference* (ISI) channel with multiple antennas at transmitter and receiver in a GSM system. Here BTS is operating as transmitter and MS is operating as receiver due to downlink mode. If we stack all the signals received at N_R receive antennas in the form $\boldsymbol{z}[n] = [z_1[n]\ z_2[n]\ \cdots\ z_{N_R}[n]]^T$, then receive symbol vector at time index n may be expressed as follows

$$\boldsymbol{z}[n] = \sum_{k=0}^{L-1} \boldsymbol{H}[k]\boldsymbol{P}\boldsymbol{u}[n-k] + \mathbf{n}[n] \tag{4.1}$$

$$or\ \boldsymbol{z}[n] = \boldsymbol{H}[n] * \boldsymbol{P}\boldsymbol{u}[n] = \boldsymbol{H}[n] * \boldsymbol{x}[n] + \mathbf{n}[n] \tag{4.2}$$

where $\boldsymbol{H}[k] = \{h_{ij}[k]\}_{i=1\cdots N_R}^{j=1\cdots N_T}$ is the $N_R \times N_T$ time-invariant MIMO channel matrix containing all the $N_R N_T$ links' *channel impulse response* (CIR) coefficients at delay index k. Here $\boldsymbol{H}[k] = \left[\boldsymbol{h}_1^T[k]\ \boldsymbol{h}_2^T[k]\ \cdots\ \boldsymbol{h}_{N_R}^T[k]\right]^T$, $\boldsymbol{h}_i[k] = [h_{i1}[k]\ h_{i2}[k]\ \cdots\ h_{iN_T}[k]]$ is the CIR vector containing all the links between the ith receive antennas and N_T transmit antennas at delay index k, L is the number of multipath components and furthermore, we assume the ij-th link is Rayleigh fading, i.e., $h_{ij} \sim \mathcal{CN}(0, \sigma_h^2)$.

The matrix $\boldsymbol{P}$ is an $N_T \times N_a$ antenna activation pattern matrix. Each column of this matrix is an antenna activation pattern which activates the antennas that are being selected by the incoming bit sequence. N_a is the number of possible activation patterns.

We assume that there are N_c RF chains, and each column of $\boldsymbol{P}$ is a vector of 0s and 1s, with the 1s indicating the antenna elements selected. There are a maximum of $\binom{N_T}{N_c}$ such vectors. We will choose $N_a = 2^{\lfloor \log_2 \binom{N_T}{N_c} \rfloor}$ so that a sequence of $p = \log_2 N_a$ bits will select the corresponding activation pattern.

The vector $\boldsymbol{u}[n-k]$ is an antenna activation vector of dimension N_a with only one non-zero component. The component that is non-zero is given a complex number from the S-QAM constellation. Each use of the channel, $p = \log_2 N_a$ bits selects the non-zero component index, and $q = \log_2 S$ bits selects the data symbol in the S-QAM constellation. The receiver must estimate both the position (activation pattern) and the data symbol itself.

If we transmit N information/pilot symbols over an L-tap ISI channel, then we receive $N+L-1$ symbols. On stacking the transmit symbols over a block of N transmit symbols, we get the following matrix-vector relation.

$$\begin{pmatrix} \boldsymbol{z}[0] \\ \boldsymbol{z}[1] \\ \vdots \\ \boldsymbol{z}[L-1] \\ \vdots \\ \boldsymbol{z}[N_o] \end{pmatrix} = \begin{pmatrix} \boldsymbol{H}[0] & \boldsymbol{O}_{N_R \times N_T} & \cdots & \boldsymbol{O}_{N_R \times N_T} \\ \boldsymbol{H}[1] & \boldsymbol{H}[0] & \cdots & \boldsymbol{O}_{N_R \times N_T} \\ \vdots & \vdots & & \vdots \\ \boldsymbol{H}[L-1] & \boldsymbol{H}[L-2] & \cdots & \boldsymbol{O}_{N_R \times N_T} \\ \boldsymbol{O}_{N_R \times N_T} & \boldsymbol{H}[L-1] & \cdots & \boldsymbol{O}_{N_R \times N_T} \\ \vdots & \vdots & & \vdots \\ \boldsymbol{O}_{N_R \times N_T} & \boldsymbol{O}_{N_R \times N_T} & \cdots & \boldsymbol{H}[0] \\ \vdots & \vdots & & \vdots \\ \boldsymbol{O}_{N_R \times N_T} & \boldsymbol{O}_{N_R \times N_T} & \cdots & \boldsymbol{H}[L-1] \end{pmatrix}$$
$$\times (\mathbf{I}_N \otimes \boldsymbol{P}) \begin{pmatrix} \boldsymbol{u}[0] \\ \boldsymbol{u}[1] \\ \vdots \\ \boldsymbol{u}[N-1] \end{pmatrix} + \begin{pmatrix} \mathbf{n}[0] \\ \mathbf{n}[1] \\ \vdots \\ \mathbf{n}[N_o] \end{pmatrix} \tag{4.3}$$

where $N_o = N + L - 2$, assuming a zero-padding between blocks of N symbols, to avoid inter-block-interference (IBI), much as a cyclic prefix is used in OFDM. The IBI is the residual interference created due to the memory in the channel. The above equation can be written in symbolic form as follows:

$$\boldsymbol{z} = \mathbf{H}\mathbf{P}\boldsymbol{u} + \mathbf{n} \tag{4.4}$$

Here $\mathbf{H}$ is the MIMO ISI channel convolution matrix in Eq. (4.3) and $\mathbf{P} = (\mathbf{I}_N \otimes \boldsymbol{P})$ is a block diagonal matrix with diagonal entries equal to $\boldsymbol{P}$, and

$$\mathbf{\Psi} = \begin{pmatrix} \boldsymbol{H}[0]\boldsymbol{P} & \boldsymbol{O}_{N_R\times N_a} & \cdots & \boldsymbol{O}_{N_R\times N_a} \\ \boldsymbol{H}[1]\boldsymbol{P} & \boldsymbol{H}[0]\boldsymbol{P} & \cdots & \boldsymbol{O}_{N_R\times N_a} \\ \vdots & \vdots & & \vdots \\ \boldsymbol{H}[L-1]\boldsymbol{P} & \boldsymbol{H}[L-2]\boldsymbol{P} & \cdots & \boldsymbol{O}_{N_R\times N_a} \\ \boldsymbol{O}_{N_R\times N_a} & \boldsymbol{H}[L-1]\boldsymbol{P} & \cdots & \boldsymbol{O}_{N_R\times N_a} \\ \vdots & \vdots & & \vdots \\ \boldsymbol{O}_{N_R\times N_a} & \boldsymbol{O}_{N_R\times N_a} & \cdots & \boldsymbol{H}[0]\boldsymbol{P} \\ \vdots & \vdots & & \vdots \\ \boldsymbol{O}_{N_R\times N_a} & \boldsymbol{O}_{N_R\times N_a} & \cdots & \boldsymbol{H}[L-1]\boldsymbol{P} \end{pmatrix} \tag{4.5}$$

Here $\mathbf{\Psi} = \mathbf{H}\mathbf{P}$ is the block Toeplitz matrix containing L weighted multipath component matrix taps on its diagonals. The dimensions of the effective channel matrix, received signal sequence, and transmitted sequence play a pivotal rule in the pursuit of CS-aided data detection and are listed in the table below.

Matrix	Name	Size
$\boldsymbol{z}$	Received Sequence	$N_R(N+L-1)\times 1$
$\mathbf{\Psi}$	Effective Channel Matrix	$N_R(N+L-1)\times NN_a$
$\boldsymbol{u}$	Antenna Activation Sequence	$NN_a \times 1$
$\mathbf{n}$	Noise Sequence	$N_R(N+L-1)\times 1$

4.2.2 Compressive Sensing Framework

In compact form, the Eq. (4.4) can be expressed as

$$\boldsymbol{z} = \boldsymbol{\Psi}\boldsymbol{u} + \mathbf{n} \tag{4.6}$$

Here $\boldsymbol{z} = \begin{pmatrix}\boldsymbol{z}[0]^T & \cdots & \boldsymbol{z}[L-1]^T & \cdots & \boldsymbol{z}[N+L-2]^T\end{pmatrix}^T$ represents the stacked measurement vector and $\boldsymbol{u} = \begin{pmatrix}\boldsymbol{u}[0]^T\boldsymbol{u}[1]^T & \cdots & \boldsymbol{u}[NN_a-1]^T\end{pmatrix}^T$. For notational convenience, we define $m = N_R(N+L-1)$ and $n = NN_a$. As N_a is quite large for tens of antennas say for $N_T = 30, 50$, the $\boldsymbol{u}$ vector is sparse: its sparsity is N because in each $\boldsymbol{u}[n]$, only one element is non-zero, so $\boldsymbol{u}$ is N-sparse. Here $\mathbf{n}$ is a complex additive white Gaussian noise (AWGN), $\mathcal{CN}(0, \sigma_n^2\mathbf{I}_m)$. As $m \ll n$, this is an ill-posed problem as there will be infinite number of solutions satisfying (4.6) (ignoring the noise, $\mathbf{n}$).

The receiver has prior knowledge of sparsity of $\boldsymbol{u}$, which can be used in estimation at the receiver. If there were no noise in the system, the signal recovery problem would be to reconstruct the signal using $\boldsymbol{l}_0$-norm minimization. This requires exhaustive search, which is intractable when the dimension of the signal to be estimated is large, as it is here. It has been established in [35] that for random matrices whose entries are independent and identically distributed (i.i.d.) Gaussian, the RIP is satisfied with high probability when $m \geqslant N\log(n/N)$, and this implies that one can replace $\boldsymbol{l}_0$ -norm minimization with $\boldsymbol{l}_1$-norm minimization, and obtain the same solution. This is the approach of Compressed/Compressive Sensing . We will assume that the RIP holds for our block Toeplitz matrix $\boldsymbol{\Psi}$. Since most of the CS algorithms are designed to solve real-valued convex minimization programs, therefore, we cast our input-output model in Eq. (4.6) into real-valued

input-output system as follows.

$$\begin{pmatrix} \Re\{\boldsymbol{z}\} \\ \Im\{\boldsymbol{z}\} \end{pmatrix} = \begin{pmatrix} \Re\{\boldsymbol{\Psi}\} & -\Im\{\boldsymbol{\Psi}\} \\ \Im\{\boldsymbol{\Psi}\} & \Re\{\boldsymbol{\Psi}\} \end{pmatrix} \begin{pmatrix} \Re\{\boldsymbol{u}\} \\ \Im\{\boldsymbol{u}\} \end{pmatrix} + \begin{pmatrix} \Re\{\mathbf{n}\} \\ \Im\{\mathbf{n}\} \end{pmatrix} \tag{4.7}$$

$$or \quad \widetilde{\boldsymbol{z}} = \widetilde{\boldsymbol{\Psi}}\widetilde{\boldsymbol{u}} + \widetilde{\mathbf{n}} \tag{4.8}$$

where $\Re\{\cdot\}$, $\Im\{\cdot\}$, and $\widetilde{\{\cdot\}}$ denote the real part, imaginary part, and the real-valued equivalent of a complex field respectively. The standard CS approach when there is noise is to solve constrained problem as follows:

$$\widehat{\widetilde{\boldsymbol{u}}} = \arg\min_{\widetilde{\boldsymbol{u}}} \|\widetilde{\boldsymbol{u}}\|_{l_1} \quad \text{subject to} \quad \|\widetilde{\boldsymbol{z}} - \widetilde{\boldsymbol{\Psi}}\widetilde{\boldsymbol{u}}\|_{l_2} \leq \epsilon \tag{4.9}$$

where $\epsilon = \sqrt{\sigma_{\mathbf{n}}^2(m + \sqrt{2m})}$.

4.2.3 Perfect Channel Knowledge

When we have perfect channel knowledge at receiver, the most widely deployed receivers are ZF and MMSE receivers. These linear receivers work much better when the system is overdetermined, i.e., the number of measurements is greater than the size of the data vector (and this is a required condition for zero-forcing). However, in our proposed system, the number of measurements $N_R(N + L - 1)$ is much less than the number of unknowns, regardless of the number of antennas. This observation motivates us to use CS techniques initially to estimate the support of the data vector using (4.9) and reduce the dimensionality of the data vector to generate a vector $\widehat{\boldsymbol{u}}_{\widehat{\mathcal{S}}}$. Now the size of data vector which is based on estimated support will only be N. If the support set $\mathcal{S}$ of $\boldsymbol{u}$ is known, (4.6) can be equivalently written as

$$\boldsymbol{z} = \boldsymbol{\Psi}_{\mathcal{S}}\boldsymbol{u}_{\mathcal{S}} + \mathbf{n} \tag{4.10}$$

This system is now overdetermined, since $\boldsymbol{\Psi}_{\mathcal{S}}$ is of size $N_R(N + L - 1) \times NN_a$, so the aforementioned linear receivers can now be applied.

4.2.4 Imperfect Channel Knowledge

In practice, the channel measurements at the receiver are subject to channel and measurement noises. Additionally, if there is some sort of feedback, then the feedback links are subject to quantization noise. In general, channel estimates are modelled as having an additional estimation noise term.

$$\widehat{\mathbf{\Psi}} = \mathbf{\Psi} + \mathbf{\Psi}_{\boldsymbol{e}} \tag{4.11}$$

where $\mathbf{\Psi}_{\boldsymbol{e}} \sim \mathcal{CN}(\mathbf{0}, \sigma_{\boldsymbol{e}}^2 \mathbf{I})$ is Gaussian estimation noise.

Algorithm 1 Compressive Sensing aided Sparse-Data Detection

1: **Input:** $\left\{\boldsymbol{z}, \widehat{\boldsymbol{\Psi}}, N_T, N_c, \epsilon\right\}$

2: **Output:** $\left\{\widehat{\mathcal{S}},\ \widehat{\boldsymbol{u}},\ \widehat{\boldsymbol{u}}_{tls},\ \widehat{\boldsymbol{u}}_{zf}\right\}$

3: Obtain crude estimate of transmit sequence $\widehat{\boldsymbol{u}}$ by running the Basis Pursuit Denoising, as in Eq. (4.9).

4: **Initialize empty set :** $\widehat{\mathcal{S}} = \emptyset$.

5: **Compute:** $\left\{\widehat{\mathcal{S}}, \widehat{\boldsymbol{u}}_{cs}\right\}$

6: **for** $i = 1 \rightarrow N$ **do**

7: $\quad j \leftarrow \arg\max_{j} \left\{\left|\widehat{\boldsymbol{u}}(j)\right| : (i-1)N_a + 1 \leq j \leq iN_a\right\}$

8: $\quad \widehat{\mathcal{S}} \leftarrow \widehat{\mathcal{S}} \cup \{j + (i-1)N_a\}$

9: **end for**

10: $\widehat{\boldsymbol{u}}_{cs}$ is the estimated signal from Eq. (4.9), all of whose elements are zero except on the estimated support $\widehat{\mathcal{S}}$

11: **Compute shrunk sensing matrix:** $\widehat{\boldsymbol{\Psi}}_{\widehat{\mathcal{S}}}$

12: $\quad \boldsymbol{E}_{\widehat{\mathcal{S}}} \leftarrow \{\delta_j : j \in \widehat{\mathcal{S}}\}$

13: $\quad \widehat{\boldsymbol{\Psi}}_{\widehat{\mathcal{S}}} \leftarrow \widehat{\boldsymbol{\Psi}} \boldsymbol{E}_{\widehat{\mathcal{S}}}$

14: **Compute:** $\{\widehat{\boldsymbol{u}}_{zf}, \widehat{\boldsymbol{u}}_{tls}\}$

15: $\quad \widehat{\boldsymbol{u}}_{\widehat{\mathcal{S}}}^{zf} \leftarrow \langle \widehat{\boldsymbol{\Psi}}_{\widehat{\mathcal{S}}}, \widehat{\boldsymbol{\Psi}}_{\widehat{\mathcal{S}}} \rangle^{-1} \langle \widehat{\boldsymbol{\Psi}}_{\widehat{\mathcal{S}}}, \boldsymbol{z} \rangle$

16: $\quad \widehat{\boldsymbol{u}}_{\widehat{\mathcal{S}}}^{tls} \leftarrow (\langle \widehat{\boldsymbol{\Psi}}_{\widehat{\mathcal{S}}}, \widehat{\boldsymbol{\Psi}}_{\widehat{\mathcal{S}}} \rangle - \sigma_{n+1}^2 \mathbf{I}) \langle \widehat{\boldsymbol{\Psi}}_{\widehat{\mathcal{S}}}, \boldsymbol{z} \rangle$

17: $\quad \widehat{\boldsymbol{u}}_{zf} \leftarrow \boldsymbol{E}_{\widehat{\mathcal{S}}} \widehat{\boldsymbol{u}}_{\widehat{\mathcal{S}}}^{zf}$

18: $\quad \widehat{\boldsymbol{u}}_{tls} \leftarrow \boldsymbol{E}_{\widehat{\mathcal{S}}} \widehat{\boldsymbol{u}}_{\widehat{\mathcal{S}}}^{tls}$

The authors in [41] propose to use TLS filtering which takes into account the noise in the channel matrix. This TLS receiver is essentially a regularized ZF receiver where the regularization takes into account the noise in the channel estimate and the received signal. Thus, its performance is better than the ZF receiver which is oblivious to the

noise in the channel estimates. In fact, the objective function of TLS attempts to correct the perturbations not only in the received signal but also in the noisy estimate of the channel matrix. The optimization problem in TLS approach attempts to minimize the perturbations of both the received signal and the estimated channel matrix. In traditional ZF approach, only the received signal is assumed to be noisy however, the channel matrix may be noisy due to modeling errors etc. The $\boldsymbol{u}_{tls}$ can be defined as follows.

$$\{\hat{\boldsymbol{u}}_{tls}, \widehat{\boldsymbol{\Psi}}_{tls}, \hat{\boldsymbol{z}}_{tls}\} := \underset{\{\boldsymbol{u}_{tls}, \widehat{\boldsymbol{\Psi}}_{tls}, \hat{\boldsymbol{z}}\}}{\arg\min} \left\| \left[\widehat{\boldsymbol{\Psi}} \middle| \boldsymbol{z}\right] - \left[\widehat{\boldsymbol{\Psi}}_{tls} \middle| \hat{\boldsymbol{z}}_{tls}\right] \right\|_F^2$$

$$subject \quad to \quad \hat{\boldsymbol{z}}_{tls} \in \mathcal{C}(\widehat{\boldsymbol{\Psi}}_{tls})$$

where $\mathbb{C}(\widehat{\boldsymbol{\Psi}}_{tls})$ is the column space of $\widehat{\boldsymbol{\Psi}}_{tls}$. Once the minimizing $\left[\widehat{\boldsymbol{\Psi}}_{tls} \middle| \hat{\boldsymbol{z}}_{tls}\right]$ are found, then any $\hat{\boldsymbol{u}}_{tls}$ satisfying $\hat{\boldsymbol{z}}_{tls} = \widehat{\boldsymbol{\Psi}}_{tls}\hat{\boldsymbol{u}}_{tls}$ is called a TLS solution. The solution to this optimization problem is given in the following theorem.

Theorem 2. *Let $\boldsymbol{U}\acute{\boldsymbol{\Sigma}}\boldsymbol{V}$ be the SVD of $\widehat{\boldsymbol{\Psi}}_{tls}$ and $\boldsymbol{U}\boldsymbol{\Sigma}\boldsymbol{V}^H$ be the SVD of $\left[\widehat{\boldsymbol{\Psi}} \middle| \boldsymbol{z}\right]$. If $\hat{\sigma}_n \geq \sigma_{n+1}$ then the signal estimate for total-least-squares filtering exists and is unique and it can be expressed as follows.*

$$\hat{\boldsymbol{u}}_{tls} = \left(\langle\widehat{\boldsymbol{\Psi}}, \widehat{\boldsymbol{\Psi}}\rangle - \sigma_{n+1}^2 \mathbf{I}_{n+1}\right)^{-1} \langle\widehat{\boldsymbol{\Psi}}, \boldsymbol{z}\rangle \tag{4.12}$$

where σ_{n+1} and $\hat{\sigma}_n$ are the smallest singular values of the augmented matrix $[\widehat{\boldsymbol{\Psi}}|\boldsymbol{z}]$ and $\widehat{\boldsymbol{\Psi}}$ respectively.

Proof:

The interested reader is referred to the proof presented in chapter 2 which is given in [41, Theorem 4.1], [42, Theorem 2.6]. Algorithm 1 is outlined above for the proposed CS aided ZF and TLS receivers.

Owing to the fact that TLS receiver's optimization problem is based on 2-norm, it is not a good choice for directly estimating the sparse signals. In practice, it performs much

better for the overdetermined case. So we will use Eq. (4.9) in first stage to estimate the support $\hat{\mathcal{S}}$ with imperfect channel knowledge in Eq. (4.11). As we know the sparsity N, so we will cast an underdetermined system of equations as in Eq. (4.10). In a second stage, we will apply the TLS receiver to the underdetermined system and this combined approach is referred to as CS-TLS. This combined approach is also adopted for a ZF receiver for the sake of comparison and is referred to as CS-ZF receiver.

4.3 Sparse Recovery for Downlink Multi-user Precoded Generalized Spatial Modulation System

Having provided the CS-aided data detection scheme, it is in order to investigate the receiver design using CS for a multi-user precoded GSM system. In the following subsections, we give the details of a novel application of CS to a multi-user GSM system.

4.3.1 Multi-user GSM System Modeling

In order to investigate GSM in multi-user MIMO systems, the idea of GSM is applied to different antenna groups of the same BTS separately. At each antenna group, the GSM mapped data is pre-processed by employing an appropriate precoder in order to mitigate the multi-user interference.

A single-cell downlink system comprising of a base station with N_T antennas and K users is considered in which data is sent from the base station to the users on the same time-frequency slot. Each user is assumed to have N_R antennas. In contrast to the traditional multi-user MIMO system in which all the N_T antennas are used simultaneously to send data from the base station to the users, the N_T transmit antennas are split up into K groups of antennas. The group 1 sends data to the user 1, group 2 sends data to user 2, and the K-th group sends data to user K. Without loss of generality, we

assume that each group of transmit antennas uses the same S-ary modulation scheme. However, the precoding scheme is applicable to the case where each group sends data on constellations of different sizes. The partitioning of base station antennas into multiple groups serves two purposes. 1) Owing to the precoding at the transmitter side, each user is decoupled from the interference signals of the users transmitted by the other groups. 2) The decoding complexity of the resultant system is reduced because due to partitioning, the multi-user system is converted into parallel single-user point-to-point systems with only N_T/K transmit antennas per user.

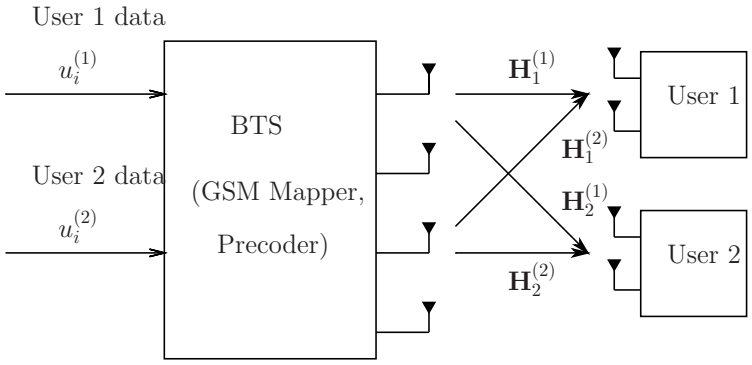

Figure 4.1: System Model of MU-GSM for $N_T = 4$, $K = 2$ users and $N_R = 2$

In order to investigate GSM systems in multi-user regime, we apply the GSM concept to each antenna group as follows. The transmit signal $\boldsymbol{x}^{(k)}$ from the k-th antenna group sent to the k-th user during each slot will be product of an antenna activation pattern matrix $\boldsymbol{P} \in \{0,1\}^{\frac{N_T}{K} \times N_a}$ and the selection vector $\boldsymbol{u}^{(k)} \in \mathbb{C}^{N_a}$.

$$\boldsymbol{x}^{(k)} = \boldsymbol{P}\boldsymbol{u}^{(k)} \tag{4.13}$$

$$= \begin{pmatrix} | & & | \\ \boldsymbol{p}_1 & \cdots & \boldsymbol{p}_{N_a} \\ | & & | \end{pmatrix} \begin{pmatrix} 0 \\ \vdots \\ u_i^{(k)} \\ \vdots \\ 0 \end{pmatrix} \tag{4.14}$$

where $u_i^{(k)} \in$ S-QAM is the complex constellation signal point emitted from the $i^{th} \in$

$\{1, ..., N_a\}$ antenna pair of the k-th group. The index of the signal $u_i^{(k)}$ is chosen by the p bits and the constellation point is chosen from the S-QAM depending upon the particular pattern of the q bits. Here $\boldsymbol{p}_i \in \mathbb{C}^{N_T}$ and is an N_c-sparse vector. Each column vector ensures which particular set of antennas are activated due to selection of the i-th column vector. In turn, this particular column vector is being selected by the index of the signal $u_i^{(k)}$. The column vector may be expressed as linear combination of some of the unit vectors of the N_T-dimensional space, i.e.,

$$\boldsymbol{p}_i = \sum_{j \in \mathcal{Z}_i} \delta_j \qquad\qquad i = 1, \cdots, N_a \tag{4.15}$$

where δ_j is the j-th unit vector of N_T-dimensional space and the set $\mathcal{Z}_i$ is the set of antenna indices being activated due to selection of $\boldsymbol{p}_i$. $\mathcal{Z}_i$ is the ordered strict subset of $\mathbb{A}$, the set comprising of all the antenna indices.

$$\mathcal{Z}_i :\subsetneq \mathbb{A} = \{1, 2, \cdots, N_T\} \tag{4.16}$$

The signal transmitted from the k-th antenna group propagates through the wireless fading channel and can be expressed as follows

$$\begin{aligned} \boldsymbol{z}^{(k)} &= \sqrt{\frac{P_s}{N_c}} \boldsymbol{H}_k^{(k)} \boldsymbol{x}^{(k)} + \sum_{\substack{j=1 \\ j \neq k}}^{K} \sqrt{\frac{P_s}{N_c}} \boldsymbol{H}_k^{(j)} \boldsymbol{x}^{(j)} + \mathbf{n}^{(k)} \\ &= \sqrt{\frac{P_s}{N_c}} \boldsymbol{H}_k^{(k)} \boldsymbol{P} \boldsymbol{u}^{(k)} + \sum_{\substack{j=1 \\ j \neq k}}^{K} \sqrt{\frac{P_s}{N_c}} \boldsymbol{H}_k^{(j)} \boldsymbol{P} \boldsymbol{u}^{(j)} + \mathbf{n}^{(k)} \end{aligned} \tag{4.17}$$

where the first term $\sqrt{\frac{P_s}{N_c}} \boldsymbol{H}_k^{(k)} \boldsymbol{x}^{(k)}$ is the desired signal component and the second term $\sum_{j=1 j \neq k}^{K} \sqrt{\frac{P_s}{N_c}} \boldsymbol{H}_k^{(j)} \boldsymbol{x}^{(j)}$ is the multi-user co-channel interference. The channel between each transmit and receive antenna in each group is assumed to be frequency-flat independent Rayleigh fading channel. Additionally, the link channel gain is assumed to be circularly symmetric complex Gaussian random variable with zero mean and variance $\sigma_h^2/2$ per dimension. $\boldsymbol{H}_j^{(i)}$ is used to denote the channel gain matrix between the group i and the

target user j. Thus, for k-th user, the direct channel gain matrix is $\boldsymbol{H}_k^{(k)}$ and $\{\boldsymbol{H}_k^{(j)} : j \neq k\}$ are considered to be interference channels. The measurement noise at each user is assumed to be AWGN process having noise variance equal to N_0 per dimension. P_s is the average total power which is divided among the active antennas of each group. In each group, as only N_c antennas are activated at one time instant so according to the principle of the GSM the power per transmit antenna in each group is P_s/N_c. As the base station has K groups of antennas serving so the total number of active antennas at the base station is KN_c. If we stack the received signals of all the K users, we will have following compact input-output relation.

$$\begin{pmatrix} \boldsymbol{z}^{(1)} \\ \vdots \\ \boldsymbol{z}^{(K)} \end{pmatrix} = \sqrt{\frac{P_s}{N_c}} \begin{pmatrix} \boldsymbol{H}_1^{(1)} & \cdots & \boldsymbol{H}_1^{(K)} \\ \vdots & \cdots & \vdots \\ \boldsymbol{H}_K^{(1)} & \cdots & \boldsymbol{H}_K^{(K)} \end{pmatrix} \times \begin{pmatrix} \boldsymbol{P} & & \\ & \ddots & \\ & & \boldsymbol{P} \end{pmatrix} \begin{pmatrix} \boldsymbol{u}^{(1)} \\ \vdots \\ \boldsymbol{u}^{(K)} \end{pmatrix} + \begin{pmatrix} \mathbf{n}^{(1)} \\ \vdots \\ \mathbf{n}^{(K)} \end{pmatrix} \tag{4.18}$$

where $\mathbf{n}^{(k)} \sim \mathcal{CN}(0, N_o\mathbf{I})$ is the AWGN. The above equation can be written more compactly as follows.

$$\boldsymbol{z} = \sqrt{\frac{P_s}{N_c}}\mathcal{H}\left(\mathbf{I}_K \otimes \boldsymbol{P}\right)\boldsymbol{u} + \mathbf{n} \tag{4.19}$$

where $(\mathbf{I}_K \otimes \boldsymbol{P})$ is the $N_T \times KN_a$ block diagonal matrix containing $\boldsymbol{P}$ on its diagonal entries, $\mathcal{H}$ is the augmented channel matrix containing the channel gains of all the users and interference channel gains, $\boldsymbol{u} = \left[\boldsymbol{u}^{(1)T} \cdots \boldsymbol{u}^{(K)T}\right]^T \in \mathbb{C}^{KN_a}$ and $\boldsymbol{z} = \left[\boldsymbol{z}^{(1)T} \cdots \boldsymbol{z}^{(K)T}\right]^T \in \mathbb{C}^{KN_R}$ are the transmitted and the received combined signal vectors respectively. The multi-user interference is created by the propagation of multi-stream signals, one from each group of antennas. This results in severe performance deterioration which can be mitigated by employing a suitable precoding scheme. The precoding scheme discussed in

the following subsection not only cancels the multi-user interference but also preserves the information encoded in the indices of the active antenna pair and the modulation symbol.

4.3.2 Precoding Scheme

Since the antenna indices contain information so the conventional ZF or MMSE are not applicable directly which cancels the channel by precoding the data with a precoder which is in general a pseudo-inverse or regularized pseudo-inverse of the channel matrix. However, we can do precoding in GSM systems by predistorting the selection vector with a precoder matrix. The resultant signal requires power normalization to satisfy the transmit power budget requirements. Let $\boldsymbol{W} = [\boldsymbol{W}_1|\cdots|\boldsymbol{W}_K] \in \mathbb{C}^{KN_a \times KN_a}$ be the combined precoding matrix of all the K users then the precoded selection vector of all the users may be expressed as follows.

$$\boldsymbol{w} = \sum_{i=1}^{K} \alpha_i \boldsymbol{W}_i \boldsymbol{u}^{(i)} \tag{4.20}$$

where $\boldsymbol{W}_i \in \mathbb{C}^{KN_a \times N_a}$ and α_i is a power normalization constant used to normalize the transmit power of each group's transmit power.

$$\alpha_i = \frac{1}{\sqrt{\langle \boldsymbol{W}_i, \boldsymbol{W}_i \rangle}} \tag{4.21}$$

where $\langle \boldsymbol{W}_i, \boldsymbol{W}_i \rangle = tr(\boldsymbol{W}_i^H \boldsymbol{W}_i)$ is the inner product of the augment matrices. Let $\boldsymbol{\Sigma} = \mathsf{diag}[\alpha_i]_{i=1}^{K} \otimes \mathbf{I}_{N_a}$, then the received signal of K users after propagation and precoding through the wireless fading channel may be expressed as follows.

$$\boldsymbol{z} = \sqrt{\frac{P_s}{N_c}} \mathcal{H} \left(\mathbf{I}_K \otimes \boldsymbol{P} \right) \boldsymbol{W} \boldsymbol{\Sigma} \boldsymbol{u} + \mathbf{n} \tag{4.22}$$

Let $\boldsymbol{W} = \left(\mathcal{H}\left(\mathbf{I}_K \otimes \boldsymbol{P}\right)\right)^{\dagger} \mathsf{diag}\left(\boldsymbol{H}_i^{(i)}\boldsymbol{P}\right)_{i=1}^{K}$, then the received signal at all the K users may be expressed as follows.

$$\begin{pmatrix} \boldsymbol{z}^{(1)} \\ \vdots \\ \boldsymbol{z}^{(K)} \end{pmatrix} = \sqrt{\frac{P_s}{N_c}} \begin{pmatrix} \alpha_1 \boldsymbol{H}_1^{(1)} & & \\ & \ddots & \\ & & \alpha_K \boldsymbol{H}_K^{(K)} \end{pmatrix} \times \begin{pmatrix} \boldsymbol{P} & & \\ & \ddots & \\ & & \boldsymbol{P} \end{pmatrix} \begin{pmatrix} \boldsymbol{u}^{(1)} \\ \vdots \\ \boldsymbol{u}^{(K)} \end{pmatrix} + \begin{pmatrix} \mathbf{n}^{(1)} \\ \vdots \\ \mathbf{n}^{(K)} \end{pmatrix} \tag{4.23}$$

The precoding cancels the interferences among different group of antennas at the transmitter exploiting the knowledge of antenna activation pattern matrix and CSIT. As a result of precoding, the received signal at each user is free of interference of all the other users and single-user GSM data detection can be employed. The above system of equations can be written more compactly as follows

$$\boldsymbol{z} = \sqrt{\frac{P_s}{N_c}} \mathsf{diag}\left(\alpha_i \boldsymbol{H}_i^{(i)}\right)_{i=1}^{K} \left(\mathbf{I}_K \otimes \boldsymbol{P}\right) \boldsymbol{u} + \mathbf{n} \tag{4.24}$$

The base station is assumed to have perfect CSI of all the links from the base station to the users. However, due to interference cancellation, the k-th user needs to know the CSI of the links between its N_R antennas and the the N_T/K antennas of the k-th group. The k-th user's received signal can be expressed as follows.

$$\boldsymbol{z}^{(k)} = \sqrt{\frac{P_s}{N_c}} \alpha_k \boldsymbol{H}_k^{(k)} \boldsymbol{P} \boldsymbol{u}^{(k)} + \mathbf{n}^{(k)} \tag{4.25}$$

Due to decomposition of multi-user GSM system into parallel single-user SM systems, multi-user GSM systems offer not only high multiplexing gains but multi-user gains are also attainable. For instance, with $N_T = 60$ BTS antennas, $N_c = 2$ RF chains and BPSK modulation, single-user GSM system can only offer $\left\lfloor \log_2 \binom{60}{2} \right\rfloor + 1 = 11$ bits per channel use (bpcu). However, if we divide the BTS antennas into four groups of 15 antennas for 4

users, then the spectral efficiency is $4\left(\left\lfloor \log_2 \binom{15}{2} \right\rfloor + 1\right) = 28$ bpcu. Thus, using the same number of BTS antennas, we can serve multiple users with significantly higher spectral efficiency at the expense of $N_c = 4$ RF chains.

Complexity Discussion

The computational complexity can be calculated using the floating-point operations [60]. For instance, given $N \times 1$ vectors $\boldsymbol{x}$ and $\boldsymbol{y}$, $M \times N$ matrix $\boldsymbol{X}$, and $N \times O$ matrix $\boldsymbol{Y}$, the inner product $\boldsymbol{x}^H\boldsymbol{y}$ requires $6N$multiplications and $2(N-1)$ additions whereas the matrix multiplication $\boldsymbol{XY}$ requires $6MNO$ multiplications and $2MO(N-1)$ additions. It can be easily shown that the computational complexity associated with calculating the pseudo-inverse in $\boldsymbol{W}$,$C_{\boldsymbol{W}}$, can be expressed as follows [61],

$$C_{\boldsymbol{W}} = KN_R\left[24(KN_R-1)(KN_a)^2 + 48(KN_R-1)^2KN_a + 54(KN_R-1)^3 + 6KN_a\right]$$

which turns out to be polynomial in number of users, number of antenna combinations, and number of receive antennas.

4.3.3 Compressive Sensing Framework

In compact form, the Eq. (4.25) can be expressed as

$$\boldsymbol{z}^{(k)} = \boldsymbol{\Psi}\boldsymbol{u}^{(k)} + \mathbf{n}^{(k)} \tag{4.26}$$

where $\boldsymbol{\Psi} = \sqrt{\frac{P_s}{N_c}}\alpha_k\boldsymbol{H}_k^{(k)}\boldsymbol{P}$ is the composite channel matrix between the N_R antennas of the k-th user and the N_T/K antennas of the k-th group at BTS. Here $\boldsymbol{z}^{(k)} \in \mathbb{C}^{N_R}$ is the received signal at the k-th user and $\boldsymbol{u}^{(k)}$ is the selection vector used at the k-th group of antennas. For notational convenience, we define $m = N_R$ and $n = N_a$. As N_a is quite large for tens of antennas say for $N_T = 20, N_c = 2$,$N_a = 128$ the $\boldsymbol{u}^{(k)}$ vector is sparse as it has only one non-zero element. In each $\boldsymbol{u}^{(k)}$, only one element is active so $\boldsymbol{u}^{(k)}$ is 1-sparse.

Here $\mathbf{n}^{(k)}$ is a complex AWGN, $\mathcal{CN}(0, \sigma_n^2 \mathbf{I}_m)$. As $m \ll n$, this is an ill-posed problem as there will be infinite number of solutions satisfying (4.26) (ignoring the noise, $\mathbf{n}^{(k)}$). However, if we have prior knowledge of sparsity of $\boldsymbol{u}^{(k)}$, then we can use the standard CS-method to reconstruct the signal which is l_0-norm minimization when the signal and measurements are free of noise. Now, it is quite straightforward to formulate an $\boldsymbol{l}_0$-norm minimization which is expressed as follows.

$$\widehat{\boldsymbol{u}^{(k)}} = \arg\min_{\boldsymbol{u}^{(k)}} \|\boldsymbol{u}^{(k)}\|_{l_0} \qquad \text{subject to} \qquad \boldsymbol{z}^{(k)} = \boldsymbol{\Psi}\boldsymbol{u}^{(k)} \tag{4.27}$$

The above solution requires exhaustive search which is intractable when the dimension of the signal to be estimated is large, as it is here. The tractable way of reconstructing a sparse signal is $\boldsymbol{l}_1$-norm minimization as in the following optimization problem :

$$\widehat{\boldsymbol{u}^{(k)}} = \arg\min_{\boldsymbol{u}^{(k)}} \|\boldsymbol{u}^{(k)}\|_{l_1} \text{ subject to } \|\boldsymbol{z}^{(k)} - \boldsymbol{\Psi}\boldsymbol{u}^{(k)}\|_{l_2} \leq \epsilon \tag{4.28}$$

where $\epsilon = \sqrt{\sigma_{\boldsymbol{n}}^2(m + \sqrt{2m})}$. It has been established in [35] that for random matrices whose entries are independent and identically distributed (i.i.d.) Gaussian, the RIP is satisfied with high probability when $m \geqslant S\log(n/S)$ where S is the sparsity of the vector of size n. The compression ratio can be defined as m/n where m is the number of measurements and n is the size of the vector to be estimated. In general, for fixed n, as m increases, the estimation performance of any CS technique improves.

4.4 Numerical Experiments

This section is devoted to numerical experiments conducted for performance evaluation of CS based detection of single and multi-user GSM systems. All the simulations are performed on the discrete event, i.e., symbol by symbol basis. For performance evaluation, we use two performance metrics : (1) Normalized mean-square error (NMSE) between

the actual and the estimated data vectors.

$$\mathsf{NMSE} = 10\log_{10}\left(\frac{1}{J}\sum_{j=1}^{J}\frac{\|\hat{\boldsymbol{x}}_j - \boldsymbol{x}_j\|^2}{\|\boldsymbol{x}_j\|^2}\right) \tag{4.29}$$

where J is the number of Monte Carlo runs. $\hat{\boldsymbol{x}}_j$ and $\boldsymbol{x}_j$ are the estimated and the original data vectors respectively at the j-th iteration respectively.(2) Bit-error rate (BER) between the transmitted data and the recovered data at receiver using the estimated data vectors. BER curves are plotted versus $1/\sigma_{\boldsymbol{n}}^2$ as the SNR: $1/\sigma_{\boldsymbol{n}}^2$ functions as the SNR per receive antenna. Each value of BER is obtained by doing Monte Carlo simulation over $10,000$ independent channel realizations.

For single-user GSM system, CS alone and CS-aided data detection algorithms for GSM systems are compared with each other. The transmit constellation is assumed to 16-QAM, $S = 16$. All the channels are assumed to be unit variance, $\sigma_h^2 = 1$. In all simulations, we assumed $N = 5, L = 5, N_R = 3, N_c = 2, N_T = 8, \sigma_{\boldsymbol{e}}^2 = 0.5$. The noise variance per receive antenna is assumed to be the same for all observations, $\sigma_1^2 = \cdots = \sigma_m^2 = \sigma_{\boldsymbol{n}}^2$.

Fig. 4.2 demonstrates the MSE performance evaluation in which NMSE (in dB) is plotted on y-axis and SNR (in dB) is plotted on x-axis. For perfect CSI, CS-ZF receiver offers 8 dB better performance than CS alone at the SNR of -10 dB. For imperfect CSI, CS-ZF offers 10 dB better performance than CS alone when the SNR is greater than -5 dB. However for imperfect CSI, CS-TLS offers 2 dB better performance than CS-ZF receiver even at low SNR. In Fig. 4.3, average uncoded BER is plotted versus SNR (in dB) per receive antenna. CS-ZF receiver with perfect CSI offers the best performance in terms of error rate. At SNR of 20 dB, it offers error rates as low as 4×10^{-3}. However, its performance deteriorates in the presence of imperfect channel knowledge. At SNR of 20 dB, CS-TLS also achieves error rates as low as 4×10^{-3}. CS-TLS receiver offers better performance than CS-ZF with imperfect channel knowledge but its performance is slightly

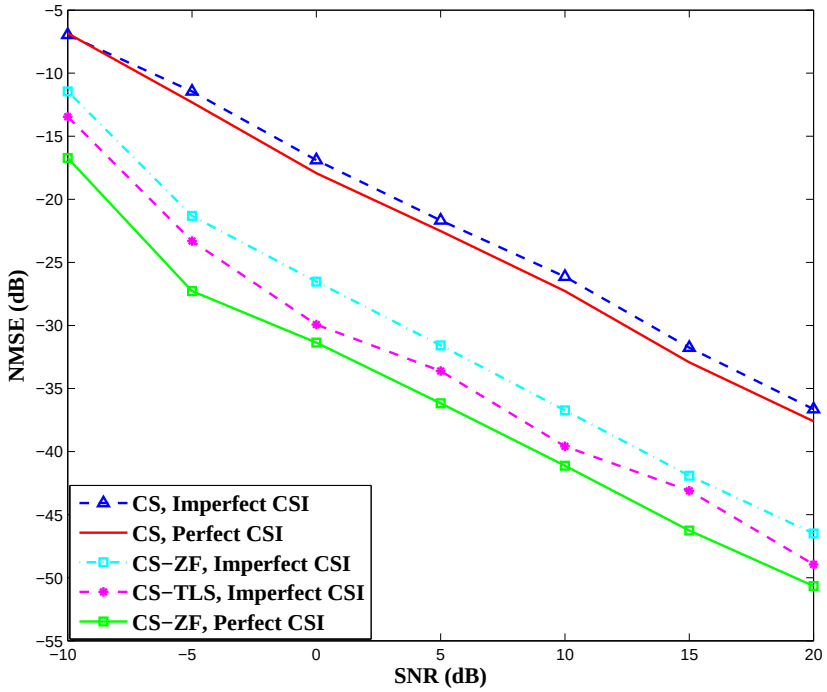

Figure 4.2: Mean Square Error Performance Evaluation in MIMO ISI channel

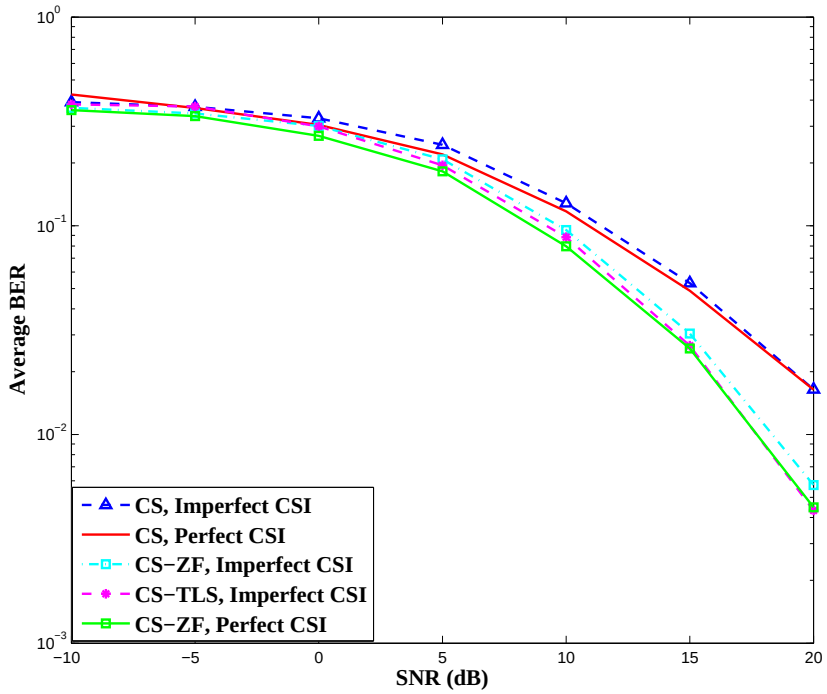

Figure 4.3: Communication Efficiency Plane in MIMO ISI channel

inferior to CS-ZF with perfect channel knowledge. Moreover, CS alone only achieve error rates of 2×10^{-2} even at high SNR of 20 dB.

For multi-user GSM systems, binary phase-shift keying (BPSK) is adopted for modulation format due to simplicity and the number of RF chains is assumed to be two, i.e., $N_c = 2$. SNR is defined to be P_s/N_o and channel variance is taken to be $\sigma_h^2 = 1$. Each value of BER is obtained by doing Monte Carlo simulation over multiple independent channel realizations.

In Fig. 4.4, the average BER for user 1 is plotted versus SNR (in dB) for different values of transmit antennas. The number of users is assumed to be four, i.e., $K = 4$ and the number of receive antennas per user is assumed to be five, i.e., $N_R = 5$. As the number of transmit antennas increases, the size of the transmitted data vector increases but as the number of measurements are fixed, the sparsity increases for fixed measurements' length. It can be observed that the performance of CS degrades as the sparsity increases for fixed number of measurements. Thus for higher number of transmit antennas, the BER is high due to limited number of measurements. For instance, at SNR of 25 dB, CS recovery offers BER as low as 1×10^{-4} for $N_T = 20$, however, as we increase the number of transmit antennas to 40, BER increases by one order of magnitude to 1×10^{-3}.

In Fig. 4.5, the average BER is plotted versus number of receive antennas for fixed value of SNR. The SNR is fixed at 20 dB and the number of users is assumed to be 4. As the number of receive antennas increases, the BER decreases in all the curves. For instance, for $N_T = 20$ antennas, the BER for user 1 is 10^{-2} at $N_R = 3$ and as the number of receive antennas are doubled, i.e., $N_R = 6$, the BER falls off to 3×10^{-4}. For fixed value of N_R, as N_T increases, the BER also increases. For example, for $N_R = 6$, the BER is 3×10^{-4} at $N_T = 20$ and the BER increases to 10^{-3} for $N_T = 40$. However, this deterioration in BER can be ameliorated by increasing the number of receive antennas as the number of transmit antennas increases. For example, at $N_T = 20$ and $N_R = 3$, BER

is 10^{-2} and same error rate can be attained at $N_T = 40$ and $N_R = 4$. Thus, by adding one extra receive antenna , i.e., $N_R = 4$, higher spectral efficiency of 24 is achieved at $N_T = 40$ in comparison to the spectral efficiency of 20 at $N_T = 20$ and $N_R = 3$ for the same error rate of 10^{-2}.

In Fig. 4.6, the average BER for interference-free single-user GSM system is compared with the average BER of the user 1 in the multi-user GSM system. For $N_T = 20$ and $N_T = 40$, the BER curves of both the schemes lie on top of each other. This validates the CS-based recovery of the the precoded system. Moreover, it shows that the interference-limited multi-user systems can approach the performance of single user systems in terms of error-rates using precoding and CS-based recovery.

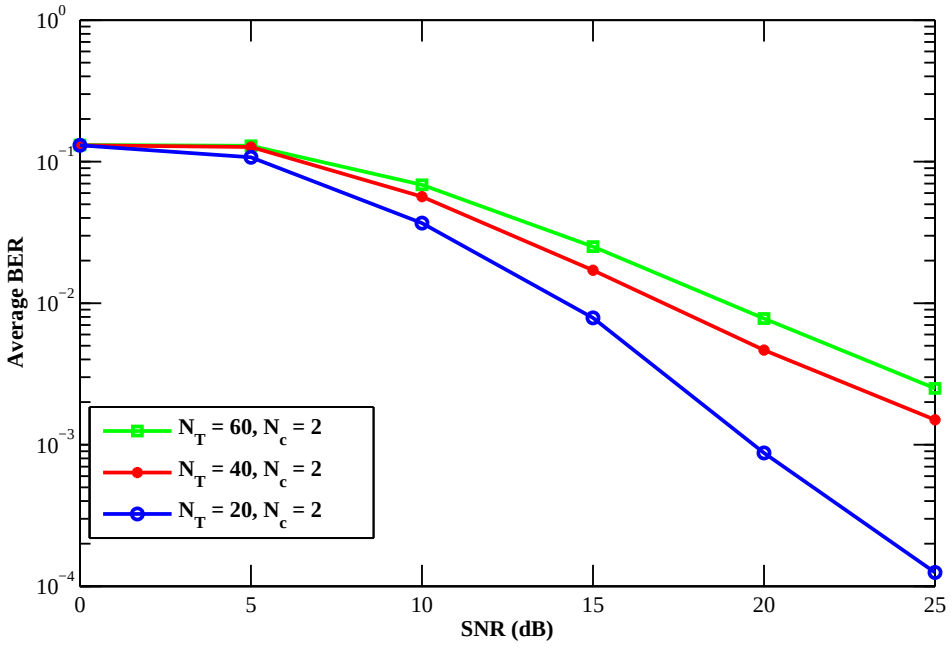

Figure 4.4: Communication Efficiency Plane for $K = 4$ users and $N_R = 5$

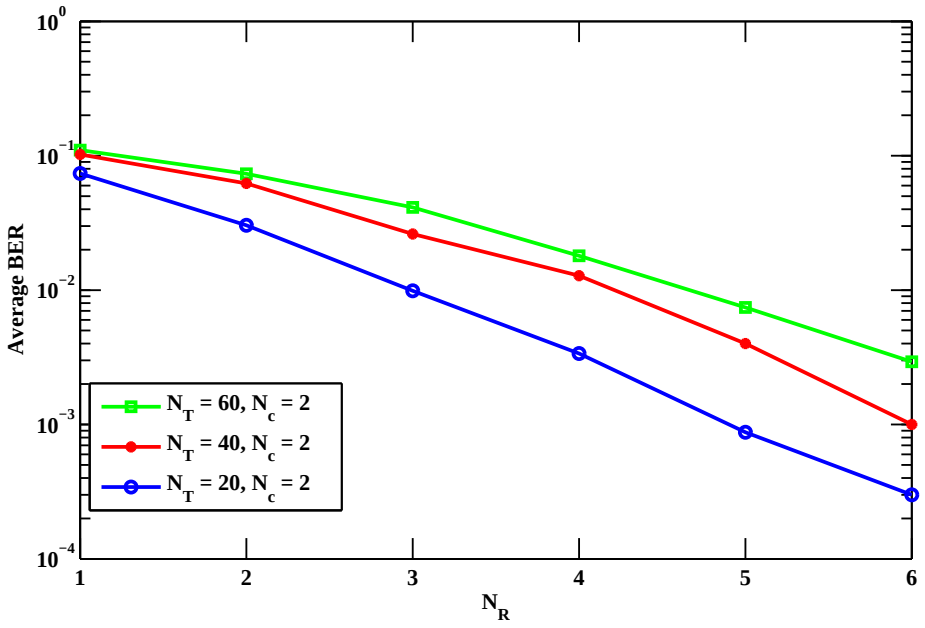

Figure 4.5: Average BER versus number of receive antennas for $K = 4$ users and $SNR = 20$ dB

4.5 Conclusion

In this chapter, we examined the CS-aided linear detection schemes for sparse reconstruction of data under MIMO ISI GSM systems. Specifically, we used CS only for support estimation of sparse-data in GSM systems. Moreover, our proposed algorithm offers reasonable accuracy under imperfect channel knowledge. CS-aided linear receivers accomplish better performance than CS-alone receivers from perspective of both the performance metrics. In practical applications requiring better quality of service, our proposed schemes can be employed despite the fact that complexity of CS-aided linear receiver is relatively higher than that of CS-alone receiver. Additionally, by exploiting the structure in the sensing matrix, computationally complexity can be reduced further. In a nutshell, CS-based data recovery can be ameliorated by subsequent application of linear receivers to combat fading. The second part of the chapter offered sparse recovery scheme for the multi-user precoded single-cell system using GSM which achieved the performance of

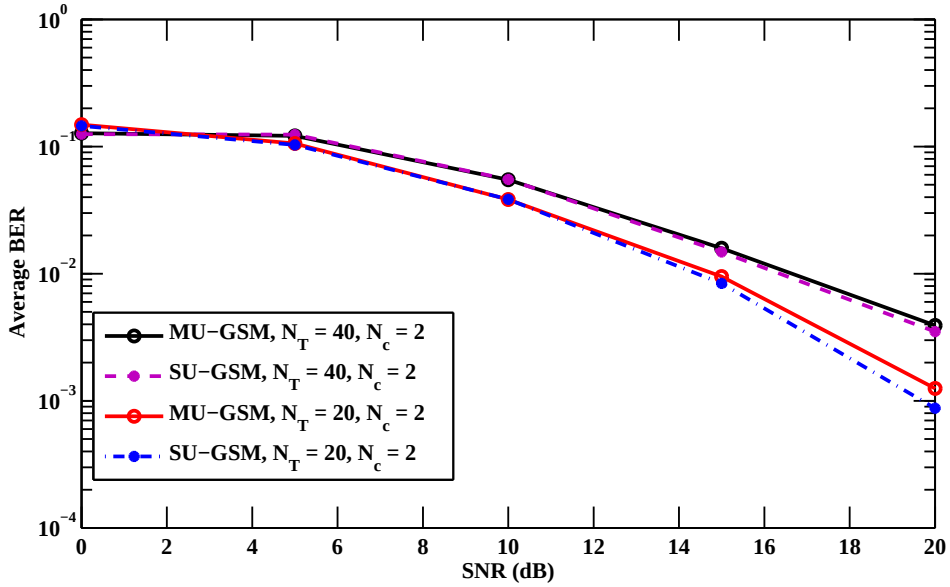

Figure 4.6: Performance Comparison of SU-GSM and MU-GSM for $K = 4$ users and $N_R = 5$

interference-free point-to-point systems in terms of BER.

Chapter 5

Achievable Rates for Generalized Spatial Modulation Massive MIMO Systems

The previous chapter was about data detection in GSM system and it was shown that GSM systems can offer reliability in terms of providing low BER. It is intriguing to investigate the achievable rates of GSM system for practical finite alphabet constraints such as QPSK, QAM etc.

This chapter is organized as follows. Section 5.1 highlights the motivation and related work. Section 5.2 illustrates the mutual information for GSM systems in which system modeling, analytical framework, calculations of entropies and mutual information are given. Section 5.3 provides the lower and upper bounds on achievable rate. Section 5.4 presents the mutual information for precoded GSM. Section 5.5 provides numerical experiments and section 5.6 concludes the chapter.

5.1 Motivation and Related Work

At the receiver, the signal detection for GSM is computationally expensive in comparison to SM systems because the activation of multiple RF chains introduces serious ICI. Until recently, most of the prior work is based on reducing the complexity of detection in GSM systems [62–64]. In [62], a new technique is devised for the construction of the multiple-antenna SM codebook using an arbitrary number of transmit antennas. The proposed technique was optimized by the maximization of the inter-symbol distance. They give a design principle for codebook construction that by carefully designing over the antenna sets and by applying the rotation angle to symbols, more diversity gains are possible. Furthermore, they propose a low-complexity detection scheme based on the signal vector space. Numerical results are used to show that the proposed scheme outperforms SM with an acceptable linear decoding complexity. In [63], an ordered block minimum mean-square error (OB-MMSE) detector for GSM was proposed in which first an ordering algorithm is used to sort the possible transmit antenna combinations. Secondly, the possible signal vector for each ordered transmit antenna combination is detected by block MMSE equalization. Afterwards, the outputs of OB-MMSE detector are compared with a preset threshold sequentially in order to judge their reliability. As a result of thresholding, if one vector is found out to be reliable, the detection process is terminated. Otherwise, the ML criterion is is used to select the best candidate. In [64], the inherent sparsity of the spatial modulation signal was exploited to present a low complexity sparse reconstruction algorithm. Particularly, they used a CS denoising scheme to counter the effect of background noise. They demonstrate better performance than ZF and MMSE receivers at lower complexity via numerical results.

An early result which quantifies the impact of finite input alphabets on the mutual information of SM has been reported in [65]. They offer a closed-form formula for mutual information and analysis of the formula results into development of a precoding scheme

to improve performance of SM. Furthermore, using the traditional constellation design, a precoding coefficient is obtained via maximization of minimum Euclidean distance. However, their analysis is limited to MISO channels, i.e., when the receiver has only one antenna. In [66], it has been proposed to combine Block Markov Superposition Transmission (BMST) with SM. The authors presented a sliding-window decoder which is executed iteratively between BMST decoder and soft-input soft-output SM demapper. Futhermore, they use Monte Carlo runs to derive the mutual information for BSMT-SM scheme under uniformly distributed input.

In [50], the capacity of GSM for Gaussian inputs has been calculated using law of large numbers. In this work, the authors conjectured the capacity of GSM using law of large numbers and classical information theory. They modelled the channel as two source multiplicative multiple access channel (MAC) in which one source is the channel and the other source is input symbol. Although, they assumed the channel's alphabet to be discrete but they assumed the data symbol to be continuous Gaussian. As a result, the results of classical capacity analysis are straightforwardly applicable. Since this result is obtained for Gaussian input symbols, so this capacity serves as an upper bound for the case of finite alphabet GSM systems. An independent work has been reported in [67] which offers capacity analysis. Their analysis covers most forms of SM such as GSM, SSK, conventional SM etc using Gaussian mixture to accurately model the spatially modulated signal using a precoding framework. However, they do not take into account the finite alphabet constraints such as QPSK, QAM etc. Since Gaussian inputs for data symbols is not a realistic assumption, so we are motivated to calculate the achievable rates for GSM systems under finite input alphabets.

In this chapter, the achievable information rate of a GSM system using a finite alphabet constraint is derived in an information theoretic framework. The impact of the finite alphabet constraint on the achievable rate of GSM has been quantified in terms of a loss

term. Additionally, we calculate the lower and upper bounds on the achievable information rate for GSM systems. Furthermore, we derive the achievable rate for a precoded GSM system. Moreover, the achievable information rates of GSM are benchmarked against the capacity expression of [50] to facilitate comparison. Additionally, we compare the performance of GSM systems with MIMO antenna selection systems [68] which has the knowledge of best channel at the transmitter.

5.2 Mutual Information for Generalized Spatial Modulation Systems

In this section, we calculate the mutual information of a GSM system in which more than one antenna is active at one time instant. One of the information symbols out of the S constellation points is transmitted from these activated antennas which are connected to information source via N_c RF chains.

5.2.1 System Modeling

In this subsection, we explain the input-output relationship of a GSM system which has been briefly discussed in previous chapter. We aim at finding out a binary-input, single-output model in order to facilitate information theoretic calculations. The input-output relation of a GSM system can be expressed as follows

$$\boldsymbol{z} = \boldsymbol{H}\boldsymbol{P}\boldsymbol{u} + \mathbf{n} \tag{5.1}$$

Here $\boldsymbol{z} \in \mathbb{C}^{N_R}$ is the received signal, $\boldsymbol{H} \in \mathbb{C}^{N_R \times N_T}$ is the MIMO channel matrix, $\boldsymbol{P} \in \mathbb{C}^{N_T \times N_a}$ is antenna activation pattern matrix, $\boldsymbol{u} \in \mathbb{C}^{N_a}$ is the antenna activation vector, and $\mathbf{n} \in \mathbb{C}^{N_R}$ represents the noise vector. In these dimensions, N_a should be ideally equal to $\binom{N_T}{N_c}$ where N_c is equal to the number of RF chains which is equal to number of

antennas activated. $\binom{N_T}{N_c}$ represents that transmitter chooses to perform data transmission over one of the N_T choose N_c combinations of antenna groups. But as the information is being encoded in the selection of a possible combination of antennas so the number of antenna combinations selected for the transmission must be a power of two. As a result, $p = \left\lfloor \log_2 \binom{N_T}{N_c} \right\rfloor$ bits are used to select one out of $N_a = 2^p$ composite channels.

5.2.2 Analytical Framework

The antenna activation pattern matrix $\boldsymbol{P}$ may be considered as a juxtaposition of the antenna activation pattern vectors as follows:

$$\boldsymbol{P} = \begin{bmatrix} | & & | \\ \boldsymbol{p}_1 & \cdots & \boldsymbol{p}_{N_a} \\ | & & | \end{bmatrix} \tag{5.2}$$

Here $\boldsymbol{p}_m \in \mathbb{C}^{N_T}$ and is a N_c-sparse vector. Each antenna activation pattern vector ensures which particular set of antennas are activated due to selection of it. In turn, this particular antenna activation pattern vector is being selected by the incoming bit sequence. The antenna activation pattern vector may be expressed as linear combination of some of the unit vectors of the N_T-dimensional space, i.e.,

$$\boldsymbol{p}_m = \sum_{j \in \mathcal{Z}_m} \boldsymbol{e}_j \qquad\qquad m = 1, \cdots, N_a \tag{5.3}$$

where $\boldsymbol{e}_j$ is the j-th unit vector of N_T-dimensional space and the set $\mathcal{Z}_m$ is the set of antenna indices being activated due to selection of $\boldsymbol{p}_m$. $\mathcal{Z}_m$ is the subset of $\mathbb{A}$, the set comprising of all the antenna indices.

$$\mathcal{Z}_m \subseteq \mathbb{A} = \{1, 2, \cdots, N_T\} \tag{5.4}$$

It is observed that the cardinality of $\mathcal{Z}_m$ is N_c, i.e., $\left|\mathcal{Z}_m\right| = N_c$. For instance, if we have $N_T = 8$ and we can activate two antennas only, i.e., $N_c = 2$, then the bits used to select

$\boldsymbol{p}_m$ will be $p = \left\lfloor \log_2 \binom{8}{2} \right\rfloor = 4$ and consequently the the total number of antenna activation pattern vectors will be 16. The antenna indices sets for these antenna activation pattern vectors are listed below for this example.

$$\mathcal{Z}_1 = \{1,2\}\,,\ \mathcal{Z}_2 = \{1,3\}\,,\ \mathcal{Z}_3 = \{1,4\}\,, \tag{5.5}$$

$$\mathcal{Z}_4 = \{1,5\}\,,\ \mathcal{Z}_5 = \{1,6\}\,,\ \mathcal{Z}_6 = \{1,7\}\,, \tag{5.6}$$

$$\mathcal{Z}_7 = \{1,8\}\,,\ \mathcal{Z}_8 = \{2,3\}\,,\ \mathcal{Z}_9 = \{2,4\}\,, \tag{5.7}$$

$$\mathcal{Z}_{10} = \{2,5\}\,,\ \mathcal{Z}_{11} = \{2,6\}\,,\ \mathcal{Z}_{12} = \{2,7\}\,, \tag{5.8}$$

$$\mathcal{Z}_{13} = \{2,8\}\,,\ \mathcal{Z}_{14} = \{3,4\}\,,\ \mathcal{Z}_{15} = \{3,5\}\,, \tag{5.9}$$

$$\mathcal{Z}_{16} = \{3,6\} \tag{5.10}$$

Now, it is in order to shed some light on the nature of the composite channels being selected by the incoming bit sequences.

$$\boldsymbol{HP} = \begin{bmatrix} | & & | \\ \boldsymbol{Hp}_1 & \cdots & \boldsymbol{Hp}_{N_a} \\ | & & | \end{bmatrix} \tag{5.11}$$

$$= \begin{bmatrix} | & & | \\ \mathbf{h}_{[1]} & \cdots & \mathbf{h}_{[N_a]} \\ | & & | \end{bmatrix} \tag{5.12}$$

Here $\mathbf{h}_{[\gamma]} \in \mathbb{C}^{N_R}$ is the γ-th composite channel which is the sum of the transmit channel vectors whose indices are being selected by the incoming bit sequence. Additionally, $\boldsymbol{HP} \in \mathbb{C}^{N_R \times N_a}$ can be recognized as effective channel matrix whose columns are effective channel vectors one of which is chosen in each transmission depending upon incoming bit sequence. So, it can be easily expressed that

$$\mathbf{h}_{[\gamma]} = \sum_{m \in \mathcal{Z}_\gamma} \boldsymbol{h}_m \qquad \gamma = 1, \cdots, N_a \tag{5.13}$$

where $\boldsymbol{h}_m$ is the transmission channel vector between the m-th transmit antenna and the N_R receive antennas. Having made this background for composite channel vectors, it is convenient to express the received signal in the following form

$$\begin{aligned} \boldsymbol{z} &= \begin{bmatrix} | & & | \\ \mathbf{h}_{[1]} & \cdots & \mathbf{h}_{[N_a]} \\ | & & | \end{bmatrix} \boldsymbol{u} + \mathbf{n} \\ \boldsymbol{z} &= \mathbf{h}_{[\gamma]} u_\nu + \mathbf{n} \qquad \gamma = 1, \cdots, N_a \qquad \nu = 1, ..., S \end{aligned} \tag{5.14}$$

In the last equation, we have exploited the fact that the sparsity of $\boldsymbol{u}$ is unity, however, the position of the non-zero element in the vector $\boldsymbol{u}$ is varying. In terms of random variables, the input-output behavioural relation of GSM may be expressed as follows

$$\boldsymbol{z} = \mathbf{H}U + \mathbf{N} \tag{5.15}$$

Here one information source is random variable U whose one particular realization $u \in \mathcal{U} = \{u_1, \cdots, u_S\}$ is emitted by the random information source. The composite channel vector over which this symbol is transmitted, is governed by the incoming bit sequences. Thus, composite channel is another random variable $\mathbf{H}$ whose one particular realization $\mathbf{h} \in \boldsymbol{\mathcal{H}} = \{\mathbf{h}_{[1]}, \cdots, \mathbf{h}_{[N_a]}\}$ is used for signalling.

Thus, our received signal is also one particular realization of of a random variable $\boldsymbol{Z}$. The proposed analytical framework results in an input-output relation for GSM systems for an information theoretic treatment. One may notice that the $\mathbf{h}_{[\gamma]}$ is not a transmit channel vector rather it is a sum of multiple transmit channel vectors whose choice changes in each signalling interval and is governed by incoming bit sequence. Nevertheless, the mutual information can be computed straightforwardly due to proposed analytical framework.

In GSM systems, we aim at finding the mutual information between pair of random variables $(\mathbf{H}, U)$ and the received measurements $\boldsymbol{Z}$, i.e., $\mathcal{I}\left((\boldsymbol{H}, U); \boldsymbol{Z}\right)$. In order to calcu-

late $\mathcal{I}((\boldsymbol{H}, U); \boldsymbol{Z})$, we invoke the definition of mutual information from Eq. (2.13).

$$\mathcal{I}((\boldsymbol{H}, U); \boldsymbol{Z}) := H((\mathbf{H}, U)) - H\left((\mathbf{H}, U)\middle|\boldsymbol{Z}\right) \tag{5.16}$$

In order to calculate $\mathcal{I}((\boldsymbol{H}, U); \boldsymbol{Z})$, we first require computations of joint and conditional entropies $H((\mathbf{H}, U))$ and $H\left((\mathbf{H}, U)\middle|\boldsymbol{Z}\right)$ which are presented in subsequent sections.

5.2.3 Calculation of $H((\mathbf{H}, U))$

The joint entropy of the composite channel vector and the information source can be calculated by the application of the chain rule for entropies (see Eq. (2.16)), so we may break up the joint entropy into a sum of entropy of composite channel vector and the entropy of the random source given the composite channel vector.

$$\begin{aligned} H(\mathbf{H}, U) &= H(\mathbf{H}) + H\left(U\middle|\mathbf{H}\right) && (5.17)\\ &= \log_2(N_a) + \log_2(S) && (5.18) \end{aligned}$$

where Eq. (5.18) follows from the fact that the composite channel and information symbols are selected by separate chunks of information bits, as a result they are statistically independent. Thus, joint entropy of the composite channel vector and the information source for GSM systems is simply the sum of the marginal entropies of information source and the composite channel vectors.

5.2.4 Calculation of $H\left((U, \mathbf{H})\middle|\boldsymbol{Z}\right)$

The calculation of $H\left(U, \mathbf{H}\middle|\boldsymbol{Z}\right)$ follows from the application of chain rule for entropies.

$$H\left(\mathbf{H}, U\middle|\boldsymbol{Z}\right) = H\left(U\middle|\boldsymbol{Z}\right) + H\left(\mathbf{H}\middle|U, \boldsymbol{Z}\right) \tag{5.19}$$

First we calculate an expression for the conditional entropy of U given $\boldsymbol{Z} = \boldsymbol{z}$ and then average it over the support of $\boldsymbol{Z}$. The above calculation requires the following conditional

distributions which can be obtained by using Bayes' Theorem.

$$p_{U|\boldsymbol{Z}}(u_\nu\big|\boldsymbol{z}) = \frac{\sum_{\gamma=1}^{N_a} e^{-\beta\|\boldsymbol{z}-\mathbf{h}_{[\gamma]}u_\nu\|^2}}{\sum_{\alpha=1}^{N_a}\sum_{\mu=1}^{S} e^{-\beta\|\boldsymbol{z}-\mathbf{h}_{[\alpha]}u_\mu\|^2}} \tag{5.20}$$

$$p_{\mathbf{H}|\boldsymbol{Z},U}(\mathbf{h}_\gamma\big|\boldsymbol{z},u_\nu) = \frac{e^{-\beta\|\boldsymbol{z}-\mathbf{h}_{[\gamma]}u_\nu\|^2}}{\sum_{\alpha=1}^{N_a} e^{-\beta\|\boldsymbol{z}-\mathbf{h}_{[\alpha]}u_\nu\|^2}} \tag{5.21}$$

where $\beta = \frac{1}{N_o}$ represents the SNR. So using the above expression for posterior pdf, the conditional entropy for $\boldsymbol{Z} = \boldsymbol{z}$ can be calculated as follows.

$$H(U|\boldsymbol{Z}=\boldsymbol{z}) = \frac{\sum_{\nu=1}^{S}\sum_{\gamma=1}^{N_a} e^{-\beta\|\boldsymbol{z}-\mathbf{h}_{[\gamma]}u_\nu\|^2}\log_2\left[\frac{\sum_{\mu=1}^{S}\sum_{\alpha=1}^{N_a} e^{-\beta\|\boldsymbol{z}-\mathbf{h}_{[\alpha]}u_\mu\|^2}}{\sum_{\gamma=1}^{N_a} e^{-\beta\|\boldsymbol{z}-\mathbf{h}_{[\gamma]}u_\nu\|^2}}\right]}{\sum_{\alpha=1}^{N_a}\sum_{\mu=1}^{S} e^{-\beta\|\boldsymbol{z}-\mathbf{h}_{[\alpha]}u_\mu\|^2}} \tag{5.22}$$

We average the above expression with respect to the channel output $\boldsymbol{z}$ to obtain the conditional entropy $H(U\big|\boldsymbol{Z})$. For interested reader, the derivation has been provided in Appendix D.

$$H(U|\boldsymbol{Z}) = \frac{1}{N_a M}\sum_{\nu=1}^{S}\sum_{\gamma=1}^{N_a}\mathbb{E}_{\mathbf{N}}\log_2\left[\frac{\sum_{\mu=1}^{S}\sum_{\alpha=1}^{N_a} e^{-\beta\|u_\nu\mathbf{h}_{[\gamma]}-u_\mu\mathbf{h}_{[\alpha]}+\mathbf{N}\|^2}}{\sum_{\gamma=1}^{N_a} e^{-\beta\|u_\mu\left(\mathbf{h}_{[\gamma]}-\mathbf{h}_{[\alpha]}\right)+\mathbf{N}\|^2}}\right] \tag{5.23}$$

Details about these calculations are omitted for the sake of brevity. In the same vein, we seek the conditional entropy for given values of $\boldsymbol{Z} = \boldsymbol{z}$ and $U = u_\nu$.

$$H(\mathbf{H}\big|U=u_\nu,\boldsymbol{Z}=\boldsymbol{z}) = \frac{\sum_{\gamma=1}^{N_a} e^{-\beta\|\boldsymbol{z}-\mathbf{h}_{[\gamma]}u_\nu\|^2}\log_2\left[\frac{\sum_{\alpha=1}^{N_a} e^{-\beta\|\boldsymbol{z}-\mathbf{h}_{[\alpha]}u_\nu\|^2}}{e^{-\beta\|\boldsymbol{z}-\mathbf{h}_{[\gamma]}u_\nu\|^2}}\right]}{\sum_{\alpha=1}^{N_a} e^{-\beta\|\boldsymbol{z}-\mathbf{h}_{[\alpha]}u_\nu\|^2}} \tag{5.24}$$

Now to obtain the conditional entropy $H(\mathbf{H}\big|\boldsymbol{Z},U)$, we average over the conditioning random variables to obtain,

$$H(\mathbf{H}\big|U,\boldsymbol{Z}) = \frac{1}{N_a S}\sum_{\nu=1}^{S}\sum_{\gamma=1}^{N_a}\mathbb{E}_{\mathbf{N}}\log_2\left[\sum_{\alpha=1}^{N_a} e^{-\left(\beta\|u_\nu\left(\mathbf{h}_{[\gamma]}-\mathbf{h}_{[\alpha]}\right)+\mathbf{N}\|^2-\beta\|\mathbf{N}\|^2\right)}\right] \tag{5.25}$$

If we add the calculated conditional entropies and subtract them from the joint entropy of two independent sources of information, we end up with the following concrete expression.

$$\begin{aligned}\mathcal{I}\left(\mathbf{H},U;\boldsymbol{Z}\right) &= \left\lfloor \log_2\binom{N_T}{N_c}\right\rfloor + \log_2(S)\\ -\frac{1}{N_a S}\sum_{\nu=1}^{S}\sum_{\gamma=1}^{N_a}\mathbb{E}_{\mathbf{N}}\log_2&\left[1+\sum_{\substack{\mu=1\\(\mu,\alpha)\neq(\nu,\gamma)}}^{S}\sum_{\alpha=1}^{N_a}\frac{e^{-\beta\left(\|u_\nu\mathbf{h}_{[\gamma]}-u_\mu\mathbf{h}_{[\alpha]}+\mathbf{N}\|^2\right)}}{e^{-\beta\|\mathbf{N}\|^2}}\right]\end{aligned} \tag{5.26}$$

where $\beta = \frac{1}{N_o}$. In Eq. (5.26), the third term is a loss term. The main reason for loss term is the finite alphabets of modulation symbols and transmit channel vectors. However, it is a decreasing function of the SNR.

Remark. *As the SNR β tends to infinity, the loss term vanishes and we are left with the maximum achievable information rate for GSM, i.e. $\lfloor\log_2\binom{N_T}{N_c}\rfloor + \log_2(S)$. For large MIMO systems, $\log_2\binom{N_T}{N_c} \approx \log_2\frac{(N_T)^{N_c}}{N_c!} = N_c\log_2(N_T) - \log_2(N_c!)$. If we double the number of transmit antennas for the same number of RF chains, then $\log_2\binom{2N_T}{N_c} \approx N_c + N_c\log_2(N_T) - \log_2(N_c!)$. Thus as the number of transmit antennas are doubled, the number of bits per channel use is increased by N_c.*

Substituting Eq. (5.13) into Eq. (5.26), we get Eq. (5.27).

$$\begin{aligned}\mathcal{I}\left(U,\mathbf{H};\boldsymbol{Z}\right) &= \left\lfloor \log_2\binom{N_T}{N_c}\right\rfloor + \log_2(S)\\ -\tfrac{1}{N_a S}\sum_{\nu=1}^{S}\sum_{\gamma=1}^{N_a}\mathbb{E}_{\mathbf{N}}\log_2&\left[1+\sum_{\substack{\mu=1\\(\mu,\alpha)\neq(\nu,\gamma)}}^{S}\sum_{\alpha=1}^{N_a} e^{-\beta\left(\|u_\nu\sum_{m\in\mathcal{Z}_\gamma}\boldsymbol{h}_m - u_\mu\sum_{m\in\mathcal{Z}_\alpha}\boldsymbol{h}_m+\mathbf{N}\|^2-\|\mathbf{N}\|^2\right)}\right]\end{aligned} \tag{5.27}$$

In general, the expectation in Eq. (5.27) is difficult to calculate and cannot be simplified further. The expression in Eq. (5.27) is a function of noise and channel realizations. Having knowledge of the CSI at receiver, we still need Monte Carlo simulation to average out the noise. Therefore, we aim at deriving upper and lower bounds which do not contain any noise terms. Furthermore, we assume perfect synchornization between transmitter and receiver. We seek to obtain a closed-form expressions for lower and upper bounds of the mutual information for finite alphabet GSM systems by harnessing the structure of the $\mathcal{I}(\mathbf{H}, U; \boldsymbol{Z})$. The derived lower bound may subsequently be used for the maximization of the mutual information.

5.3 Lower and Upper Bounds on Achievable Rate

In this subsection, we provide lower and upper bounds on the achievable rates in the Proposition 1 and 2 respectively.

Proposition 1. *For finite alphabets, achievable rates for GSM can be lower bounded as follows*

$$\begin{aligned}\mathcal{I}(\mathbf{H}, U; \boldsymbol{Z}) \geqslant & \left\lfloor \log_2 \binom{N_T}{N_c} \right\rfloor + \log_2(S) - N_R \log_2(e) \\ & + N_R - \frac{1}{N_a S} \sum_{\nu=1}^{S} \sum_{\gamma=1}^{N_a} \log_2 \left[\sum_{\mu=1}^{S} \sum_{\alpha=1}^{N_a} e^{-\frac{1}{2N_o}(\|u_\nu \mathbf{h}_{[\gamma]} - u_\mu \mathbf{h}_{[\alpha]}\|^2)} \right] \end{aligned} \tag{5.28}$$

Proof. It follows from Eq. (5.27) that

$$\begin{aligned}\mathcal{I}(\mathbf{H}, U; \boldsymbol{Z}) = & \left\lfloor \log_2 \binom{N_T}{N_c} \right\rfloor + \log_2(S) - N_R \log_2(e) \\ & - \frac{1}{N_a S} \sum_{\nu=1}^{S} \sum_{\gamma=1}^{N_a} \mathbb{E}_{\mathbf{N}} \log_2 \left[\sum_{\mu=1}^{S} \sum_{\alpha=1}^{N_a} e^{-\frac{1}{N_o}\left(\|u_\nu \mathbf{h}_{[\gamma]} - u_\mu \mathbf{h}_{[\alpha]} + \mathbf{N}\|^2\right)} \right] \end{aligned} \tag{5.29}$$

Here $N_R \log_2(e)$ term arises from applying the expectation operator on the squared norm of noise only term in Eq. (5.27). Using Jensen's inequality and the concavity of the $\log(x)$

function, we can upper bound the expectation by swapping the expectation and logarithm operation.

$$\mathbb{E}_{\mathbf{N}} \log_2 \left[\sum_{\mu=1}^{S} \sum_{\alpha=1}^{N_a} e^{-\frac{1}{N_o}\left(\|u_\nu \mathbf{h}_{[\gamma]} - u_\mu \mathbf{h}_{[\alpha]} + \mathbf{N}\|^2\right)} \right]$$
$$\leq \log_2 \left[\sum_{\mu=1}^{S} \sum_{\alpha=1}^{N_a} \mathbb{E}_{\mathbf{N}} e^{-\frac{1}{N_o}\left(\|u_\nu \mathbf{h}_{[\gamma]} - u_\mu \mathbf{h}_{[\alpha]} + \mathbf{N}\|^2\right)} \right] \tag{5.30}$$

The norm square in the exponent is a non-central chi-square random variable $\chi^2_{2N_R}(s^2)$ with degrees of freedom equal to $2N_R$ and non-centrality parameter equal to $s^2 = \left\|u_\nu \mathbf{h}_{[\gamma]} - u_\mu \mathbf{h}_{[\alpha]}\right\|^2$. Let $\mathbf{Q} = \|\mathbf{N} + u_\nu \mathbf{h}_{[\gamma]} - u_\mu \mathbf{h}_{[\alpha]}\|^2$, then its moment generating function (MGF) is given as

$$\mathcal{M}_{\mathbf{Q}}(t) = \frac{1}{(1 - tN_o)^{N_R}} \exp\left(\frac{t\left\|u_\nu \mathbf{h}_{[\gamma]} - u_\mu \mathbf{h}_{[\alpha]}\right\|^2}{1 - tN_o} \right) \tag{5.31}$$

where $\mathcal{M}_{\mathbf{Q}}(t) = \mathbb{E}\left[e^{t\mathbf{Q}}\right]$. Calculating the above MGF at $t = -\frac{1}{N_o}$ yields the following expression.

$$\mathbb{E}_{\boldsymbol{Q}} \left[e^{-\frac{1}{N_o}\left(\|u_\nu \mathbf{h}_{[\gamma]} - u_\mu \mathbf{h}_{[\alpha]} + \mathbf{N}\|^2\right)} \right]$$
$$= \mathbb{E}_{\mathbf{Q}} \left[e^{-\frac{\mathbf{Q}}{N_o}} \right] = \log_2 \left[\sum_{\mu=1}^{S} \sum_{\alpha=1}^{N_a} \left(\frac{1}{2}\right)^{N_R} e^{-\frac{\|u_\nu \mathbf{h}_{[\gamma]} - u_\mu \mathbf{h}_{[\alpha]}\|^2}{2N_o}} \right] \tag{5.32}$$

On re-arrangement of the terms, we obtain Eq. (5.28). □

It can be observed clearly from Eq. (5.28) and Eq. (5.27) that at high SNR, the exponential terms die down. Thus, at high SNR, the gap between the achievable rate and the lower bound is $N_R(\log_2(e) - 1)$ which is independent of the channel realization, data symbol, modulation order and the number of transmit antennas.

Proposition 2. *For finite alphabets, achievable rates for GSM can be upper bounded as follows*

$$\mathcal{I}_U = \left\lfloor \log_2 \binom{N_T}{N_c} \right\rfloor + \log_2(S) \tag{5.33}$$
$$- \frac{1}{N_a S} \sum_{\nu=1}^{S} \sum_{\gamma=1}^{N_a} \log_2 \sum_{\mu=1}^{S} \sum_{\alpha=1}^{N_a} \exp\left(-\beta\left(\|u_\nu \mathbf{h}_{[\gamma]} - u_\mu \mathbf{h}_{[\alpha]}\|^2\right)\right)$$

Proof. As $\log \sum_k \exp(x_k)$ is a convex function, Jensen's inequality can be applied to the expression of average mutual information to derive an upper bound. We know for convex function $\varphi(x)$, Jensen's inequality reads,

$$\varphi(\mathbb{E}[\boldsymbol{x}]) \leq \mathbb{E}[\varphi(\boldsymbol{x})] \tag{5.34}$$

Thus, the expectation term with respect to noise can be lower bounded as follows.

$$\mathbb{E}_{\mathbf{N}} \log_2 \left[\sum_{\mu=1}^{S} \sum_{\alpha=1}^{N_a} \exp\left(-\beta \left(\|u_\nu \mathbf{h}_{[\gamma]} - u_\mu \mathbf{h}_{[\alpha]} + \mathbf{N}\|^2 - \|\mathbf{N}\|^2 \right)\right) \right] \tag{5.35}$$

$$\geq \log_2 \sum_{\mu=1}^{S} \sum_{\alpha=1}^{N_a} \exp\left(-\beta \mathbb{E}_{\mathbf{N}} \left(\|u_\nu \mathbf{h}_{[\gamma]} - u_\mu \mathbf{h}_{[\alpha]} + \mathbf{N}\|^2 - \|\mathbf{N}\|^2 \right)\right) \tag{5.36}$$

The expectation with respect to noise is calculated initially,

$$\mathbb{E}_{\mathbf{N}} \quad \left(\|u_\nu \mathbf{h}_{[\gamma]} - u_\mu \mathbf{h}_{[\alpha]} + \mathbf{N}\|^2 - \|\mathbf{N}\|^2 \right) \tag{5.37}$$

$$= \quad \mathbb{E}_{\mathbf{N}} \left[\|u_\nu \mathbf{h}_{[\gamma]} - u_\mu \mathbf{h}_{[\alpha]}\|^2 + 2\Re\{\mathbf{N}^H \left(u_\nu \mathbf{h}_{[\gamma]} - u_\mu \mathbf{h}_{[\alpha]} \right)\} \right] \tag{5.38}$$

$$= \quad \|u_\nu \mathbf{h}_{[\gamma]} - u_\mu \mathbf{h}_{[\alpha]}\|^2 \tag{5.39}$$

Now, the inequality in Eq. (5.36) can be simplified as follows.

$$\mathbb{E}_{\mathbf{N}} \log_2 \left[\sum_{\mu=1}^{S} \sum_{\alpha=1}^{N_a} \exp\left(-\beta \left(\|u_\nu \mathbf{h}_{[\gamma]} - u_\mu \mathbf{h}_{[\alpha]} + \mathbf{n}\|^2 - \|\mathbf{N}\|^2 \right)\right) \right]$$

$$\geq \log_2 \sum_{\mu=1}^{S} \sum_{\alpha=1}^{N_a} \exp\left(-\beta \left(\|u_\nu \mathbf{h}_{[\gamma]} - u_\mu \mathbf{h}_{[\alpha]}\|^2 - \|\mathbf{N}\|^2 \right)\right) \tag{5.40}$$

Using the inequality in Eq. (5.40), the upper bound of mutual information can be calculated as follows.

$$\mathcal{I}_U \quad = \left\lfloor \log_2 \binom{N_T}{N_c} \right\rfloor + \log_2(S) \tag{5.41}$$

$$- \quad \frac{1}{N_a S} \sum_{\nu=1}^{S} \sum_{\gamma=1}^{N_a} \log_2 \sum_{\mu=1}^{S} \sum_{\alpha=1}^{N_a} \exp\left(-\beta \left(\|u_\nu \mathbf{h}_{[\gamma]} - u_\mu \mathbf{h}_{[\alpha]}\|^2 \right)\right)$$

□

The gap between the lower and the upper bounds can be calculated as follows,

$$\begin{aligned}
\mathcal{I}_U &- \mathcal{I}_L = N_R \log_2(e) - N_R && (5.42)\\
&+ \frac{1}{N_a S}\sum_{\nu=1}^{S}\sum_{\gamma=1}^{N_a}\log_2\sum_{\mu=1}^{S}\sum_{\alpha=1}^{N_a}\exp\left(-\frac{\beta}{2}\left(\|u_\nu \mathbf{h}_{[\gamma]} - u_\mu \mathbf{h}_{[\alpha]}\|^2\right)\right)\\
&- \frac{1}{N_a S}\sum_{\nu=1}^{S}\sum_{\gamma=1}^{N_a}\log_2\sum_{\mu=1}^{S}\sum_{\alpha=1}^{N_a}\exp\left(-\beta\left(\|u_\nu \mathbf{h}_{[\gamma]} - u_\mu \mathbf{h}_{[\alpha]}\|^2\right)\right) && (5.43)\\
&= N_R \log_2(e) - N_R && (5.44)\\
&+ \frac{1}{N_a S}\sum_{\nu=1}^{S}\sum_{\gamma=1}^{N_a}\left[\log_2\frac{\sum_{\mu}\sum_{\alpha}\exp\left(-\frac{\beta}{2}\left(\|u_\nu \mathbf{h}_{[\gamma]} - u_\mu \mathbf{h}_{[\alpha]}\|^2\right)\right)}{\sum_{\mu=1}^{S}\sum_{\alpha=1}^{N_a}\exp\left(-\beta\left(\|u_\nu \mathbf{h}_{[\gamma]} - u_\mu \mathbf{h}_{[\alpha]}\|^2\right)\right)}\right]
\end{aligned}$$

In high SNR regime, the gap between the lower and the upper bounds of mutual information can be expressed as follows.

$$\lim_{\beta\to\infty}(\mathcal{I}_U - \mathcal{I}_L) = N_R(\log_2(e) - 1) \tag{5.45}$$

Similarly, in the low SNR regime the gap between the lower and the upper bounds of mutual information can be expressed as follows.

$$\lim_{\beta\to 0}(\mathcal{I}_U - \mathcal{I}_L) = N_R(\log_2(e) - 1) \tag{5.46}$$

Remark. *For a given number of receive anetnnas, the gap between lower and upper bounds in the regimes of low and high SNRs, is fixed and is independent of the channel realization, data symbol, modulation order and the number of transmit antennas.*

5.4 Mutual Information for Precoded Generalized Spatial Modulation Systems

The conventional spatial and GSM systems require CSI only at receiver to either perform maximal-ratio combining (MRC) technique for detection of antenna index or using

maximum-likelihood (ML) rule for joint detection of antenna indices and I-Q modulation symbols. The symbol error performance of these receivers becomes better as the SNR increases. In order to further boost the receiver SNR, we use maximum-ratio transmission (MRT), which requires the CSIT. As we are assuming downlink transmissions here and CSIT is available at BTS due to Massive MIMO regime, so we attempt to use MRT in which information symbol is transmitted along the most dominant eigen-mode of the transmission channel. As a result, SNR is boosted which ultimately improves the BER performance.

5.4.1 System Modeling

In precoded GSM system, first a subset of antennas is selected based on incoming bit pattern. Then a corresponding smaller-scale MIMO system is considered corresponding to those selected antennas. Afterwards, conventional eigen-beamforming vectors are calculated for smaller-scale MIMO system which are sparse if we take into account the anetnna domain of the actual large-scale MIMO systems where many antennas are deactivated. This process is illustrated with help of Fig. (5.1) where the activated antennas are shaded and the deactivated antennas are unshaded. In precoded GSM systems, the matrix-vector relation between the multi-antenna transmitter and the multi-antenna receiver may be expressed as follows.

$$\boldsymbol{z} = \boldsymbol{H}\mathbf{W}\boldsymbol{u} + \mathbf{n} \tag{5.47}$$

The dimensions of quantities in above relation follows $\boldsymbol{z} \in \mathbb{C}^{N_R}$, $\boldsymbol{H} \in \mathbb{C}^{N_R \times N_T}$, $\mathbf{W} \in \mathbb{C}^{N_T \times N_a}$, $\boldsymbol{u} \in \mathbb{C}^{N_a}$, and $\mathbf{n} \in \mathbb{C}^{N_R}$. In this setting, N_a like GSM systems, is equal to $2^{\lfloor \log_2 \binom{N_T}{N_c} \rfloor}$ where N_c is equal to the number of RF chains. The only difference from the modeling of the GSM systems is the presence of a precoding matrix $\mathbf{W}$ instead of an antenna activation matrix $\boldsymbol{P}$.

5.4.2 Analytical Framework

Let matrix $\mathbf{W}$ be a juxtaposition of eigenbeamforming vectors instead of antenna activation pattern vectors, then it can be mathematically expressed as follows.

$$\mathbf{W} = \begin{bmatrix} | & & | \\ \mathbf{w}_1 & \cdots & \mathbf{w}_{N_a} \\ | & & | \end{bmatrix} \tag{5.48}$$

The product of the transmission channel and the precoding matrix is an $N_R \times N_a$ matrix $\mathbf{\Phi}$ whose columns are precoded channel vectors onto one of them the symbol transmission is performed.

$$\mathbf{\Phi} = \boldsymbol{H}\mathbf{W} = \begin{bmatrix} | & & | \\ \boldsymbol{h}_1 & \cdots & \boldsymbol{h}_{N_T} \\ | & & | \end{bmatrix} \begin{bmatrix} | & & | \\ \mathbf{w}_1 & \cdots & \mathbf{w}_{N_a} \\ | & & | \end{bmatrix} \tag{5.49}$$

$$= \begin{bmatrix} | & & | \\ \boldsymbol{H}\mathbf{w}_1 & \cdots & \boldsymbol{H}\mathbf{w}_{N_a} \\ | & & | \end{bmatrix} \tag{5.50}$$

$$\mathbf{\Phi} = \begin{bmatrix} | & & | \\ \boldsymbol{\phi}_1 & \cdots & \boldsymbol{\phi}_{N_a} \\ | & & | \end{bmatrix} \in \mathbb{C}^{N_R \times N_a} \tag{5.51}$$

The precoded channel vector $\boldsymbol{\phi}_m = \boldsymbol{H}\mathbf{w}_m \in \mathbb{C}^{N_R}$ and is an N_c-sparse vector. Each precoding vector $\mathbf{w}_m$ ensures which particular set of antennas are activated due to the selection of the m-th precoding vector and consequently which particular transmission sub-channel is precoded. Moreover, the m-th particular precoding vector is itself being selected by the incoming bit sequence. The non-zero or active components of the precoding vector are taken from the right singular vector corresponding to the most dominant eigen-mode of the sub-channel matrix $\boldsymbol{H}\boldsymbol{E}_m$ which is the sub-matrix of the transmission channel $\boldsymbol{H}$.

Here $\boldsymbol{E}_m$ itself is a sub-matrix of identity matrix of order N_T whose columns are essentially unit vectors of N_T-dimensional space. The partial identity matrix $\boldsymbol{E}_m$ is a collection of unit vectors $\{\boldsymbol{e}_k\}_{k\in\mathcal{Z}_m}$ whose indices are being chosen from the underlying index set $\mathcal{Z}_m$ whose cardinality is N_c. Like GSM system, the index set is an ordered subset of the universal set of antennas' indices $\mathbb{A}$, i.e., $\mathcal{Z}_m :\subsetneq \mathbb{A} = \{1, 2, \cdots, N_T\}$. Thus, succinctly the precoding vector $\boldsymbol{w}_m$ and the partial identity matrix $\boldsymbol{E}_m$ may be expressed as

$$\boldsymbol{w}_m = \boldsymbol{E}_m \boldsymbol{v}_1 \left(\boldsymbol{H}\boldsymbol{E}_m\right) \tag{5.52}$$

$$\boldsymbol{E}_m = \left(\boldsymbol{e}_k\right)_{k\in\mathcal{Z}_m} \in \{0,1\}^{N_T\times|\mathcal{Z}_m|} \tag{5.53}$$

where $\boldsymbol{v}_1(\cdot)$ is the first column vector of the right singular matrix $\mathbf{V}$ in the singular value decomposition (SVD) of the the sub-channel matrix $\boldsymbol{\psi}_m = \boldsymbol{H}\boldsymbol{E}_m$ where SVD of $\boldsymbol{\psi}_m$ may be expressed as

$$\boldsymbol{\psi}_m = \mathbf{U}\boldsymbol{\Sigma}\mathbf{V}^{\dagger} \in \mathbb{C}^{N_R\times N_c} \tag{5.54}$$

Here $\mathbf{V} = [\boldsymbol{v}_1, \cdots, \boldsymbol{v}_{N_c}] \in \mathbb{C}^{N_c\times N_c}$ is the right singular matrix of sub-channel matrix $\boldsymbol{\psi}_m$, $\boldsymbol{\Sigma} = \mathsf{diag}\left[\sigma_1, \cdots, \sigma_r, 0, \cdots, 0\right] \in \mathbb{C}^{N_R\times N_c}$ is the diagonal matrix containing the singular values of $\boldsymbol{\psi}_m$ and $\mathbf{U} = [\boldsymbol{u}_1, \cdots, \boldsymbol{u}_{N_c}] \in \mathbb{C}^{N_R\times N_R}$ is the left singular matrix of $\boldsymbol{\psi}_m$. Here $r \leqslant \min\{N_R, N_c\}$ is the rank of $\boldsymbol{\psi}_m$. Thus, the precoded channel matrix $\boldsymbol{\Phi}$ can be expressed as follows

$$\boldsymbol{\Phi} = \begin{bmatrix} \Big| & & \Big| \\ \sum\limits_{i\in\mathcal{Z}_1} w_1(i)\boldsymbol{h}_i & \cdots & \sum\limits_{i\in\mathcal{Z}_{Na}} w_{N_a}(i)\boldsymbol{h}_{N_a} \\ \Big| & & \Big| \end{bmatrix} \tag{5.55}$$

Here $\boldsymbol{\Phi} \in \mathbb{C}^{N_R\times N_a}$ is the precoded channel matrix whose columns are beamformed composite channel vectors. Each of these columns is a weighted sum of different combination of transmit channel vectors of the physical transmission channel matrix where the weights

are complex scalars $\{w_k(i)\}_{i\in\mathcal{Z}_k}$. In each signalling interval, one of these beamformed composite channel vectors is modulated depending upon the incoming bit sequence. Under this analytical framework of signalling, it is convenient to express the received signal in the following form.

$$\boldsymbol{z} = \begin{bmatrix} | & & | \\ \boldsymbol{\phi}_1 & \cdots & \boldsymbol{\phi}_{N_a} \\ | & & | \end{bmatrix} \boldsymbol{u} + \mathbf{n} \tag{5.56}$$

$$\boldsymbol{z} = \boldsymbol{\phi}_\gamma u_\nu + \mathbf{n} \qquad \gamma = 1, \cdots, N_a \qquad \nu = 1, \cdots, S \tag{5.57}$$

Eqs. (5.56) and (5.57) are compatible owing to the fact that the sparsity of $\boldsymbol{u}$ is unity and the value of that active element is equal to u_ν. In terms of random variables, the input-output relation of the precoded GSM may be expressed as follows.

$$\boldsymbol{Z} = \boldsymbol{\Phi} U + \mathbf{N} \tag{5.58}$$

Here one information source is a random variable U whose one particular realization $u \in \mathcal{U} = \{u_1, u_2, \cdots, u_S\}$ is emitted by the random information source. The precoded sub-channel $\boldsymbol{\phi}_\gamma$ onto which a particular realization of u, i.e. , u_γ is sent is also selected by the incoming bits. Thus, precoded sub-channel is another random variable $\boldsymbol{\Phi}$ whose one particular realization $\boldsymbol{\phi} \in \boldsymbol{\Psi} = \{\boldsymbol{\phi}_1, \cdots, \boldsymbol{\phi}_{N_a}\}$ is used for signalling.

In precoded GSM systems, the information symbols and the precoded sub-channels are jointly mapped from the block of bits $p + q$ taken from the incoming datastreams. p bits are encoded to select a particular beamformed composite channel vector $\boldsymbol{\phi}_\gamma$ onto which a complex symbol is sent. q bits are encoded to select one out of $S = 2^q$ symbols, i.e., $\boldsymbol{u}_\nu$ which is then transmitted over the γ-th precoded composite channel. As a result, the received signal is also one particular realization of a random variable $\boldsymbol{Z}$. The proposed analytical framework results in an input-output relation for precoded GSM system which is useful for information theoretic treatment. It can be noticed easily that the precoded

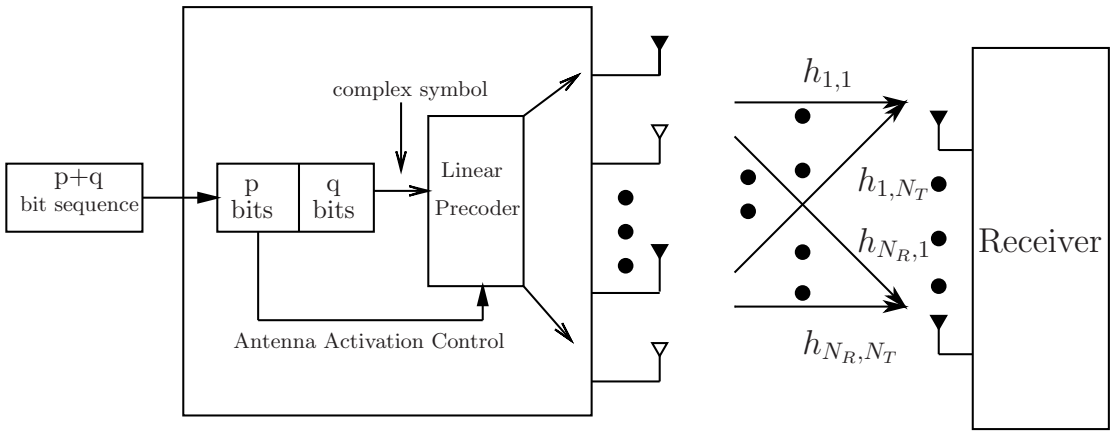

Figure 5.1: System model of single-user GSM precoder

sub-channel $\boldsymbol{\phi}_\gamma$ is not a linear combination of some transmit channel vectors instead it is a weighted sum of some transmit channel vectors where the complex weights perform precoding/beamforming. Nonetheless it is now straightforward to calculate mutual information owing to affine relationship between random variables U and $\boldsymbol{Z}$. The mutual information between the pair of random variables $(\boldsymbol{\Phi}, u)$ and the random variable $\boldsymbol{Z}$, $\mathcal{I}_{PGSM}$, can be defined as follows.

$$\mathcal{I}_{PGSM}((\boldsymbol{\Phi}, U)\,;\boldsymbol{Z}) := H((\boldsymbol{\Phi}, u)) - H((\boldsymbol{\Phi}, u)\,\big|\boldsymbol{Z}) \tag{5.59}$$

Thus, the calculation of $\mathcal{I}_{PGSM}((\boldsymbol{\Phi}, U)\,;\boldsymbol{Z})$ necessitates the computations of the joint and conditional entropies $H((\boldsymbol{\Phi}, U))$ and $H((\boldsymbol{\Phi}, U)\,\big|\boldsymbol{Z})$ which are performed in the upcoming sections.

5.4.3 Calculation of $H((\boldsymbol{\Phi}, U))$

The joint entropy of the precoded sub-channel and the information source can be simplified by the application of chain rule for entropies. Thus, the joint entropy is the sum of the entropy of the random information source and the conditional entropy of the precoded

sub-channel given the random information source.

$$H((\mathbf{\Phi}, U)) = H(U) + H(\mathbf{\Phi}\big|U) \tag{5.60}$$

Since the random information source and the precoded sub-channel are statistically independent, so the conditional entropy is equal to the unconditional entropy.

$$\begin{aligned} H((\mathbf{\Phi}, U)) &= H(U) + H(\mathbf{\Phi}) && (5.61)\\ &= \log_2(S) + \log_2 \left\lfloor \binom{N_T}{N_c} \right\rfloor && (5.62) \end{aligned}$$

5.4.4 Calculation of $H((\mathbf{\Phi}, U)\,\big|\boldsymbol{Z})$

The application of the chain rule of entropies results in the following breakdown.

$$H((\mathbf{\Phi}, U)\,\big|\boldsymbol{Z}) = H(U\big|\boldsymbol{Z}) + H(\mathbf{\Phi}\big|U, \boldsymbol{Z}) \tag{5.63}$$

The calculation of $H(U\big|\boldsymbol{Z})$ follows from taking the joint expectation of the function $\log_2 p_{U|Z}(u\big|\boldsymbol{Z})$ with respect to underlying random variables U and $\boldsymbol{Z}$.

$$\begin{aligned} H(U\big|\boldsymbol{Z}) &= -\mathbb{E}_{U,\boldsymbol{Z}}\left[\log_2 p_{U|Z}(U\big|\boldsymbol{Z})\right] && (5.64)\\ &= -\sum_{\boldsymbol{\phi}\in\mathbf{\Psi}} \mathbb{E}_{U,\boldsymbol{Z}|\mathbf{\Phi}}\left[\log_2 p_{U|Z}(U\big|\boldsymbol{Z})\right] p_{\mathbf{\Phi}}(\boldsymbol{\phi}) && (5.65)\\ &= -\mathbb{E}_{\mathbf{\Phi}}\mathbb{E}_{U,\boldsymbol{Z}|\mathbf{\Phi}}\left[\log_2 p_{U|Z}(U\big|\boldsymbol{Z})\right] && (5.66)\\ &= -\mathbb{E}_{U,\boldsymbol{Z},\mathbf{\Phi}}\left[\log_2 p_{U|Z}(U\big|\boldsymbol{Z})\right] && (5.67)\\ &= -\mathbb{E}_{(U,\mathbf{\Phi})}\mathbb{E}_{\boldsymbol{Z}|(U,\mathbf{\Phi})}\left[\log_2 p_{U|Z}(U\big|\boldsymbol{Z})\right] && (5.68)\\ &= -\frac{1}{N_a S}\sum_{\nu=1}^{S}\sum_{\gamma=1}^{N_a} \mathbb{E}_{\boldsymbol{Z}|(U,\mathbf{\Phi})}\left[\log_2 p_{U|Z}(U\big|\boldsymbol{Z})\right] && (5.69) \end{aligned}$$

Here the second equation follows from averaging out the underlying randomness of $\mathbf{\Phi}$. The averaging is performed by summing the products of expectation conditioned on a given realization of $\mathbf{\Phi}$ and probability of corresponding realization for all the realizations.

Now, we focus on the inner expectation in the last equation and compute it via insertion of log-likelihood function.

$$H(U\big|\boldsymbol{Z}) = -\frac{1}{N_a S}\sum_{\nu=1}^{S}\sum_{\gamma=1}^{N_a}\mathbb{E}_{\boldsymbol{Z}|(U,\boldsymbol{\Phi})}\log_2\left[\frac{\displaystyle\sum_{\alpha=1}^{N_a}\exp\left(-\beta\left\|\boldsymbol{z}-\boldsymbol{\phi}_\alpha u_\nu\right\|^2\right)}{\displaystyle\sum_{\alpha=1}^{N_a}\sum_{\mu=1}^{S}\exp\left(-\beta\left\|\boldsymbol{z}-\boldsymbol{\phi}_\alpha u_\mu\right\|^2\right)}\right]$$

where $\beta = \frac{1}{N_o}$. Since the random variable $\boldsymbol{Z}$ is conditional on U and $\boldsymbol{\Phi}$ in the above expectation, so the main randomness in $\boldsymbol{Z}$ owes to the underlying noise random variable $\mathbf{N}$. As a result, we deem it feasible to make the substitution $\boldsymbol{z} = \boldsymbol{\phi}_\gamma u_\nu + \mathbf{n}$ to have the following simplification.

$$H(U|\boldsymbol{Z}) = \frac{1}{N_a S}\sum_{\nu=1}^{S}\sum_{\gamma=1}^{N_a}\mathbb{E}_{\mathbf{N}}\log_2\left[\frac{\displaystyle\sum_{\mu=1}^{S}\sum_{\alpha=1}^{N_a}\exp\left(-\beta\left\|u_\nu\boldsymbol{\phi}_\gamma - u_\mu\boldsymbol{\phi}_\alpha + \mathbf{N}\right\|^2\right)}{\displaystyle\sum_{\gamma=1}^{N_a}\exp\left(-\beta\left\|u_\mu\left(\boldsymbol{\phi}_\gamma - \boldsymbol{\phi}_\alpha\right) + \mathbf{N}\right\|^2\right)}\right]$$

The evaluation of $H(\boldsymbol{\Phi}\big|U,\boldsymbol{Z})$ is quite involved and it needs application of chain rule of entropies and the law of iterated expectations. The conditional entropy may be calculated by taking the negative expectation of $\log_2 p_{\boldsymbol{\Phi}|U,\boldsymbol{Z}}(\boldsymbol{\phi}|u,\boldsymbol{z})$ with respect to underlying random variables $U, \boldsymbol{Z}, \boldsymbol{\Phi}$.

$$H(\boldsymbol{\Phi}\big|U,\boldsymbol{Z}) = -\mathbb{E}_{\boldsymbol{Z},\boldsymbol{\Phi},U}\left[\log_2 p_{\boldsymbol{\Phi}|(u,\boldsymbol{z})}(\boldsymbol{\phi}|u,\boldsymbol{z})\right] \tag{5.70}$$

Now it is quite straightforward to apply law of iterated expectations to have the following conditional and marginal expectations.

$$\begin{aligned} H(\boldsymbol{\Phi}\big|U,\boldsymbol{Z}) &= -\mathbb{E}_{(U,\boldsymbol{\Phi})}\mathbb{E}_{\boldsymbol{Z}|(U,\boldsymbol{\Phi})}\left[\log_2 p_{\boldsymbol{\Phi}|(U,\boldsymbol{Z})}(\boldsymbol{\phi}|u,\boldsymbol{z})\right] &(5.71)\\ &= -\frac{1}{N_a S}\sum_{\nu=1}^{S}\sum_{\gamma=1}^{N_a}\mathbb{E}_{\boldsymbol{Z}|(U,\boldsymbol{\Phi})}\left[\log_2 p_{\boldsymbol{\Phi}|(U,\boldsymbol{Z})}(\boldsymbol{\phi}|u,\boldsymbol{z})\right] &(5.72)\end{aligned}$$

Using Bayes' rule, the posterior pdf $p_{\boldsymbol{\Phi}|(U,\boldsymbol{Z})}(\boldsymbol{\phi}|u,\boldsymbol{z})$ may be expressed as follows.

$$p_{\boldsymbol{\Phi}|(U,\boldsymbol{Z})}(\boldsymbol{\phi}|u,\boldsymbol{z}) = \frac{\exp\left(-\beta\left\|\boldsymbol{z}-\boldsymbol{\phi}_\gamma u_\nu\right\|^2\right)}{\sum_{\alpha=1}^{N_a}\exp\left(-\left\|\boldsymbol{z}-\boldsymbol{\phi}_\alpha u_\nu\right\|^2\right)} \tag{5.73}$$

Substituting the above posterior pdf into Eq. (5.72) yields,

$$H(\boldsymbol{\Phi}\big|U=u,\boldsymbol{Z}) = \frac{1}{N_a S}\sum_{\nu=1}^{S}\sum_{\gamma=1}^{N_a}\mathbb{E}_{\boldsymbol{Z}|(U,\boldsymbol{\Phi})}\log_2\left[\sum_{\alpha=1}^{N_a}\exp\left(\beta\left\|\boldsymbol{z}-\boldsymbol{\phi}_\gamma u_\nu\right\|^2-\beta\left\|\boldsymbol{z}-\boldsymbol{\phi}_\alpha u_\nu\right\|^2\right)\right]$$

where in above substitution, we have absorbed the minus sign into the argument of the logarithm. Since $\boldsymbol{Z}$ is conditional on $\boldsymbol{\Phi}$ and U, therefore, it is convenient to do the substitution $\boldsymbol{z}=\boldsymbol{\phi}_\gamma u_\nu+\mathbf{n}$ in order to make the following changes.

$$H(\boldsymbol{\Phi}\big|U,\boldsymbol{Z}) = \frac{1}{N_a S}\sum_{\nu=1}^{S}\sum_{\gamma=1}^{N_a}\mathbb{E}_{\mathbf{N}}\left[\log_2\left(\sum_{\alpha=1}^{N_a}\exp\left\{\beta\|\mathbf{N}\|^2-\beta\left\|u_\nu\boldsymbol{\phi}_\gamma-\boldsymbol{\phi}_\alpha+\mathbf{N}\right\|^2\right\}\right)\right]$$

Now to obtain the conditional entropy $H((\boldsymbol{\Phi},U)\,\big|\boldsymbol{Z})$, we add the $H(U\big|\boldsymbol{Z})$ and $H(\boldsymbol{\Phi}\big|U,\boldsymbol{Z})$ to have the following expression.

$$H((\boldsymbol{\Phi},U)\,\big|\boldsymbol{Z}) = \frac{1}{N_a S}\sum_{\nu=1}^{S}\sum_{\gamma=1}^{N_a}\mathbb{E}_{\mathbf{N}}\left[\sum_{\mu=1}^{S}\sum_{\alpha=1}^{N_a}\exp\left\{\beta\left(\|\mathbf{N}\|^2-\left\|u_\nu\boldsymbol{\phi}_\gamma-u_\mu\boldsymbol{\phi}_\alpha+\mathbf{N}\right\|^2\right)\right\}\right]$$

Substituting values in Eq. (5.59) yields the following result.

$$\mathcal{I}_{PGSM}\left((\boldsymbol{\Phi},U);\boldsymbol{Z}\right) = \left\lfloor\log_2\tbinom{N_T}{N_c}\right\rfloor+\log_2(S) \tag{5.74}$$

$$-\tfrac{1}{N_aS}\sum_{\nu=1}^{S}\sum_{\gamma=1}^{N_a}\mathbb{E}_{\mathbf{N}}\log_2\left[1+\sum_{\substack{\mu=1\\(\mu,\alpha)\neq(\nu,\gamma)}}^{M}\sum_{\alpha=1}^{N_a}\exp\left\{\frac{1}{N_o}\left(\|\mathbf{N}\|^2-\left\|u_\nu\boldsymbol{\phi}_\gamma-u_\mu\boldsymbol{\phi}_\alpha+\mathbf{N}\right\|^2\right)\right\}\right] \tag{5.75}$$

Using Eq. (5.4.2) into above equation, we obtain

$$\mathcal{I}_{PGSM}\left((\boldsymbol{\Phi},u);\boldsymbol{z}\right) = \left\lfloor\log_2\binom{N_T}{N_c}\right\rfloor+\log_2(S)-\frac{1}{N_aS}\sum_{\nu=1}^{S}\sum_{\gamma=1}^{N_a}\mathbb{E}_{\mathbf{N}}$$

$$\log_2\left[1+\sum_{\substack{\mu=1\\(\mu,\alpha)\neq(\nu,\gamma)}}^{S}\sum_{\alpha=1}^{N_a}\exp\left\{\beta\left(\|\mathbf{N}\|^2-\left\|u_\nu\sum_{m\in\mathcal{Z}_\gamma}w_\gamma(m)\boldsymbol{h}_m-u_\mu\sum_{m\in\mathcal{Z}_\alpha}w_\alpha(m)\boldsymbol{h}_m+\mathbf{N}\right\|^2\right)\right\}\right]$$

where $\beta=\frac{1}{N_o}$ represents the channel SNR.

5.5 Numerical Experiments

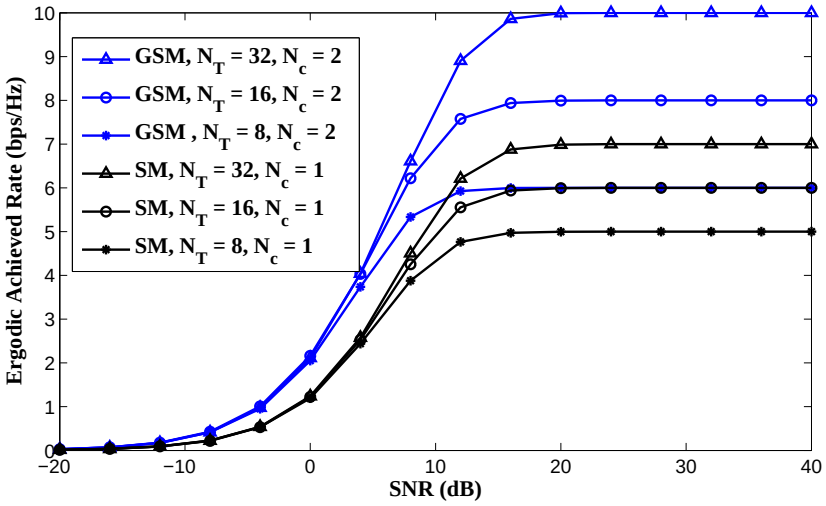

Figure 5.2: Achievable Rates verus SNR for SM and GSM

All the discussion so far is for a fixed $N_R \times N_T$ matrix $\boldsymbol{H}$. However, the ergodic achievable rate when $\boldsymbol{H}$ is random and known at the receiver is easily shown to be the expectation of the mutual information calculated in Eq. (5.27), averaged over $\boldsymbol{H}$. The numerical results below are for the i.i.d. Rayleigh model with independent channel coefficients, $N_R = 3$ and N_T is varied. Without loss of generality, the modulation scheme is assumed to be QPSK, i.e., $S = 4$. Due to high numerical complexity incurred due to huge number of antenna combinations, the number of Monte Carlo runs is set to be equal to ten for GSM simulations.

In Fig. 5.2, the achieved mutual information (in bps/Hz) is plotted versus SNR (in dB) for GSM and SM to facilitate comparison. It is evident from the figure that GSM

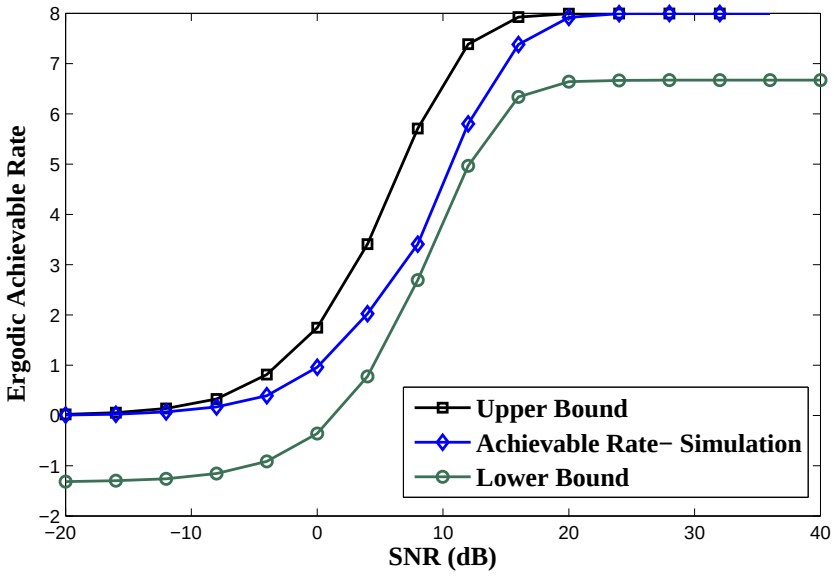

Figure 5.3: Achieved Rates comparison of GSM with 3×3 MIMO

beats SM in terms of achievable rates for the same numbers of transmit and receive antennas. For instance for $N_T = 8$, GSM spectral efficiency is 6 bps/Hz and SM spectral efficiency is 5 bps/Hz. Moreover in SM, if we double the number of transmit antennas, the improvement in spectral efficiency is only 1 bps/Hz, however, in GSM, the improvement is N_c bps/Hz. For $N_T = 16$, the GSM spectral efficiency is 8 bps/Hz and for $N_T = 32$, the GSM spectral efficiency is 10 bps/Hz and the increase in spectral efficiency is 2 bps/Hz which is the number of activated RF chains. For $N_T = 16$, SM offers spectral efficiency of 6 bps/Hz and for $N_T = 8$, GSM offers the same spectral efficiency. Thus the size of channel matrix is halved for same spectral efficiency which leads to decrease in cost of channel measurements.

In Fig. 5.3, the ergodic achievable rates, which are the Monte-Carlo average of Eq. (5.27) with respect to channel realizations, of a GSM system with $N_T = 16, N_c = 2$ is simulated. The expressions of the lower and upper bounds for same parameters are plotted. The upper bound coincides with the simulated achievable rate in low and high SNR regimes. The gap between upper and lower bounds in the low and high SNR regimes

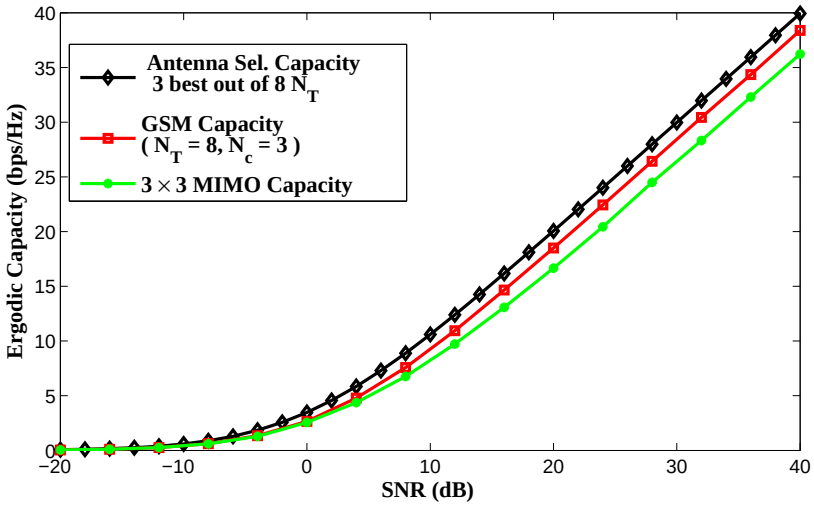

Figure 5.4: Capacity comparison of GSM with 3×3 MIMO and Antenna Selection MIMO

is fixed. In low and high SNR regimes, upper bound coincides with simulated rate and in medium SNR regime lower bound is more close to the simulated rate in terms of rate gap.

In Fig. 5.4, the capacity of a GSM system is compared with the capacity results of some previous schemes. The antenna selection capacity and MIMO capacity curves are averaged over $10,000$ channel realizations. The antenna selection capacity curve is when the transmitter knows the channel matrix and can select the best 3 antennas [68]. The GSM capacity curve is the capacity with 8 transmit antennas, 3 RF chains and 3 receive antennas with no constraint on the input alphabet, as calculated in [50]. The 3×3 MIMO capacity curve is the capacity of traditional MIMO with 3 transmit antennas and 3 receive antennas. 3×3 MIMO is used as a baseline because we are evaluating the performance of GSM using only 3 RF chains at transmitter and receiver and 3×3 MIMO also uses the same amount of RF chains on both sides. The GSM capacity beats the 3×3 MIMO capacity because of the extra information stored in the antenna indices. Moreover, it performs nearly as well as antenna selection without the need for channel knowledge at the transmitter. The GSM scheme does not need any CSIT whereas antenna selection requires

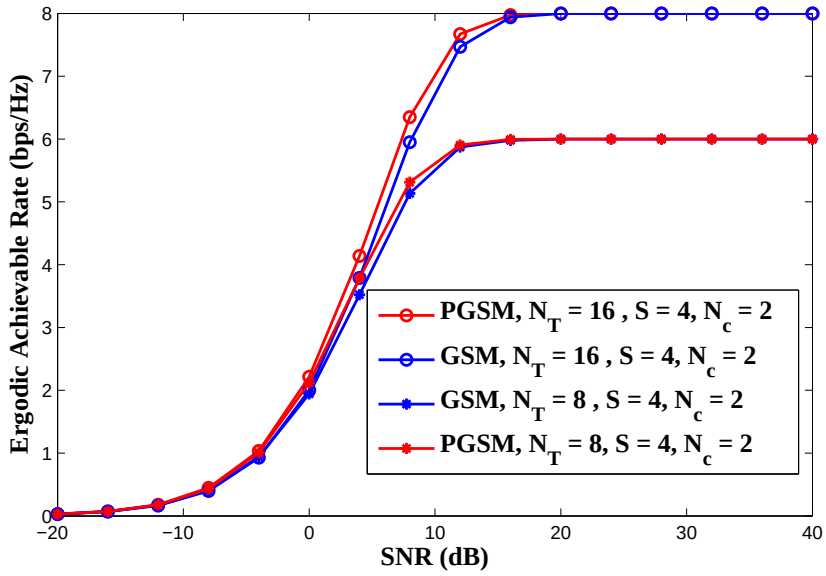

Figure 5.5: Achievable Rates verus SNR for Precoded GSM

CSIT in order to select the best antennas. Thus, antenna selection MIMO achieves better performance than GSM MIMO at the expense of CSIT.

In Fig. 5.5, the ergodic achievable rates for precoded GSM and GSM are compared for $N_T = 8, 16, N_c = 2$. In low and high SNR regimes, the rate performance of precoded GSM and that of GSM is same. However, in the medium SNR regime, i.e., $0 - 10$ dB, precoded GSM outperforms the GSM and for higher number of transmit antennas for fixed number of RF chains, the rate improvement increases. This rate improvement comes from extra degrees of freedom arising from more antennas although the activated antennas are same in both cases.

5.6 Conclusion

This chapter provided a closed-form expression for the achievable information rate of GSM systems using finite input alphabets. Reasonably tight upper and lower bounds

were calculated in an information-theoretic framework. We showed that a GSM system can offer same information rate as the SM system but using less transmit antennas and with a lower channel estimation burden. Additionally, the achievable rate for a precoded GSM system is derived whose performance is shown to be superior to GSM system via numerical results. As the capacity of antenna selection is more than that of GSM system for fixed parameters, we focus on antenna selection aided beamforming for massive MIMO in next chapter.

Chapter 6

Large System Analysis of Antenna Selection aided Downlink Beamforming in Massive MISO under RF Chains Constraint

The previous chapter was about GSM in which a group of antennas is selected based on incoming data. We have shown through numerical results in last chapter that capacity of antenna selection is better than that of GSM for same number of transmit antennas and RF chains. Thus, antenna selection is a promising solution to deal with limited number of RF chains in massive MIMO. Antenna selection can exploit the massive spatial degrees of freedom offered by huge number of antenna elements under RF chains constraint. In this chapter, we focus on performing a large system analysis of antenna selection aided single-user massive MISO setup with a huge array of transmit antennas sending data to a single user. This analysis enables us to investigate how the capacity scales asymptotically with the number of transmit antennas without conducting extensive Monte Carlo simulations.

This chapter is organized as follows. Section 6.1 highlights the motivation and the related work. Section 6.2 presents the system modelling and the problem statement for the considered system. Section 6.3 illustrates the large system analysis and Section 6.4 provides the associated lower and upper bounds on the capacity of the antenna selection aided beamforming system. Section 6.5 provides numerical experiments and Section 6.6 concludes the chapter.

6.1 Motivation and Related Work

Antenna Selection is a well-studied technique for traditional MIMO systems. In antenna selection, a subset of transmit antennas is chosen at every signaling instant and RF chains are connected to those chosen transmit antennas only. The chosen transmit antennas are the ones which have best channel conditions. The selection criterion can be maximization of channel capacity, SNR at the receiver, or the maximization of minimum eigenvalue of the channel [68]. The reduction of active transmit antennas leads to reduction of required RF chains which results in significant savings while preserving the advantages of full MIMO system. When the number of antennas at the BTS is large, there are multiple links between the transmit antennas at the BTS and the antennas at the user thereby creating much more spatial selectivity from which the system performance can be greatly enhanced. When the number of antennas is large, the antenna selection scheme will have a large number of subsets of transmit antennas from which BTS selects the subset with the best channel conditions and then the RF chains will be connected to the chosen transmit antennas.

Antenna Selection has been studied recently for massive MIMO. It has been considered feasible for massive MIMO by the experimental results, because only a subset of the antennas actually contributes to the achieved sum rate in many scenarios [69]. In [70],

transmit antenna selection is studied using channels taken from practical measurement campaigns. The authors used convex optimization to select the best antenna subset which maximizes the dirty-paper coding (DPC) capacity. Thus, they used the knowledge of measured channels to find the subset of antennas which maximize the DPC capacity for a given number of antennas to be selected for transmission. Their results show that in the regime of more transmit antennas than the RF chains, the antenna selection can greatly enhance the system performance. In [71], a robust constant-envelope (CE) precoding with antenna-subset selection in a large scale MIMO system is studied under the assumption that only imperfect channel knowledge is available at the transmitter. CE precoding enables the use of cheap but highly power-efficient amplifiers and antenna selection is known for reducing the number of RF chains. The combination of antenna selection with CE precoding, leads to cost cutting in hardware implementation. Particularly, the authors formulate a power minimisation problem for antenna selection CE precoding where symbol-error rate (SER) is less than a preset threshold. Further, they propose an approximation for NP-hard optimisation problem based on greedy knapsack approximation. In [72], the authors propose an algorithm for downlink massive MIMO systems under the constraint of a finite number of RF chains. The proposed algorithm enables joint antenna selection and user scheduling to take advantage of spatial selectivity and multi-user diversity gains offered by antenna selection and user scheduling respectively. Specifically, the proposed algorithm successively eliminates both undesired users and BTS antennas which yield minor contribution to system's performance. Numerical results show that the joint optimization strategy performs close to optimal exhaustive search. In [73], an antenna selection algorithm for massive MIMO uplink is proposed under the assumption of imperfect CSI and correlated channels. In their work, they exploited the sparsity of channel gain vectors at the BTS end. Particularly, they use a compressive sensing algorithm namely orthogonal-matching pursuit (OMP) to estimate the sparse structure of

beamformer. Simulation results indicate that the proposed scheme can offer comparable performance to MRC notwithstanding imperfect CSI and spatial correlation among BTS antennas.

GSM system can offer enhanced spectral efficiency in massive MIMO under limited RF chains. However, this comes at the cost of increase in receiver complexity. Moreover, MS must need to know the CSI in order to do data detection. In massive MIMO operating in TDD mode, as CSI is measured at BTS so it is an overhead to send the channel information of all the links to the MS via feedback link. In antenna selection, the MS do not need to know the individual link gains. It just needs the knowledge of sum power gain of the channel which being a scalar can be reported to MS via feedback link with less overhead. Thus, we focus on antenna selection capacity analysis in this chapter in the large system dimensions.

In this chapter, we provide the deterministic equivalent of the capacity of antenna selection based beamforming in massive MISO systems. We use the fact that once we know the best transmit antennas and their corresponding channel gains, conjugate beamforming at the transmitter side is optimal [74]. The capacity of the considered system is a random variable and changes as the channel realization changes, but in our scaling regime the fluctuations become small as the number of antennas grows large, in a law of large numbers (see Theorem 3). It provides a capacity scaling law using a law of large numbers for single-user massive MISO systems under RF chains constraint when antenna selection is employed. Deterministic upper and lower bounds on the capacity are derived. The derived capacity deterministic equivalent can be used for calculating the required number of RF chains for a given capacity and fixed number of transmit antennas in the large system dimensions.

6.2 System modeling and Problem Statement

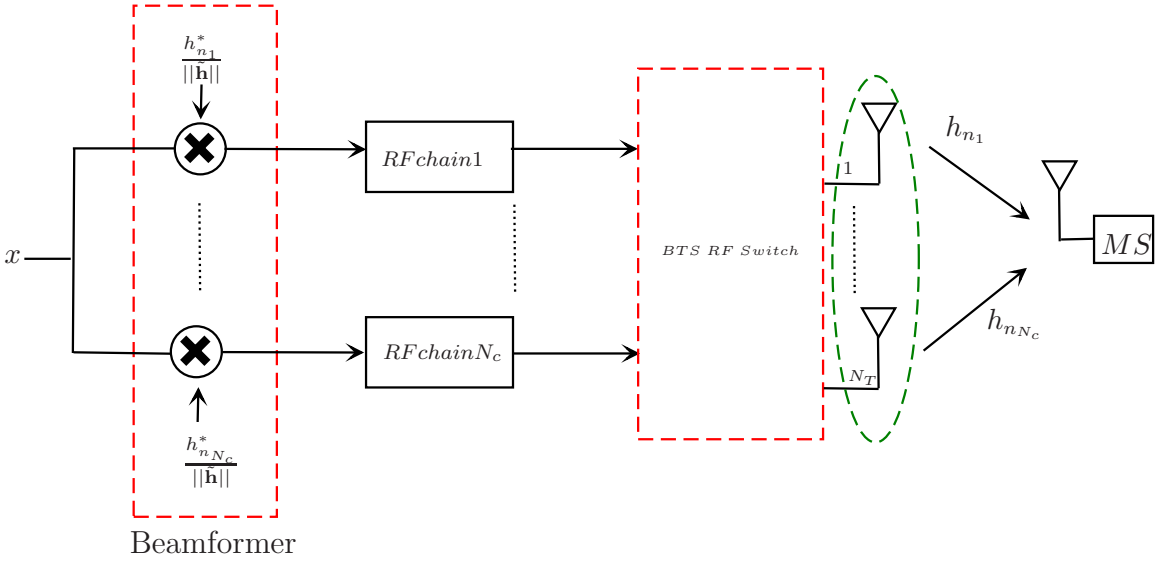

Figure 6.1: Schematic of Antenna Selection based Beamforming in Massive MIMO

A point-to-point massive MIMO system is considered in which a BTS has N_T transmit antennas and it sends data to a single-antenna MS in the downlink mode. The transmission channel between any of the N_T transmit antennas and the MS is assumed to be frequency-flat Rayleigh fading channel. The $1 \times N_T$ complex equivalent baseband channel can be expressed as follows.

$$\boldsymbol{h} = [h_1 \cdots h_{N_T}] \tag{6.1}$$

where $h_i \sim \mathcal{CN}(0, \sigma_h^2)$ is the complex channel gain of the link between the i-th transmit antenna of the BTS and the MS. Let N_c be the number of RF chains.

The transmitter is assumed to have perfect knowledge of all the channel gains $\{h_i\}_{i=1}^{N_T}$. The channel estimation is performed by first sending pilot symbols from the MS to the BTS in the uplink mode thanks to the TDD mode assumption in massive MIMO systems. More specifically, we connect the N_c RF chains to N_c different antennas out of N_T antennas in each training slot. Thus, in N_T/N_c training slots, we can sound all the link gains. As we know the training symbol at the BTS, employing the least square channel estimation

amounts to dividing the received signal vector by the training symbol at the BTS. For instance, for 100 antennas at BTS with 10 RF chains, we need 10 training slots to estimate all the 100 link gains. Owing to limited number of RF chains, we need proportionately higher number of training slots to estimate all the channel gains.

In order to boost the receiver SNR, beamforming is performed. Owing to the fact that we have limited number of RF chains, the N_c best transmit antennas are first selected and then the RF chains are connected to selected N_c transmit antennas. After choosing the best N_c transmit antennas, a beamforming vector is chosen which maximizes the received SNR. The schematic of antenna selection based beamforming in Massive MIMO is shown in Fig. 6.1. The beamforming vector is constructed using the CSI. Now, the received signal at the MS can be expressed as follows.

$$z = \boldsymbol{h}\boldsymbol{w}x + \mathsf{n} \tag{6.2}$$

Here $z \in \mathbb{C}$ is the received signal at the MS, $\boldsymbol{w}$ is an $N_T \times 1$ beamforming vector, $x \in \mathbb{C}$ is the transmitted symbol from the BTS and $\mathsf{n} \sim \mathcal{CN}(0, \sigma_{\mathsf{n}}^2)$ is circularly-symmetric complex AWGN. The signal power is assumed to be P, i.e., $\mathbb{E}\left[|x|^2\right] = P$. Let $\mathcal{I}^{(N_T)}$ be the subset of $\{1, 2, \cdots N_T\}$ which consists of the indices of the N_c antennas which corresponds to the best channel gains. Thus, we may express $\mathcal{I}^{(N_T)}$ as follows,

$$\mathcal{I}^{(N_T)} = \{n_1, n_2, \cdots, n_{N_c}\} \tag{6.3}$$

where $n_1, n_2, \cdots, n_{N_c}$ are the antennas' indices whose channel gains would be ordered as follows,

$$|h_{n_1}|^2 \geq |h_{n_2}|^2 \geq \cdots \geq |h_{n_{N_c}}|^2 \tag{6.4}$$

where $n_1 = \arg\max_i |h_i|^2$, and $|h_{n_{N_c}}|^2$ is smaller than all the link gains. Thus, $\mathcal{I}^{(N_T)}$ consists of the indices of the N_c largest components of $\{|h_1|, |h_2|, \cdots, |h_{N_T}|\}$.

Let $\tilde{\boldsymbol{h}}$ represent the subset of channel gains which are used for data transmission. The components of $\tilde{\mathbf{h}}$, i.e., $\tilde{\boldsymbol{h}}_n$'s will be zero when n is not an element of $\mathcal{I}^{(N_T)}$ and $\tilde{\boldsymbol{h}}_n$ will be equal to $\boldsymbol{h}_n$ when n is an element of $\mathcal{I}^{(N_T)}$.

$$\tilde{\boldsymbol{h}}_n = \begin{cases} 0 & : n \notin \mathcal{I}^{(N_T)} \\ \boldsymbol{h}_n & : n \in \mathcal{I}^{(N_T)} \end{cases}$$

The precoding vector has the same sparsity pattern as $\tilde{\boldsymbol{h}}$. However, its active components are normalized so that the maximum sum power radiated by the N_c transmit antennas during one symbol duration is P regardless of the number of RF chains used. Thus,

$$\boldsymbol{w}_n = \begin{cases} 0 & : n \notin \mathcal{I}^{(N_T)} \\ \frac{\tilde{\boldsymbol{h}}_n^*}{\sqrt{\sum_{n \in \mathcal{I}^{(N_T)}} |\boldsymbol{h}_n|^2}} & : n \in \mathcal{I}^{(N_T)} \end{cases}$$

The product of the actual channel vector and the precoding vector can be simplified as follows.

$$\begin{aligned} \boldsymbol{h}\boldsymbol{w} &= \frac{\sum_{n \in \mathcal{I}^{(N_T)}} |\boldsymbol{h}_n|^2}{\sqrt{\sum_{n \in \mathcal{I}^{(N_T)}} |\boldsymbol{h}_n|^2}} && (6.5) \\ &= \sqrt{\sum_{n \in \mathcal{I}^{(N_T)}} |\boldsymbol{h}_n|^2} && (6.6) \\ &= \|\tilde{\mathbf{h}}\| && (6.7) \end{aligned}$$

Thus, our system is equivalent to a SISO system with channel gain equal to $\|\tilde{\mathbf{h}}\|$ where $\|\tilde{\mathbf{h}}\|^2$ is the power of the vector which represents the subset of antennas with N_c largest

channel gains. Now, the received SNR can be expressed as follows.

$$\begin{aligned}
\mathsf{SNR} &= \frac{P\|\tilde{\boldsymbol{h}}\|^2}{\sigma_n^2} && (6.8)\\
&= \frac{P}{\sigma_n^2}\sum_{n\in\mathcal{I}^{(N_T)}}|h_n|^2 && (6.9)\\
&= \frac{P}{\sigma_n^2}\sum_{i=1}^{N_c}|h_{n_i}|^2 && (6.10)\\
&= \frac{PN_T}{\sigma_n^2}\frac{1}{N_T}\sum_{i=1}^{N_c}|h_{n_i}|^2 && (6.11)
\end{aligned}$$

Thus, the channel capacity of the RF-chains constrained beamforming system can be expressed as follows.

$$\begin{aligned}
C=&\log_2\left(1+\frac{PN_T}{\sigma_n^2}\frac{1}{N_T}\sum_{i=1}^{N_c}|h_{n_i}|^2\right) && (6.12)\\
=&\log_2(\gamma N_T)+\log_2\left(\frac{1}{N_T}\sum_{i=1}^{N_c}|h_{n_i}|^2\right)+\mathcal{O}\left(\frac{1}{N_T}\right) && (6.13)
\end{aligned}$$

where $\gamma=\frac{P}{\sigma_n^2}$ is the transmit SNR.

For large system dimensions, it is numerically expensive task to find the statistical average of above expression which motivates us to do large system's analysis in the following section.

6.3 Large System's Analysis

We proceed to the large system's analysis of the capacity in Eq. (6.13) in the limit as N_c, N_T grow large while keeping the ratio of the number of RF chains to the total number of transmit antennas $\beta=\frac{N_c}{N_T}$ fixed. The basic idea is to apply the strong law of large numbers to the term $\frac{1}{N_T}\sum_{n\in\mathcal{I}^{(N_T)}}|h_n|^2$. Using strong law of large numbers, we obtain an deterministic equivalent of $\frac{1}{N_T}\sum_{n\in\mathcal{I}^{(N_T)}}|h_n|^2$ which will be used to calculate the deterministic equivalent of the channel capacity of the considered system. Furthermore, we calculate the lower and upper bounds on the asymptotic capacity C^*.

Theorem 3. *Let* $\frac{1}{N_T}\sum_{i\in\mathcal{I}^{(N_T)}}|h_i|^2$ *be the normalized channel power gain of an antenna selection based MISO beamforming system with* N_T *transmit antennas and bounded link gains* $(\mathbb{E}(|h|^2)<\infty)$*, then* $\frac{1}{N_T}\sum_{i\in\mathcal{I}^{(N_T)}}|h_i|^2$ *as* $N_T\uparrow\infty$ *with* β *held fixed, converges almost surely as follows*

$$\frac{1}{N_T}\sum_{i\in\mathcal{I}^{(N_T)}}|h_i|^2 \xrightarrow[N_T\uparrow\infty]{a.s.} \int_{\zeta(\beta)}^{\infty}\zeta dF_{|h|^2}(\zeta) \tag{6.14}$$

where β *is the ratio of the activated RF chains to the total number of transmit antennas and* $\mathbb{P}\left(|h|^2\geq\zeta(\beta)\right)=\beta$*. Consequently,*

$$C-\log_2\left(\gamma N_T\right)\xrightarrow[N_T\uparrow\infty]{a.s.} log_2\left(\int_{\zeta(\beta)}^{\infty}\zeta dF_{|h|^2}(\zeta)\right) \tag{6.15}$$

where $\gamma=\frac{P}{\sigma_n^2}$ *is the transmit SNR.*

Proof. Define the function $\beta(\zeta):=\mathbb{P}\left(|h|^2\geq\zeta\right)$ which is a non-increasing left-continuous, right-limits function with $\beta(0)=1$ and $\beta(\infty)=0$. Then there is a unique non-increasing right-continuous, left-limits inverse function $\zeta(\beta)$ such that $\mathbb{P}\left(|h|^2\geq\zeta(\beta)\right)=\beta$. For any $\beta'\in(0,1)$, define

$$\mathcal{I}_{\beta'}^{(N_T)}:=\{i:|h_i|^2\geq\zeta(\beta')\} \tag{6.16}$$

and

$$B_{\beta'}^{(N_T)}:=\frac{|\mathcal{I}_{\beta'}^{(N_T)}|}{N_T} \tag{6.17}$$

For any $\beta'\in(0,1)$ the following inequalities hold: (i) if $B_{\beta'}^{(N_T)}\leq\beta$ then $\mathcal{I}_{\beta'}^{(N_T)}\subseteq\mathcal{I}^{(N_T)}$ and (ii) if $B_{\beta'}^{(N_T)}\geq\beta$ then $\mathcal{I}^{(N_T)}\subseteq\mathcal{I}_{\beta'}^{(N_T)}$. But by the strong law of large numbers,

$$B_{\beta'}^{(N_T)}=\frac{1}{N_T}\sum_{i=1}^{N_T}\mathbb{I}\left[|h_i|^2\geq\zeta(\beta')\right]\xrightarrow[N_T\uparrow\infty]{a.s.}\mathbb{P}(|h|^2\geq\zeta(\beta'))=\beta'. \tag{6.18}$$

Thus, for any $\epsilon>0$, $B_{\beta-\epsilon}^{(N_T)}\xrightarrow[N_T\uparrow\infty]{a.s.}\beta-\epsilon$ and $B_{\beta+\epsilon}^{(N_T)}\xrightarrow[N_T\uparrow\infty]{a.s.}\beta+\epsilon$. Thus, for any $\epsilon>0$ and for N_T large enough,

$$\mathcal{I}_{\beta-\epsilon}^{(N_T)}\subseteq\mathcal{I}^{(N_T)}\subseteq\mathcal{I}_{\beta+\epsilon}^{(N_T)}. \tag{6.19}$$

By definition,

$$\frac{1}{N_T}\sum_{i\in\mathcal{I}_{\beta'}^{(N_T)}}|h_i|^2=\frac{1}{N_T}\sum_{i=1}^{N_T}|h_i|^2\mathbb{I}\left[|h_i|^2\geq\zeta(\beta')\right]. \tag{6.20}$$

Applying the strong law of large numbers to the right-hand side of (6.20) we get

$$\frac{1}{N_T}\sum_{i\in\mathcal{I}_{\beta'}^{(N_T)}}|h_i|^2\xrightarrow[N_T\uparrow\infty]{a.s.}\int_{\zeta(\beta')}^{\infty}\zeta dF_{|h|^2}(\zeta). \tag{6.21}$$

Thus,

$$\frac{1}{N_T}\sum_{i\in\mathcal{I}_{\beta-\epsilon}^{(N_T)}}|h_i|^2\xrightarrow[N_T\uparrow\infty]{a.s.}\int_{\zeta(\beta-\epsilon)}^{\infty}\zeta dF_{|h|^2}(\zeta), \tag{6.22}$$

and

$$\frac{1}{N_T}\sum_{i\in\mathcal{I}_{\beta+\epsilon}^{(N_T)}}|h_i|^2\xrightarrow[N_T\uparrow\infty]{a.s.}\int_{\zeta(\beta+\epsilon)}^{\infty}\zeta dF_{|h|^2}(\zeta). \tag{6.23}$$

Applying the set inequalities in (6.19), we obtain that

$$\begin{aligned}\limsup_{N_T\uparrow\infty}\frac{1}{N_T}\sum_{i\in\mathcal{I}^{(N_T)}}|h_i|^2 &\leq \lim_{\epsilon\downarrow 0}\int_{\zeta(\beta+\epsilon)}^{\infty}\zeta dF_{|h|^2}(\zeta)\\ &= \int_{\zeta(\beta)}^{\infty}\zeta dF_{|h|^2}(\zeta)\end{aligned} \tag{6.24}$$

and

$$\begin{aligned}\liminf_{N_T\uparrow\infty}\frac{1}{N_T}\sum_{i\in\mathcal{I}^{(N_T)}}|h_i|^2 &\geq \lim_{\epsilon\downarrow 0}\int_{\zeta(\beta-\epsilon)}^{\infty}\zeta dF_{|h|^2}(\zeta)\\ &= \int_{\zeta(\beta)}^{\infty}\zeta dF_{|h|^2}(\zeta)\end{aligned} \tag{6.25}$$

Using the fact that for convergent sequence, $\limsup = \liminf = \lim$ and Eqs. (6.24) and (6.25), we obtain

$$\lim_{N_T\uparrow\infty}\sum_{i\in\mathcal{I}^{(N_T)}}|h_i|^2=\int_{\zeta(\beta)}^{\infty}\zeta dF_{|h|^2}(\zeta) \tag{6.26}$$

In order to have finite $\int_{\zeta(\beta)}^{\infty}\zeta dF_{|h|^2}(\zeta)$, the condition $\mathbb{E}(|h|^2)<\infty$ is sufficient because $\int_{\zeta(\beta)}^{\infty}\zeta dF_{|h|^2}(\zeta)\leq\int_{0}^{\infty}\zeta dF_{|h|^2}(\zeta)=\mathbb{E}(|h|^2)$. [1]

□

[1] In practice, real-world channels have bounded link power gains.

Now we calculate the asymptotic limit for the particular case of Rayleigh fading. The magnitude square of the random channel vector whose probability distribution is complex Gaussian, will be distributed according to an exponential distribution. We assume that the channel power is unity because the variance of real and imaginary parts of the complex Gaussian is assumed to be half, i.e., $\sigma_h^2 = 1$. Thus, the distribution function of the channel power gain $|h|^2$ denoted by $F_{|h|^2}(\zeta)$ in our case may be expressed as follows

$$F_{|h|^2}(\zeta) \;=\; 1 - e^{-\zeta} \qquad \zeta > 0 \tag{6.27}$$

Substituting the distribution in Eq. (6.27) into Eq. (6.14), we obtain the following limit:

$$\frac{1}{N_T} \sum_{n \in \mathcal{I}^{(N_T)}} |h_i|^2 \xrightarrow[N_T \uparrow \infty]{a.s.} \frac{N_c}{N_T} \left[1 - \ln \frac{N_c}{N_T} \right] \tag{6.28}$$

Thus, the asymptotic channel capacity may be expressed as follows:

$$C - \log_2(\gamma N_T) \xrightarrow[N_T \uparrow \infty]{a.s.} \log_2 \left(\beta(1 - \ln(\beta)) \right), \tag{6.29}$$

where $\gamma = \frac{P}{\sigma_n^2}$.

The above limit is significant because it enables us to estimate the capacity of a system which uses the best channel gains to do beamforming under finite RF chains constraint. This capacity limit is independent of the channel gains which enables us to predict the capacity of such a system without the knowledge of best channel gains using Eq. (6.29).

Remark. *For a target capacity and fixed number of transmit antennas, our proposed capacity deterministic equivalent enables us to calculate the required number of RF chains to achieve the target capacity asymptotically.*

6.4 Lower and Upper Bounds on Asymptotic Limit

The asymptotic limit in Eq. (6.14) can be lower and upper bounded for Rayleigh fading as follows,

$$\begin{aligned}
\int_{\zeta(\beta)}^{\infty} \zeta dF_{|h|^2}(\zeta) &= \int_{\zeta(\beta)}^{\infty} \zeta f_{|h|^2}(\zeta) d\zeta && (6.30)\\
&\geq \zeta(\beta) \int_{\zeta(\beta)}^{\infty} f_{|h|^2}(\zeta) d\zeta && (6.31)\\
&= \ln \frac{1}{\beta} \int_{\ln \frac{1}{\beta}}^{\infty} e^{-\zeta} d\zeta && (6.32)\\
&= \beta \ln \frac{1}{\beta} && (6.33)
\end{aligned}$$

Thus, a lower bound can be calculated as follows,

$$\beta \ln \frac{1}{\beta} \leq \frac{1}{N_T} \sum_{i \in \mathcal{I}^{(N_T)}} |h_i|^2 \; as \; N_T \uparrow \infty \tag{6.34}$$

In order to calculate an upper bound of the asymptotic limit, it can be observed that the asymptotic limit is in fact the partial mean of a positive random variable which may be upper bounded by the statistical mean of the underlying random variable.

$$\begin{aligned}
\int_{\zeta(\beta)}^{\infty} \zeta dF_{|h|^2}(\zeta) &= \int_{\zeta(\beta)}^{\infty} \zeta f_{|h|^2}(\zeta) d\zeta && (6.35)\\
&\leq \int_{0}^{\infty} \zeta f_{|h|^2}(\zeta) d\zeta && (6.36)\\
&= 1 && (6.37)
\end{aligned}$$

Thus, the upper bound can be calculated as follows.

$$\frac{1}{N_T} \sum_{i \in \mathcal{I}^{(N_T)}} |h_i|^2 \leq 1 \tag{6.38}$$

From Eq. (6.34) and Eq. (6.38), we obtain the following

$$\beta \ln \left(\frac{1}{\beta} \right) \leq \frac{1}{N_T} \sum_{i \in \mathcal{I}^{(N_T)}} |h_i|^2 \leq 1 \tag{6.39}$$

The above equation can be expressed in terms of system parameters as follows.

$$N_c \ln\left(\frac{N_T}{N_c}\right) \leq \sum_{i \in \mathcal{I}^{(N_T)}} |h_i|^2 \leq N_T \tag{6.40}$$

Substituting Eq. (6.40) into Eq. (6.12), we get the following capacity bounds,

$$\log_2\left(1 + \gamma N_c \ln\left(\frac{N_T}{N_c}\right)\right) \leq_{N_T} C^* \leq_{N_T} \log_2\left(1 + \gamma N_T\right) \tag{6.41}$$

where C^* is the asymptotic deterministic value of capacity of the considered system.

6.5 Numerical Results

In this section, numerical experiments are conducted to verify the large system analysis and associated bounds in the previous sections. In all the results, link and noise power are assumed to be unity, i.e., $\sigma_h^2 = \sigma_n^2 = 1$ and SNR is the transmit SNR.

Fig. 6.2 demonstrates how the channel capacity in Eq. (6.12) randomly varies around the asymptotic mean value of channel capacity in Eq. (6.29) as N_c, N_T grow large while maintaining fixed ratio $\beta = \frac{N_c}{N_T}$. In this figure, we use one hundred realizations of the channel vector $\boldsymbol{h}$ for a particular value of SNR. It can be observed from the figure that the deviations of the random capacity values are centered on the asymptotic value. In Fig. 6.3, the randomly generated capacity values are compared with the asymptotic value for $N_T = 500$ while maintaining fixed ratio of $\beta = \frac{1}{5}$. It can be noticed easily from the figures that the spread of the random capacity values around the asymptotic value for finite N_c and N_T start decreasing as N_T increases while β is held fixed. Specifically, for $N_T = 500$ and $\beta = \frac{1}{5}$, the randomly generated values are very close to the asymptotic value. Thus, law of large number's analysis enables us to estimate the channel capacity and provides us insights into key system parameters.

In Fig. 6.4, the upper and lower bounds on the asymptotic limit are plotted for $N_T = 500$ and $\beta = \frac{1}{5}$. All the randomly generated capacities lie in the gap between lower

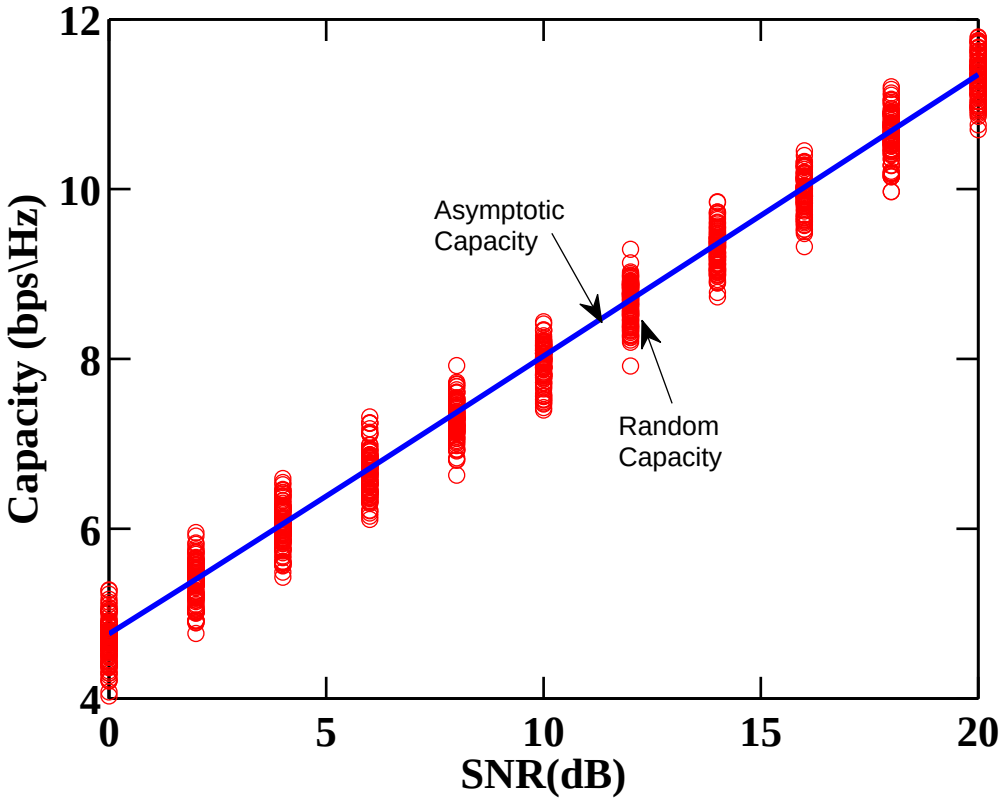

Figure 6.2: Comparison of randomly generated Capacity and Asymptotic Capacity for $\beta = \frac{1}{5}$ and $N_T = 50$

and upper bounds.

6.6 Conclusion

In this chapter, we have provided an asymptotic limit of the normalized channel power gain of the antenna selection based beamforming in massive MISO using the strong law of large numbers. It is shown that the deterministic equivalent specifically in case of Rayleigh fading channel only depends on the ratio of the total number of RF chains to the total number of transmit antennas. Our proposed deterministic equivalent leads to important insights into the system's behaviour. The proposed expression is independent

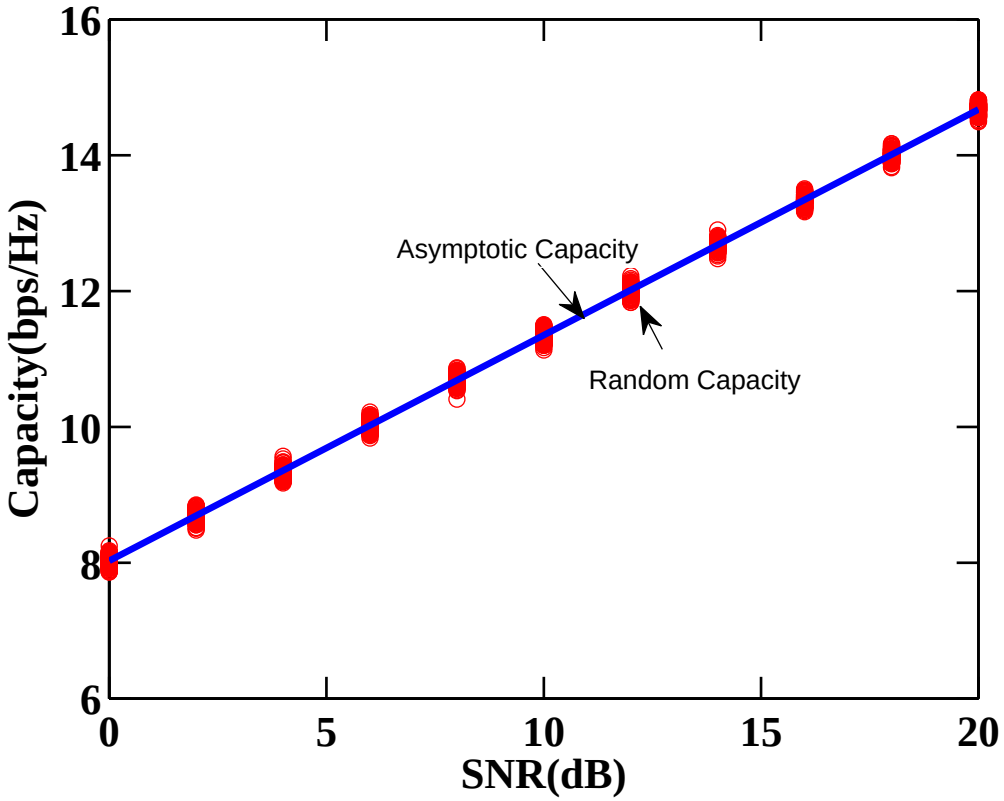

Figure 6.3: Comparison of randomly generated Capacity and Asymptotic Capacity for $\beta = \frac{1}{5}$ and $N_T = 500$

of the channel realizations and can be used to simulate the considered system's behaviour without carrying out the extensive Monte Carlo simulations. More importantly, the proposed capacity deterministic equivalent enables us to compute the required number of RF chains for a given number of transmit antennas and target capacity asymptotically. The capacity performance of the antenna selection is difficult to study for finite dimensions but becomes feasible by investigating our proposed capacity approximation in the regime of large system dimensions. Numerical results have validated the accuracy of our proposed limit for relatively small N_c, N_T as well. We would like to emphasize that our proposed upper bound holds for arbitrary fading channels as well under the condition of finite power channel gains.

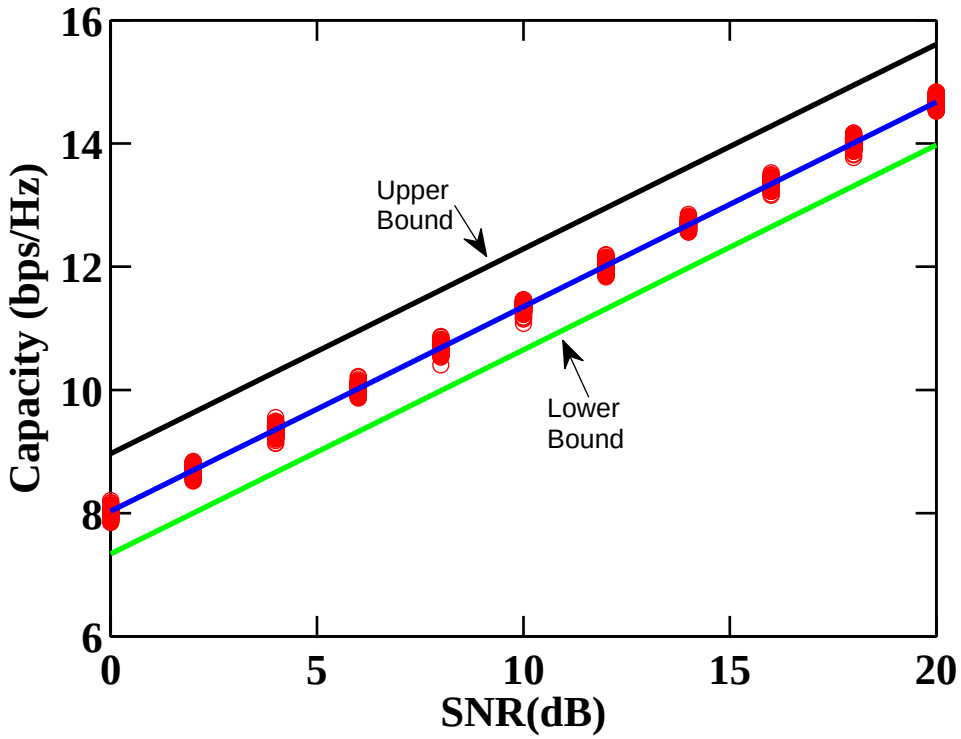

Figure 6.4: Upper and Lower Bounds of Asymptotic Capacity for $N_T = 500$ and $\beta = 1/5$

Chapter 7

Beam Alignment Schemes for Millimeter-Wave Massive MIMO systems under RF Chains Constraint

A mmWave massive MIMO system is a strong candidate for delivering gigabits-per-second throughputs due to abundant unlicensed spectrum in the mmWave band. Owing to enormous vacant bandwidth, mmWave massive MIMO has potential to deliver huge throughputs under the constraint of RF chains. To cope with the incurred path loss at mmWave frequencies, mmWave massive MIMO systems will deploy high-gain electronically steerable directional antennas. Due to pencil-sharp narrow beams produced by high-gain antennas, beam alignment problem becomes much more crucial. In this chapter, we focus on investigating beam-alignment problem in mmWave massive MIMO systems under RF chains constraint.

This chapter is organized as follows. Section 7.1 provides motivation and the related work. Section 7.2 presents the system modeling of the continuous-time mmWave link. Section 7.3 illustrates the problem statement of the mmWave Beam Alignment problem.

Section 7.4 provides algorithms for threshold based hierarchical search. Section 7.5 enlightens the statistical analysis of beam misalignment. Section 7.6 presents the numerical experiments and simulation results and section 7.7 concludes the chapter.

7.1 Motivation and Related Work

Owing to the spectrum scarcity in the lower-frequency bands, it is recently envisaged to use the huge bandwidths offered by the mmWave spectrum for future cellular systems and wireless local area networks [75]. Most past research was aimed at enhancing link spectral efficiency by employing orthogonal frequency-division multiplexing (OFDM), MIMO, efficient channel coding and interference management because limited spectrum had been licensed for commercial cellular bands. To improve the area spectral efficiency, network densification has also been an active area of research which encompasses the deployment of heterogeneous infrastructure (picocells, femtocells, relays, distributed antennas). However, increased area spectral efficiency does not suffice to meet the high per-user data rate requirement. As there is little scope for further improvement at the physical layer and the widespread deployment of massive MIMO and heterogeneous networks is a daunting challenge due to many practical problems, these proposals on their own may not be sufficient to satisfy the huge traffic demands induced by the bandwidth-hungry web applications of smart phones and tablets. A mmWave cellular system, which operates in the 10-300 GHz band, is a desirable candidate for fifth-generation cellular systems because it has enormous vacant spectrum bands capable to support multiple gigabit-per-second data rates.

The mmWave band has been successfully employed to offer gigabits-per-second data rates in fixed outdoor wireless systems [76] and indoor wireless systems [77, 78]. The recent improvements in mmWave hardware and the less-congested spectrum in mmWave bands have ignited the interest of wireless industry to explore the mmWave band for

outdoor cellular systems [79, 80]. In order to realize mmWave systems in practice, the propagation characteristics and channel impairments of mmWave band must be dealt with properly. The bottleneck in mmWave propagation is an orders-of-magnitude increased path loss which is caused by the ten-folds increase in carrier frequency compared to legacy microWave cellular systems which can be mitigated by keeping the antenna aperture fixed at both transmit and receive sides. Additionally in mmWave bands, scattering is limited which reduces the available diversity and non-line-of-sight (NLOS) paths are weaker which leads to blockage and consequently, coverage holes become much more pronounced [81].

Another considerable impairment in mmWave bands is high noise power which stems from the large width of spectrum bands. As a result, mmWave systems are noise-limited in constrast to legacy cellular systems which are interference-limited. To overcome this problem, high SNR at the receiver can only be achieved by deploying high-gain electronically steerable directional antennas.

High-gain antennas can be realized by packing an orders-of-magnitude more antenna elements than current cellular arrays in arrays of practical dimensions, thanks to the small wavelengths associated with the mmWave band. Large arrays not only provide the huge beamforming gain to cope with the huge path loss but also support multiple data streams (or multiple single-antenna users) by deploying multiple RF chains which would potentially improve spectral efficiency and enable mmWave systems to approach the network capacity. However, owing to the high power consumption of mixed signal components and costly RF chains, digital baseband beamforming is difficult for practical realization. For single stream transmission, analog beamsteering is a practical choice whereby all the antennas are connected to a single RF chain via a network of low-cost RF phase shifters [82–85].

In order to reap the benefits of digital beamforming and analog beamsteering simultaneously, a hybrid precoding was proposed which facilitates multi-user/multi-stream trans-

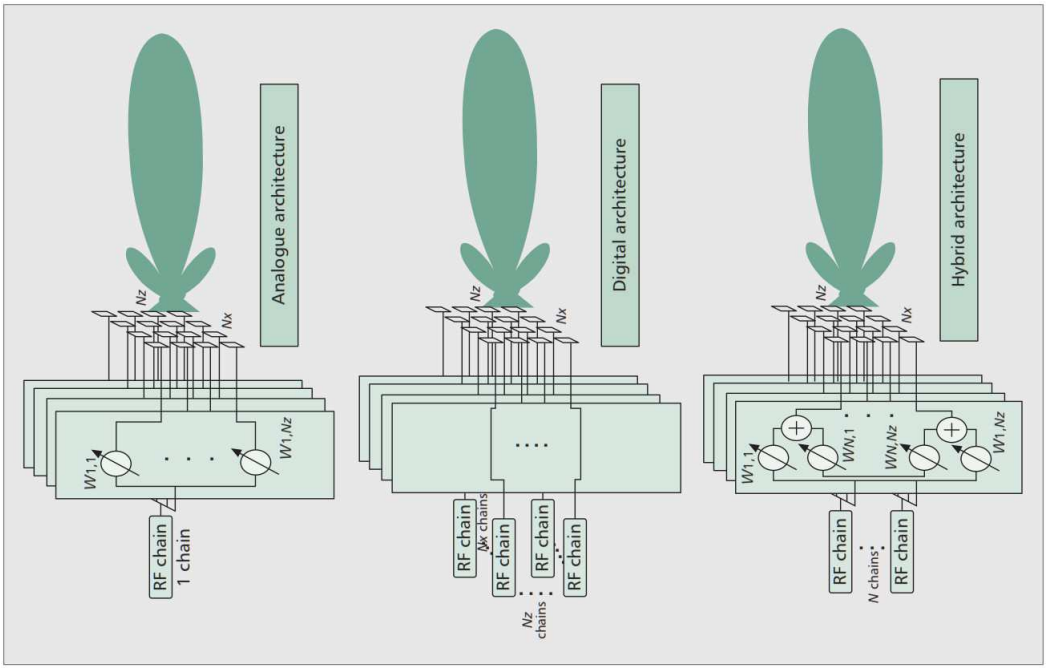

Figure 7.1: Analogue versus Digital versus Hybrid Architectures [86]

mission where a few RF chains are tied to huge array of antennas via a network of cheap phase shifters [87, 88]. It has been developed primarily to support spatial multiplexing while taking into account the RF chains' limitation in mmWave massive MIMO realm. The term *precoding* implies the use of multiple beamforming vectors, one for each spatial direction. In hybrid precoding, most of precoding is performed in RF analogue domain while some precoding is performed in baseband digital domain. Let $\boldsymbol{W}$ be precoding matrix then it can be decomposed as $\boldsymbol{W} = \boldsymbol{W}_{rf}\boldsymbol{W}_{bb}$ where $\boldsymbol{W}_{rf}$ is an $N_T \times N_c$ matrix corresponding to analogue beamforming coefficients and $\boldsymbol{W}_{bb}$ is an $N_c \times N_s$ matrix of digital precoding coefficients. The parameter N_c specifies the number of RF chains and the number of spatial streams to be multiplexed, N_s, must satisfy the constraint $N_s \leq N_c$. Thus, N_c is the so-called DOF for the spatial streams. The design of precoding matrices under the constraint of constant envelope phase shifters is an interesting problem. However, if designed properly results in comparable performance to unconstrained digital precoding.

Some design approaches aim at exploiting the sparsity in mmWave channel due to few multipath components (MPCs). Fig. 7.1 illustrates the architectures of analogue, digital and hybrid beamforming schemes. Regardless of hybrid precoding, entry-wise channel estimation of mmWave channel matrix is time consuming due to massive antenna array and there is a significant room for devising new time-efficient beam alignment algorithms which align the beam of the BTS to the angular-direction from which user's signal is arriving.

Exploiting the fact that mmWave channel is sparse in the angular domain owing to limited scattering in this band, compressive sensing tools have been leveraged to estimate the steering angles of different MPCs [87,89–92]. In [90], the authors propose a new adaptive compressive sensing (ACS) algorithm to estimate the mmWave channel parameters with low training overhead considering single-user multi-stream transmission. A hierarchical codebook is designed to construct training beamforming vectors with different beamwidths for hybrid precoding. Simulation results are used to show that the proposed algorithm achieves precoding gains comparable to exhaustive training algorithms. In [91], multi-user downlink transmission in mmWave realm is proposed and evaluated. The proposed scheme is based on CS channel estimation and conjugate analogue beamforming. Specifically, they show that the number of measurements need to be optimized in order to account for tradeoff between channel estimation accuracy and the training overhead. The approach in [92] is to append virtual antenna elements into physical antenna array which improves upon estimation accuracy of the ACS algorithm of [90]. The authors propose a compressive angle estimation method with less training overhead and delay than the ACS algorithm. Particularly, the proposed algorithm eliminates the constraint on resolution posed by the number of antenna elements in physical array thereby achieving better resolution without any physical change in size of array.

For the analog beamsteering architecture, two types of methods are adopted. In

[82, 83, 93, 94], an iterative beam training method is applied whereby the beamsteering vector on one end (BTS or MS) is alternately optimized by fixing the beamsteering vector on the other end, and this approach is repeated iteratively to enhance the beamforming gain over prior iterations. However, in [84, 85, 95] a beamforming codebook approach is followed where the angular search space is partitioned into multiple bins and each bin corresponds to a codeword in the beamforming codebook. The best transmit/receive beam is found by traversing through the beamforming codebook. Both the methodologies are applicable in different scenarios with their own advantages.

In this chapter, we focus on single-stream beamforming which has been shown to be capacity achieving in the very low SNR case [18]. Furthermore, single-stream beamforming can be modified to the more practical hybrid precoding case [90]. For the beamforming codebook approach, an exhaustive search might be applied whereby all the beam directions are searched sequentially in the angular domain and the best pair of transmit/receive beamforming codewords are determined. This sequential approach gives very high resolution at the cost of prohibitive time complexity as the number of beam directions is typically high due to required high resolution in mmWave band. In order to minimize the time complexity, a hierarchical codebook approach had been adopted in [22, 84, 85, 96, 97]. In hierarchical codebook approach, search process is executed in multiple stages. Initial stages have few beamforming vectors corresponding to low resolution beams and as the stage number increases, the number of beamforming vectors increases to take into account higher resolution beams. In each stage, the best beam direction is chosen and based on that chosen beam, the corresponding angular region is further partitioned into high resolution beams and beam search process is continued.

The performance evaluation of the hierarchical codebook is impacted by the radiation pattern of codebook beamforming vectors. The probability of beam misalignment and the search time can be minimized by effective design of the hierarchical codebook. In [84, 85],

it is proposed to choose wider beams to minimize the search time, however, the design methodologies for codebook are not investigated. In [96], the wider beams are designed by the superposition of two narrower beams but the resultant beamforming vectors do not admit constant envelope constraint. In [22], a sub-array approach is followed which broadens the beamwidth by pointing the beams of subarray in slightly-gapped directions but a complete hierarchical codebook is not explicitly designed, and this approach might not be able to design very wide beams in initial low resolution stages. In [90], hybrid precoding was employed to construct negligible side-lobe beams by exploiting ZF structure but deep sinks appear in the beam zone if the number of RF chains are not large enough. In [97], a binary search tree is employed for hierarchical codebook search and wider beams are generated by deactivation (or turning off of) antennas, however, they do not offer beam misalignment analysis. In [23], the authors state two basic criteria for arbitrary hierarchical codebook designs, and proposed an efficient hierarchical codebook by exploiting sub-array and antenna deactivation simultaneously. They do not outline complete algorithms to perform beam search and they do not offer beam misalignment analysis.

In this chapter, we propose two novel algorithms namely iterative-thresholding hierarchical search (ITHS) and refined-hierarchical search (RHS) in which all the antennas are activated in all training slots to reap the benefits of huge beamforming gain equally in all stages. Furthermore, we do complete analysis of beam misalignment exploiting the orthogonality among the columns of beamforming codebook. We propose a Bayesian approach which offers better performance in terms of beam-alignment over traditional beamforming energy based methods. Analytical expression for probability of beam misalignment for conventional exhaustive search estimator and for a newly proposed Bayesian estimator are derived and compared with simulation error-rates and are found to be reasonably accurate. Numerical experiments and simulations are conducted to corroborate

the superiority of proposed algorithms over existing hierarchical and exhaustive search.

It is pertinent to mention here that the scattering properties of the uplink and downlink modes are quite different. In urban environments, the scattering environment of the mobile station is typically rich. This is due to the abundance of objects surrounding the mobile station in urban settings. On the contrary, the scattering environment of the base station is assumed to be limited scattering. This assumption stems from the fact that the base stations are typically mounted quite high. Consequently, direction-of-arrival estimation is practically done at the base station to exploit the sparse structure offered by the line-of-sight model of the uplink mode. Fig. 7.2 shows a multi-user setup in which a BTS electronically aligns the beams towards multiple users using an antenna array at the BTS. In the next section, we focus on the system modeling of continuous-time point-to-point mmWave link.

7.2 System Modeling of continuous-time mmWave Link

We consider a single cell single-input multiple-output (SIMO) wireless system operating in the mmWave band. The MS is assumed to have one omni-directional antenna and the BTS is equipped with N_T antenna elements uniform-linear array (ULA) and is receiving the signal transmitted by MS. Consider a continuous-time baseband uplink signalling transmission in which MS is transmitting N pilot symbols in a fixed amount of time T to the BTS. Let $\boldsymbol{y}(t) \in \mathbb{C}^{N_T}$ represent the signal received by the BTS which has passed through the wireless channel $\boldsymbol{h}(\phi) \in \mathbb{C}^{N_T}$ then the signal received at the BTS may be expressed as follows.

$$\boldsymbol{y}(t) = \sqrt{\rho} \sum_{k=0}^{N-1} \boldsymbol{h}(\phi) s\left(t - k\frac{T}{N}\right) + \boldsymbol{n}(t) \qquad 0 < t < T \tag{7.1}$$

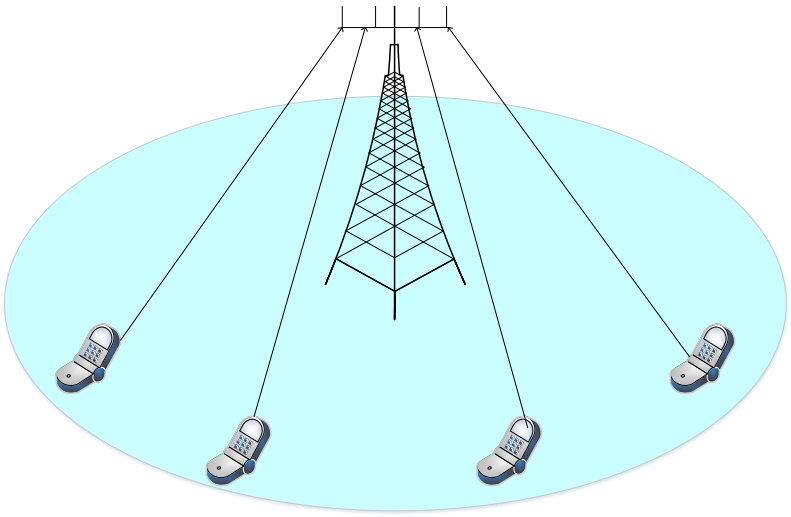

Figure 7.2: A multi-user mmWave setup in which a BTS electronically aligns the pencil beams towards multiple users using an antenna array during beam-alignment

where $\boldsymbol{n}(t) \in \mathbb{C}^{N_T}$ is the circularly-symmetric complex AWGN, $\boldsymbol{n} \sim \mathcal{CN}(\mathbf{0}, \boldsymbol{I})$, $s(t)$ is the baseband transmitted pilot waveform of unit amplitude and time support of width $\frac{T}{N}$ where T is the total transmission time allocated for beam alignment phase. Here $\boldsymbol{h}(\phi)$ represents the directional transmission channel vector which is characterized by the physical direction-of-arrival (DOA) ϕ of the signal coming from the MS. ρ models the transmit SNR minus the path-loss and other attenuation factors like rainfall and penetration losses. In this work, with slight abuse of terminology we will refer to the parameter ρ as received SNR and will assume that it takes on values less than unity for high path-loss and other attenuation factors.

In a typical mmWave link, the highly directional and quasi-optical nature of electromagnetic wave propagation leads to few multi-path components in the mmWave band. A mmWave channel comprises a line-of-sight (LOS) propagation component and a set of few single bounce non-line-of-sight (NLOS) propagation paths. Consequently, the wireless channel in mmWave band is considered to have limited scattering hence it is modeled

as a sparse channel in terms of multi-path components. The well-known sparse channel model in terms of BTS steering vectors (a.k.a. array response vectors) for ULAs can be expressed as follows.

$$\boldsymbol{h}(\phi) = \sqrt{N_T\rho}\boldsymbol{a}(\phi_{los}) + \sqrt{N_T}\sum_{j=1}^{L}\sqrt{\rho}_j\boldsymbol{a}(\phi_{nlos}^{(j)}) \tag{7.2}$$

where

$$\boldsymbol{a}(\phi) = \frac{1}{\sqrt{N_T}}\begin{bmatrix}1 & e^{j2\pi\delta\cos(\phi)} & \cdots & e^{j2\pi(N_T-1)\delta\cos(\phi)}\end{bmatrix}^T \tag{7.3}$$

Here ϕ_{los} represents the DOA of the LOS path, $\phi_{nlos}^{(j)}$ represents the physical direction-of-arrival of j-th NLOS path and $\delta = \frac{d}{\lambda}$ denotes the inter-antenna element spacing d normalized by the wavelength. In this work, we assume super-critical spacing, i.e., $\delta = \frac{1}{2}$ [18]. It is noteworthy that the array steering vector in Eq. (7.3) has its power normalized to unity and hence the normalization constant $\sqrt{N_T}$ is incorporated in Eq. (7.2). In general, the DOA of LOS or NLOS path takes on value in the angular range $(\phi_{low}, \phi_{high})$. Let $\mathcal{A}_{N_T}$ denote the set of all the steering vectors in the physical angular range $(\phi_{low}, \phi_{high})$, then

$$\mathcal{A}_{N_T} = \left\{\boldsymbol{a}(\phi) \in \mathbb{C}^{N_T} : \phi_{low} < \phi < \phi_{high}\right\} \tag{7.4}$$

If a mmWave channel has LOS link, then the NLOS paths have marginal effect on the received signal. This owes to the fact that the path loss of the NLOS propagation paths is much higher in comparison to that of LOS propagation paths ; the link power associated with the NLOS paths is typically 20 dB weaker than that of LOS path [98]. When there is no LOS path due to severe blockage, it is argued that the mmWave communication may take place through a NLOS path with highly directional beamsteering [98]. In both cases, very few propagation paths exist and as a result, in many research works for mmWave communication [99–106], single-path channel model has been adopted by assuming one path which may be dominant LOS path if it exists or a dominant NLOS path if a LOS

path does not exist due to severe blockage. In order to render the problem tractable and gain insights into beam alignment in highly-directional mmWave MIMO, we adopt the single-path channel model considering the dominant LOS path. In contrast to existing literature, we do not assume that the dominant path gain is Gaussian. By taking into account all the stated assumptions, the mmWave channel model can be expressed as follows.

$$\boldsymbol{h} = \sqrt{N_T \rho}\boldsymbol{a}(\phi_{los}) \tag{7.5}$$

Similar single-path channel model has been adopted previously in [99,100] and was termed as uniform-random single-path (UR-SP) channel model. It can be noticed that the power of the UR-SP channel model can be obtained from $\mathbb{E}\left[\|\boldsymbol{h}\|^2\right] = N_T$. Hence the channel power gain (or the array gain) increases linearly with N_T. The same linear increase in channel power gain is typically observed in the rich scattering Rayleigh fading channel model where $\boldsymbol{h} \sim \mathcal{CN}(\boldsymbol{0}, \boldsymbol{I})$. Therefore, the power radiated by the MS in the space is concentrated by the ULA mounted on the BTS. In the light of these assumptions, we can model our input-output relationship as follows.

$$\boldsymbol{y}(t) = \sqrt{N_T \rho}\sum_{k=0}^{N-1}\boldsymbol{a}(\phi)s\left(t - k\frac{T}{N}\right) + \boldsymbol{n}(t) \tag{7.6}$$

The bandwidth of the baseband pulse is proportional to $\frac{N}{T}$ which can be transmitted easily thanks to the huge bandwidths offered by mmWave systems.

7.3 Problem Statement of the mmWave Beam Alignment

7.3.1 Analogue Beam Steering

In single-stream transmission, the BTS employs an antenna array to receive one data stream. An analogue beamforming vector is one where all its weights couple one RF chain with all antennas and all the weights have constant-amplitude constraint. Let $\boldsymbol{w}_{rf}$ denote the analogue beamforming vector, then the SNR at the output of beamformer can be expressed as follows.

$$\mathsf{SNR}(\phi) = \rho|\boldsymbol{w}_{rf}^{\dagger}\boldsymbol{h}(\phi)|^2 \tag{7.7}$$

The primary aim of analogue beamforming is to maximize the SNR at the output of beamformer. When the channel is a dominant LOS channel as discussed earlier or when the number of scatterers is small, it is reasonable to construct the beamforming vectors in order to enhance the beamforming gain in a particular direction ϕ. This process is termed as "beamsteering" in the literature. The fundamental approach of performing beamsteering is to adjust the beamforming vector phase (ϕ_k) to match the array response vector of the channel vector in Eq. (7.5). This is achieved by setting $\boldsymbol{w}_{rf} = \boldsymbol{a}(\phi_k)$ and by varying ϕ_k, we choose the ϕ_k which is close to the actual DOA ϕ. This process generates a radiation pattern with main lobe pointing in the actual DOA.

Other codebook designs that trade main lobe directivity with side-lobe level are only possible when we have variable-gain amplifiers but this requires a separate RF chain for each antenna to simultaneously adjust the amplitudes of complex weights of beamforming vector from the baseband. Another approach to shape the beam-pattern is hybrid beamforming in which multiple RF chains and additional processing layer at baseband is required. In this approach, the number of RF chains is less than the number of transmit

antennas and are higher than the number of users in the system. In hybrid beamforming, all the beamforming is split up into analogue and digital beamforming where analogue beamforming is done at RF level and digital beamforming is done in the baseband. Hybrid beamforming offers performance very close to digital beamforming, however, for single user analogue beamforming performance suffices so henceforth in this chapter, we focus on beam-alignment algorithmic design under analogue beamforming.

In order to design cost-effective single-user systems, we restrict ourselves to constant-envelope low-cost RF phase shifters and design analog beamsteering algorithms under this constraint without additional RF chains and baseband digital beamforming as one RF chain is required for one user in the single user setting.

The processed signal $r_k(t)$ at the output of analogue beamformer may be expressed as

$$r_k(t) = \boldsymbol{a}(\phi_k)^\dagger \boldsymbol{y}(t) \qquad k = 0, \cdots, N-1 \qquad \frac{kT}{N} < t < (k+1)\frac{T}{N} \tag{7.8}$$

It is well known that matched-filter or correlator maximizes the SNR so we use a baseband matched-filter which is used to collect the energy in the pilot waveform. The pilot waveform is assumed to be known at the BTS. Let q_k denote the output of baseband matched-filter, then the output of baseband matched-filter can be expressed as follows.

$$q_k = \int_{k\frac{T}{N}}^{(k+1)\frac{T}{N}} r_k(t) s\left(t - k\frac{T}{N}\right) dt \tag{7.9}$$

Let $q_k = m_k + n_k$ where m_k represents the signal part and n_k represents the noise part, then

$$m_k = \sqrt{\rho N_T}\boldsymbol{a}^\dagger(\phi_k)\boldsymbol{a}(\phi) \int_{k\frac{T}{N}}^{(k+1)\frac{T}{N}} s^2\left(t - \frac{kT}{N}\right) dt \tag{7.10}$$

$$= \sqrt{\rho N_T}\frac{T}{N}\boldsymbol{a}^\dagger(\phi_k)\boldsymbol{a}(\phi) \tag{7.11}$$

$$n_k = \boldsymbol{a}^\dagger(\phi_k) \int_{k\frac{T}{N}}^{(k+1)\frac{T}{N}} \boldsymbol{n}(t) s\left(t - \frac{kT}{N}\right) dt \tag{7.12}$$

In general, the number of transmissions can be arbitrarily large. However, in case of mutually orthogonal beamforming vectors, the maximum value of N is equal to number

of antennas N_T. Henceforth, in this work we assume $N = N_T$ in order to ensure mutual orthogonality of beamforming vectors unless stated otherwise. In this case, it is evident that as the pilot transmission time is fixed, increasing the number of beamforming vectors results in a reduction of signal part's energy which offsets the beamforming gain. It is noteworthy that the beamforming gain due to increased N is cancelled by the power loss from shorter pulse-width. Thus, as we go to higher resolutions, the energy collected per beam reduces due to shorter time support of pilot waveform. However, as the noise power is also reduced due to shorter observation window, the overall SNR after beamforming stays constant for a given pilot transmission time.

Since $\boldsymbol{n}(t)$ is a linear functional of Gaussian process and $\boldsymbol{a}(\phi_j)$ has complex exponential entries due to channel's Vandermonde structure, it follows that $n_j's$ admit white Gaussian distribution. The statistical mean of the processed noise can be expressed as follows.

$$\mathbb{E}\left[n_k\right] = \boldsymbol{a}^{\dagger}(\phi_k) \int_{k\frac{T}{N}}^{(k+1)\frac{T}{N}} \mathbb{E}\left[\boldsymbol{n}(t)\right] s\left(t - \frac{kT}{N}\right) dt = 0 \tag{7.13}$$

where the last equality follows from the assumption that $\boldsymbol{n}(t)$ is zero-mean Gaussian process. It is in order to compute the covariance of the noise samples n_i, n_j on two different time epochs.

$$\begin{aligned}
\mathrm{Cov}(n_i, n_j) &= \mathbb{E}\left[n_i n_j^{\dagger}\right] && (7.14)\\
&= \mathbb{E}\left[\boldsymbol{a}^{\dagger}(\phi_i) \int_{i\frac{T}{N}}^{(i+1)\frac{T}{N}} \boldsymbol{n}(t) s\left(t - i\frac{T}{N}\right) dt \int_{j\frac{T}{N}}^{(j+1)\frac{T}{N}} \boldsymbol{n}^{\dagger}(\tau) s\left(\tau - j\frac{T}{N}\right) d\tau \boldsymbol{a}(\phi_j)\right]\\
&= \boldsymbol{a}^{\dagger}(\phi_i)\boldsymbol{a}(\phi_j) \int_{i\frac{T}{N}}^{(i+1)\frac{T}{N}} \int_{j\frac{T}{N}}^{(j+1)\frac{T}{N}} \delta(t-\tau) s\left(t - i\frac{T}{N}\right) s\left(\tau - j\frac{T}{N}\right) dt d\tau && (7.15)\\
&= \frac{T}{N}\delta_{ij} && (7.16)
\end{aligned}$$

Thus, the noise samples $\{n_i\}_{i=0}^{N-1}$ at the output of baseband matched-filter are temporally uncorrelated and zero-mean. As a result, the noise is temporally white with variance $\frac{T}{N}$ per sample. Thus, the noise sample's energy also reduces as we increase the number of

beamforming vectors. Consequently, the energy-to-noise ratio at the output of baseband matched filter can be increased by either increasing the pilot transmission time or by increasing the transmit energy for the case of mutually orthogonal beamforming vectors at the BTS.

7.3.2 Review of Code-Book Design for Hierarchical Search

Most of the earlier work on beam alignment is directed towards multi-resolution hierarchical schemes [90, 97, 107] where in each stage of hierarchical framework, the resolution improves upon that of the preceding stage. Let $\theta = \cos(\phi)$ denote the spatial frequency(aka directional cosine) corresponding to DOA ϕ [108] where $\phi \in (0, \pi)$ covers the physical angular range and correspondingly $\theta \in (-1, 1)$ covers the one-sided spatial horizon as the mapping between the physical angle and spatial frequency is one-to-one. For $1 \leq s \leq S$, the s-th stage codebook $\mathcal{W}^{(s)} = \left\{ \boldsymbol{w}_1^{(s)}, \cdots, \boldsymbol{w}_{|\mathcal{W}^{(s)}|}^{(s)} \right\}$ is constructed in such a way so as to cover the spatial horizon $(-1, 1)$ where $|\mathcal{W}^{(s)}|$ denotes the cardinality of s-th stage codebook which is the total number of beamforming vectors in s-th stage. As the resolution of s-th stage's beamforming vector is higher than that of $(s-1)$-th stage's beamforming vector so the cardinality of successive stage is greater than that of preceding stage, i.e., $|\mathcal{W}^{(1)}| < \cdots < |\mathcal{W}^{(S)}|$. As the spatial frequency range of the s-th stage codebook is partitioned into $|\mathcal{W}^{(s)}|$ spatial intervals where each beamforming vector $\boldsymbol{w}_i^{(s)}$ covers a specific spatial interval $AoA_i^{(s)} \subset (-1, 1)$ and the union of all such intervals span the entire search space, i.e., $\bigcup_{i=1}^{|\mathcal{W}^{(s)}|} AoA_i^{(s)} = (-1, 1)$. Let $AoA_i^{(s)}$ denote the spatial region covered by the i-th beamforming vector of s-th stage and $AoA^{(s)}$ denote the total spatial zone searched in the s-th stage, then

$$AoA_i^{(s)} = \left\{ \theta : \theta \subset (-1, 1), \bigcup_{i=1}^{K} AoA_i^{(s)} = AoA^{(s)} \right\} \tag{7.17}$$

where K is the number of beamforming vectors sounded in each stage. The length of the spatial interval $AoA_i^{(s)}$ covered by any beamforming vector in s-th stage or the beamwidth of the radiation pattern generated by the i-th beamforming vector in the s-th stage can be approximated as follows.

$$\pi(AoA_i^{(s)}) = \int_{D_\theta} \mathbb{I}(\theta \in AoA_i^{(s)}) d\theta = \frac{2}{2^s} \tag{7.18}$$

where $D_\theta = \{\theta : -1 \leq \theta \leq 1\}$ is the total support in the spatial domain and $\mathbb{I}(\cdot)$ denotes the indicator function and $\pi(\cdot)$ denotes the Lebesgue measure. In the S-th stage, when $2^S = N$, the beamwidth of each codeword becomes $\frac{2}{N}$ which is the beamwidth of orthogonal beamforming vectors. Thus, as the stage of beamforming vector increases, the angular region covered by it decreases so it is termed as multi-resolution beamforming [90].

An example of radiation patterns in different stages of multi-resolution beamforming is given in Figs. 7.3-7.8 for $K = 2$ and $N = 8$. It is clear that the side-lobe levels are high in radiation patterns corresponding to physical angle and those corresponding to spatial frequency are low. The fundamental problem with hierarchical search is that in presence of noise, side-lobes enhance the noise and once we make decision in favour of a side-lobe, then due to error-propagation effect, we make wrong decisions in subsequent stages as the decision metric in all the existing hierarchical schemes is power. In each stage, we select the beamforming vector whose output power is higher than its competitors. Up till now, all the research is focused on the design of radiation patterns to minimize the side-lobe levels.

The problem in mmWave beam alignment is the error propagation effect which arises when low resolution wide beams are used in initial stages of hierarchical search. Furthermore, as less time is spent in initial stages, the probability of beam misalignment enhances in initial stages. In the next section, we propose two hierarchical schemes in which we use fixed resolution beams in all the stages of hierarchical search instead of using the multi-resolution approach where initial stages use low-resolution wide beams and

the final stage uses high-resolution narrow beams. Moreover, we allocate more training time in the initial stages in order to find the correct region in which MS lies with more reliability.

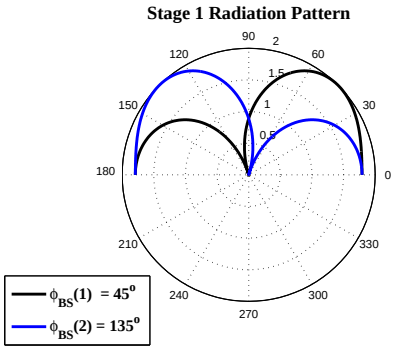

Figure 7.3: Radiation Pattern of Stage 1

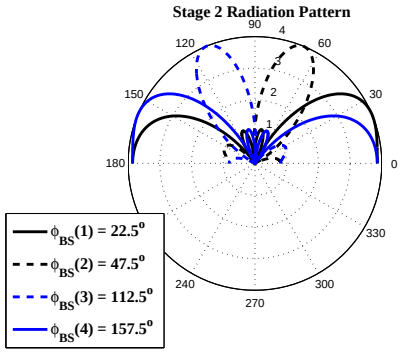

Figure 7.4: Radiation Pattern of Stage 2

7.4 Algorithms for Threshold based Hierarchical Search

In order to cope with the problem of enhanced sidelobe levels, we propose two novel hierarchical search schemes in which all the antennas are activated in all stages. We call Algorithm 1 an "iterative-thresholding hierarchical search" scheme in which the threshold is modified in each stage of hierarchical search. In particular, the BTS spends one half of pilot transmission time on testing the $\frac{N}{2}$ beam directions in $(-1, 0)$ so as to get the reliable estimate of MS's DOA in initial stages. The average energy corresponding to all the test directions is compared with a threshold which is calculated from received SNR, number of directions tested and the total number of antennas. If the average energy in first stage is above the threshold, then first half of $(-1, 0)$ is searched again via $\frac{N}{4}$ beam directions otherwise the first half of $(0, 1)$ is searched via $\frac{N}{4}$ beam directions. In each stage, the number of directions tested is halved until we end up with only one test beam which is chosen if it contains energy above the threshold otherwise its competitor is chosen.

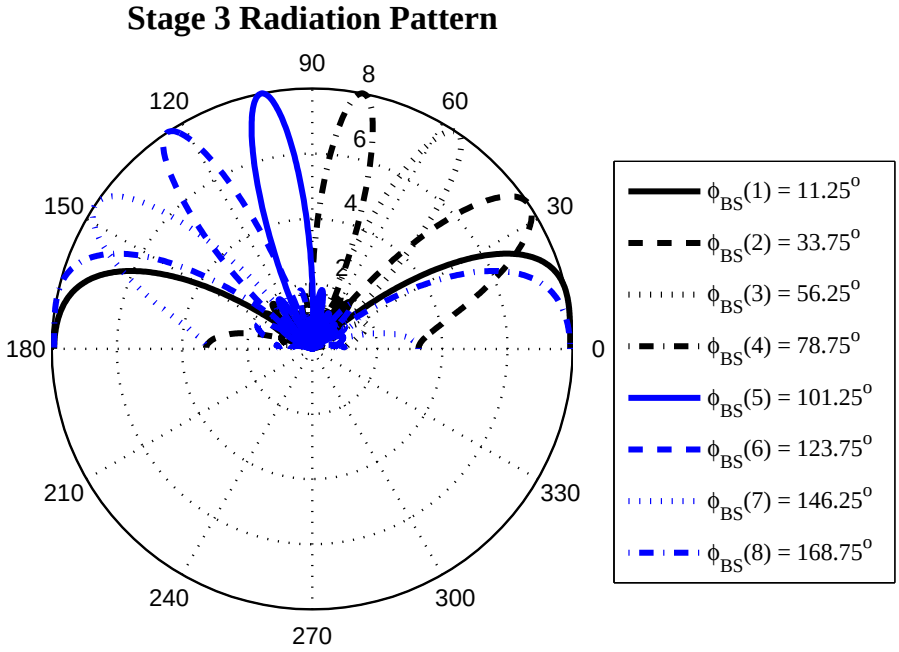

Figure 7.5: Radiation Pattern of Stage 3

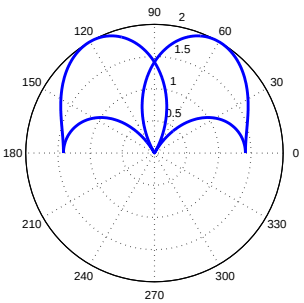

Figure 7.6: Spatial frequency radiation pattern of stage 1

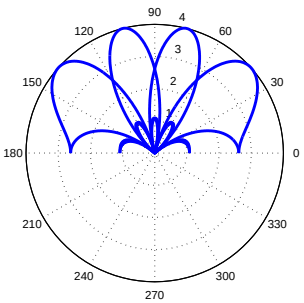

Figure 7.7: Spatial frequency radiation pattern of stage 2

Algorithm 2 is based on the refinement of searched beam directions via an additional search round cycle. Particularly, two cycles of half a second duration are employed to obtain a refined estimate of the MS's DOA. In first round cycle, all the beams are tested

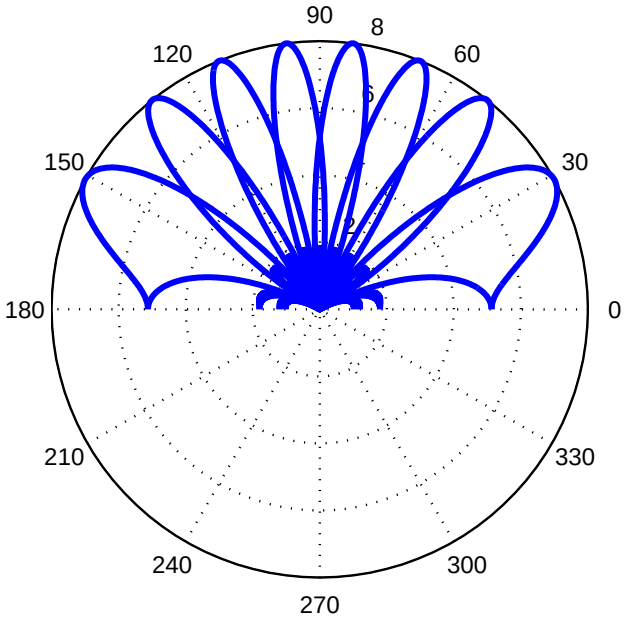

Figure 7.8: Spatial frequency radiation pattern of stage 3

at the BTS, however, only a subset of test directions which contain energy above a pre-set threshold are chosen for next cycle. In the next cycle, the remaining second half is consumed for testing the chosen search directions in the previous round and the one with the highest energy is selected. In the worst case, when all the beams in first round cycle are below the threshold, the maximum of all the beams is selected.

Algorithm 2 Iterative-Thresholding Hierarchical Search for LOS mmWave Channel

Input: $\{N_T, N, \boldsymbol{y}(t)\}$

Output: $\hat{\phi}$

Initialize the extreme indices of beamforming vectors, :

Start $\leftarrow 0$, End $\leftarrow \frac{N}{2}$

Initialize loop controlling parameters : P $\leftarrow N_T$, $k_p \leftarrow 2$.

while $P > 1$ **do**

  $\Delta \leftarrow$ End $-$ Start $+ 1$

  for $i = Start \rightarrow End$ **do**

    Record energy outputs of baseband matched-filter

    $u_i \leftarrow |\boldsymbol{w}_i^{\dagger} \boldsymbol{y}(t)|^2 \frac{1}{k_p \Delta}$

  end for

  $Average \leftarrow \frac{1}{\Delta} \sum_{i=Start}^{End} u_i$

  $\eta \leftarrow \frac{\rho N_T}{2 k_p \Delta^2}$

  if $Average > \eta$ **then**

    if $Start = End$ **then**

      Result $\leftarrow$ Start

    else

      End $\leftarrow$ End $- \frac{\mathrm{P}}{4}$

    end if

  else if $Start = End$ **then**

    Result $\leftarrow$ End $+ 1$

  else

    End $\leftarrow$ End $+ \frac{\mathrm{P}}{4}$

    Start $\leftarrow$ Start $+ \frac{\mathrm{P}}{2}$

  end if

  P $\leftarrow \frac{P}{2}$, $k_p \leftarrow 2 \times k_p$

end while

$\hat{\phi} \leftarrow \boldsymbol{\phi}_{bs}$(result)

Algorithm 3 Refined-Hierarchical Search for LOS mmWave Channel

Input: $\{\rho, N, \boldsymbol{y}(t)\}$

Output: $\hat{\phi}$

Initialize the pulse width of $s(t)$ to be $\frac{1}{2N}$.

Initialize the threshold for Refinement : $\eta \leftarrow \frac{\rho}{10}$.

for $i = 1 \rightarrow N$ **do**

    Record energy outputs of baseband matched-filter.

    $u_i \leftarrow |\boldsymbol{w}_i^{\dagger} \boldsymbol{y}(t)|^2 \frac{1}{2N}$

end for

Find indices of energy entries greater than threshold.

indices $\leftarrow$ find$(u_i > \eta)$.

Calculate the length of indices vector.

$L \leftarrow$ length(indices)

if $L > 0$ **then**

    for $j = 1 \rightarrow L$ **do**

        $t_j \leftarrow |\boldsymbol{w}_{\text{indices}(j)}^{\dagger} \boldsymbol{y}(t)|^2 \frac{1}{2L}$

    end for

    $l \leftarrow \arg\max_j t_j$

    index $\leftarrow$ indices(l)

else

    $\boldsymbol{t} \leftarrow \boldsymbol{u}$

    index $\leftarrow \arg\max_j t_j$

end if

$\hat{\phi} \leftarrow \boldsymbol{\phi}_{bs}$(index)

7.5 Statistical Analysis of Beam Misalignment

In order to do statistical analysis, it is assumed that DOAs can only take values on a grid of N points uniformly sampled from $(-1, 1)$, i.e., $\theta \in \{-1 + \frac{2k-1}{N}\}$, $k = 1, 2, \cdots, N$. In practice, the DOAs are continuous-valued, so off-grid schemes like sparse regularized total-least squares filtering or continuous-basis pursuit can be invoked to mitigate the grid quantization errors arising due to off-grid DOAs [109,110]. The following lemma illustrates that the beamforming vectors are mutually orthogonal if their spatial frequencies are outcomes of uniform sampling of the underlying search space. Similar result exists in [18] but are presented here for illustrative purposes.

Lemma 2. *If the spatial frequencies of beamforming steering vectors are chosen by uniformly sampling the search space in spatial frequency domain* $(-1, 1)$ *with spatial resolution proportional to integral multiple of* $\frac{2}{N}$*, then all the beamforming steering vectors are mutually orthogonal.*

Proof

Let $\boldsymbol{a}(\phi_1)$ and $\boldsymbol{a}(\phi_2)$ be the beamforming steering vectors corresponding to physical angles ϕ_1 and ϕ_2 then

$$\boldsymbol{a}^{\dagger}(\phi_1)\boldsymbol{a}(\phi_2) = \frac{1}{N}\sum_{m=0}^{N-1}\exp(jm\pi(\cos(\phi_1) - \cos(\phi_2))) \tag{7.19}$$

$$= \frac{1}{N}\frac{1 - \exp(-j\pi N_T(\cos(\phi_2) - \cos(\phi_1)))}{1 - \exp(-j\pi(\cos(\phi_2) - \cos(\phi_1)))} \tag{7.20}$$

$$\Rightarrow |\boldsymbol{a}^{\dagger}(\phi_1)\boldsymbol{a}(\phi_2)| = \frac{1}{N}\left|\frac{\sin(\frac{\pi N}{2}(\cos(\phi_2) - \cos(\phi_1)))}{\sin(\frac{\pi}{2}(\cos(\phi_2) - \cos(\phi_1)))}\right| \tag{7.21}$$

The absolute value of the cross-correlation will be zero when

$$\frac{\pi N}{2}(\cos(\phi_1) - \cos(\phi_2)) = l\pi \qquad l \in \mathbb{Z} \tag{7.22}$$

$$\Rightarrow \cos(\phi_2) - \cos(\phi_1) = \frac{2l}{N} \qquad l \in \mathbb{Z} \tag{7.23}$$

Our chosen beamforming directinal cosines have structure

$$\cos(\phi_2) = -1 + \frac{2k-1}{N} \qquad k \in \mathbb{Z}_+ \tag{7.24}$$

$$\cos(\phi_1) = -1 + \frac{2m-1}{N} \qquad m \in \mathbb{Z}_+ \tag{7.25}$$

The difference between two directional cosines can be manipulated as follows

$$\cos(\phi_2) - \cos(\phi_1) = \frac{2(k-m)}{N} \quad (k,m) \in (\mathbb{Z}_+, \mathbb{Z}_+) \tag{7.26}$$

$$\cos(\phi_2) - \cos(\phi_1) = \frac{2l}{N} \qquad l \in \mathbb{Z} \tag{7.27}$$

For $N = 16$, the cross-correlation of the beamforming vectors is plotted versus the difference of directional cosines. It is clear from the figure that for $\cos(\phi_2) - \cos(\phi_1) = \left\{\frac{1}{8}, \frac{1}{4}, \frac{3}{8}, \cdots, 1\right\}$, the beamforming steering vectors are orthogonal. We choose the spacing between two steering angles to be $\frac{1}{8}$ which is minimum to obtain maximum number of beamforming vectors (N = 16) in the search space $(-1, 1)$ of width 2.

7.5.1 Statistical Analysis for Exhaustive Search

For exhaustive search over all the possible beam alignments, it is assumed that DOAs take on discrete values as explained in previous subsection and all the possible beam directions are equiprobable. Moreover, under the assumption of discrete-valued DOAs, we can exhaustively search in finite number of time slots because the true DOA will align with only one beamforming vector at the BTS and its cross-correlation with other beamforming vectors will be very low due to presence of noise despite orthogonality of beamforming vectors. Furthermore, it is assumed that the signal and noise are statistically uncorrelated so the process of baseband matched filtering amounts to measuring the energy by taking the product of instantaneous power with $\frac{1}{N}$ when total pilot transmission time is assumed to be one. Now, the received signal when the transmitted signal's DOA is taking value

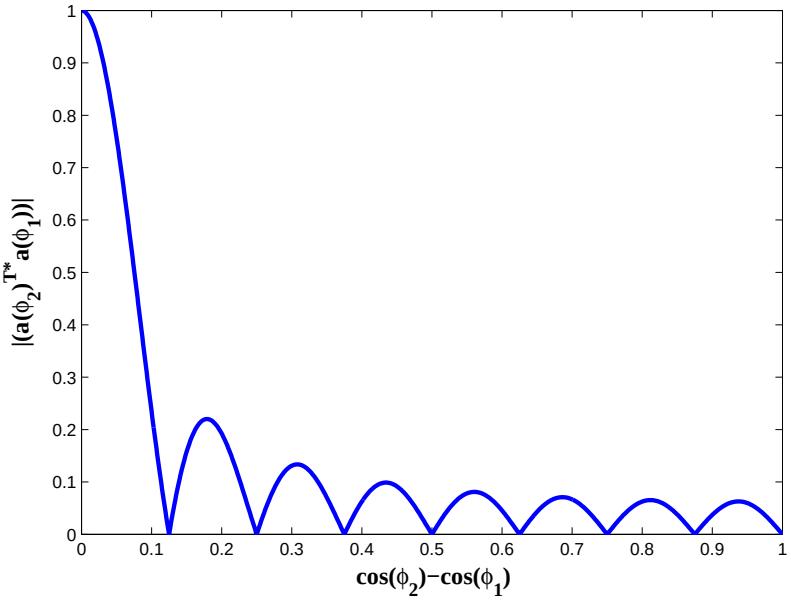

Figure 7.9: Absolute Cross-Correlation of beamforming vectors plotted verus difference of spatial frequencies for N = 16

on the i-th point on the grid, can be expressed as follows.

$$\boldsymbol{y} = \sqrt{\rho N}\boldsymbol{a}(\phi_i)s + \boldsymbol{n} \tag{7.28}$$

At BTS, the received signal is processed through a beamformer and energy is measured via a baseband matched-filter. After N measurements, the energy outputs $\frac{|\boldsymbol{w}_i^\dagger \boldsymbol{y}|^2}{N}$ are compared with each other. The energy outputs can be expressed as follows.

$$\frac{|\boldsymbol{w}_i^\dagger \boldsymbol{y}|^2}{N} = \frac{|\sqrt{\rho N}s + \boldsymbol{w}_i^\dagger \boldsymbol{n}|^2}{N} \tag{7.29}$$

$$\frac{|\boldsymbol{w}_j^\dagger \boldsymbol{y}|^2}{N} = \frac{|\boldsymbol{w}_j^\dagger \boldsymbol{n}|^2}{N} \qquad \forall j \neq i \tag{7.30}$$

where we have dropped the time dependence with slight abuse of notation. For $1 \leq j \leq N$, $\boldsymbol{w}_j^\dagger \boldsymbol{n}$ is complex AWGN with variance 1 ($\frac{1}{2}$ per real and imaginary dimension). Let $\boldsymbol{r}_i = \boldsymbol{w}_i^\dagger \boldsymbol{y}$ and $\boldsymbol{r}_j = \boldsymbol{w}_j^\dagger \boldsymbol{y} \quad \forall j \neq i$, then the envelope of i-th beamformer output admits Rician distribution and and that of other beamformer outputs $\{\boldsymbol{r}_j\}_{\forall j \neq i}$ admit

Rayleigh distribution. It is well known that the square of Rician distribution follows non-central chi square distribution with degrees of freedom equal to two and the square of Rayleigh distribution admits exponential distribution. The PDFs of energies of i-th and j-th matched filters can be expressed as follows.

$$f_{\mathcal{E}_i}(w) = \frac{1}{2\sigma^2} \exp\left(-\frac{Nw+\nu^2}{2\sigma^2}\right) \mathrm{I}_0\left(\frac{\sqrt{Nw}}{\sigma^2}\nu\right) u(w) \tag{7.31}$$

$$f_{\mathcal{E}_j}(z) = \frac{1}{2\sigma^2} \exp\left(-\frac{Nz}{2\sigma^2}\right) u(z) \qquad \forall j \neq i \tag{7.32}$$

where $\nu = \sqrt{\rho N}$ is non-centrality parameter and $\sigma^2 = \frac{1}{2}$ is noise power per dimension at the output of the matched filter, $\mathrm{I}_0(\cdot)$ is modified Bessel function of first kind and zero order and $u(\cdot)$ is Heaviside unit step function. The BTS will make an error in beam alignment if the energy of the beamformed signal corresponding to the correct direction becomes less than that of beamformed signals corresponding to other directions. Without loss of generality, it is assumed that the transmitted signal $\boldsymbol{a}(\phi_i)s$ lies in the 1st bin of the search space, then the BTS makes a correct decision if $\{\mathcal{E}_j < \mathcal{E}_1\}_{\forall j \neq i}$. Thus, the probability of correct decision can be expressed as follows.

$$\begin{aligned} \mathrm{P}_c &= \mathrm{Prob}\left\{\mathcal{E}_2 < \mathcal{E}_1, \cdots, \mathcal{E}_N < \mathcal{E}_1\right\} && (7.33)\\ &= \int_0^\infty \mathrm{Prob}\left\{\mathcal{E}_2 < w, \cdots, \mathcal{E}_N < w \middle| \mathcal{E}_1 = w\right\} f_{\mathcal{E}_1}(w) dw && (7.34)\\ &= \int_0^\infty \left[\mathrm{Prob}\left\{\mathcal{E}_2 < w\right\}\right]^{N-1} f_{\mathcal{E}_1}(w) dw && (7.35) \end{aligned}$$

Now, using the CDF of the exponential distribution, we get

$$\mathrm{Prob}\left\{\mathcal{E}_2 < w\right\} = \left(1 - \exp\left(-Nw\right)\right) u(w) \tag{7.36}$$

The application of the Binomial expansion yields,

$$\left[\mathrm{Prob}\left\{\mathcal{E}_2 < w\right\}\right]^{N-1} = \sum_{n=0}^{N-1} \binom{N-1}{n} (-1)^n \exp\left(-Nwn\right) \tag{7.37}$$

The probability of the correct decision can be expressed as follows.

$$\begin{aligned} \mathrm{P}_c &= \sum_{n=0}^{N-1} \binom{N-1}{n} (-1)^n \int_0^{\infty} \exp\left(-Nw(n+1)+\nu^2\right) \\ &\times \mathrm{I}_0\left(2\sqrt{Nw}\nu\right) dw \end{aligned} \tag{7.38}$$

Substituting $Nw(n+1) = u$ and doing some manipulations, we obtain

$$\begin{aligned} \mathrm{P}_c = &\sum_{n=0}^{N-1} \binom{N-1}{n} \frac{(-1)^n}{n+1} \exp\left(-\nu^2\left(\frac{n}{n+1}\right)\right) \\ &\times \int_0^{\infty} \exp\left(-u+\frac{\nu^2}{n+1}\right) \mathrm{I}_0\left(2\sqrt{u}\frac{\nu}{\sqrt{n+1}}\right) du \end{aligned} \tag{7.39}$$

The integrand is the PDF of non-central chi-square with non-centrality parameter $\frac{\nu^2}{n+1}$ so it integrates to unity. Substituting $\nu^2 = \rho N$, we obtain

$$\mathrm{P}_c = \sum_{n=0}^{N-1} \binom{N-1}{n} \frac{(-1)^n}{n+1} \exp\left(-\rho\frac{nN}{n+1}\right) \tag{7.40}$$

Using $\mathrm{P}_e = 1 - \mathrm{P}_c$, Eq. (7.41) follows.

Theorem 4. *For a spatial frequency resolution of $\frac{2}{N}$, the BTS succeeds in estimating the beam direction under energy detection criterion with probability of error P_e where,*

$$P_e = \sum_{n=1}^{N-1} \binom{N-1}{n} \frac{(-1)^{n+1}}{n+1} \exp\left(-\rho\frac{nN}{n+1}\right) \tag{7.41}$$

where ρ is the received SNR.

7.5.2 Bayesian Approach for Beam Alignment

During the beam alignment phase, estimating the direction in which BTS 'listens' to the signal can be performed by designing a N-ary hypothesis testing problem. In prior literature [90], the beam which has highest power among a set of beams is selected so the criterion for selection of a beam is signal power at output of beamformer. However, due to presence of noise in signal, the received power contains noise power which perturbs

the beams at the output of beamformer in erroneous directions. As a result if a wrong direction is selected due to noise perturbation, the hierarchical search typically fails due to error-propagation.

In this section, we propose a Bayesian approach which aims at minimizing the probability of estimation error. The Maximum-a-Posteriori (MAP) detector, which is a Bayesian risk minimizer, boils down to ML detector under the assumption that signal can take on any direction with equal probability. We begin by formulating the N hypotheses that the signal can take on any of N directions.

$$\mathcal{H}_1 : \quad \boldsymbol{y} = \sqrt{\rho N}\boldsymbol{a}(\phi_1) + \boldsymbol{n} \tag{7.42}$$

$$\vdots \tag{7.43}$$

$$\mathcal{H}_N : \quad \boldsymbol{y} = \sqrt{\rho N}\boldsymbol{a}(\phi_N) + \boldsymbol{n} \tag{7.44}$$

where $\boldsymbol{n} \sim \mathcal{CN}(\mathbf{0}, \mathbf{I})$ is the complex AWGN with noise covariance matrix $\mathbf{I}$. Without loss of generality, we have assumed the pilot symbol to be one. Let all the ϕ_i's be equiprobable, then the Bayesian detector selects the hypothesis $\mathcal{H}_i$ which maximizes the conditional likelihood function.

$$\mathcal{H}_i = \arg\max_{\mathcal{H}_l} f_{\boldsymbol{n}}(\boldsymbol{y}|\mathcal{H}_l) \tag{7.45}$$

$$= \arg\max_{l} \frac{1}{\det(\pi \boldsymbol{I})} \exp\left(-\left\|\boldsymbol{y} - \sqrt{\rho N}\boldsymbol{a}(\phi_l)\right\|_2^2\right) \tag{7.46}$$

Maximizing the log-likelihood function and doing some manipulations lead to following detector.

$$\mathcal{H}_i = \arg\max_{l} \Re\left(\boldsymbol{y}^\dagger \boldsymbol{a}(\phi_l)s\right) - \frac{\sqrt{\rho N}}{2}\left\|\boldsymbol{a}(\phi_l)\right\|_2^2 \tag{7.47}$$

It can be readily observed from the estimation rule in Eq. (7.47) that the BTS must measure the received SNR in order to align the beam towards the user. However, due to the Vandermonde structure of ULA steering vectors, all steering vectors have equal energy,

thus rendering the second term constant. Consequently, we can simplify the estimation criterion as follows.

$$\mathcal{H}_i = \arg\max_{l} \quad \Re\left(\boldsymbol{y}^{\dagger}\boldsymbol{a}(\phi_l)\right) \tag{7.48}$$

Here we have omitted the pilot waveform as after baseband matched-filtering, all the hypotheses acquire same amount of energy inversely proportional to N. Thus, the optimum detector cross-correlates the received signal with all the candidate beamforming vectors at the BTS and chooses the one which maximizes the output of cross-correlators. Hence, the above detector can be interpreted as "beam-correlator" or "beam matched filter" because it matches the received signal with different potential beamforming vectors. Let $\mathbb{T}(\boldsymbol{y}) = \mathcal{R}\left(\boldsymbol{y}^{\dagger}\boldsymbol{a}(\phi_l)\right)$ represent the test statistic under an arbitrary hypothesis then the conditional test statistic under true hypothesis $\mathcal{H}_i$ and the conditional test statistic under rest of hypotheses can be defined as follows.

$$\mathbb{T}_i(\boldsymbol{y}) \;:=\; \mathbb{T}(\boldsymbol{y}\big|\mathcal{H}_i) \tag{7.49}$$

$$\mathbb{T}_j(\boldsymbol{y}) \;:=\; \mathbb{T}(\boldsymbol{y}\big|\mathcal{H}_j) \qquad \forall j \neq i \tag{7.50}$$

The probability distribution of the conditional test statistic under the true and the rest of the hypotheses are characterized in the following lemma.

Lemma 3. *Under Bayeisan estimation approach, the test statistics of true and false hypotheses* $\mathbb{T}(\boldsymbol{y}|\mathcal{H}_i)$ *and* $\mathbb{T}(\boldsymbol{y}|\mathcal{H}_j) \;\; \forall j \neq i$ *admit Gaussian distributions which can be expressed as follows.*

$$\mathbb{T}_i(\boldsymbol{y}) \;\sim\; \mathcal{N}\left(\boldsymbol{y}; \sqrt{\rho N}, \frac{1}{2}\right) \tag{7.51}$$

$$\mathbb{T}_j(\boldsymbol{y}) \;\sim\; \mathcal{N}\left(\boldsymbol{r}; 0, \frac{1}{2}\right) \tag{7.52}$$

Proof Under $\mathcal{H}_i$, the cross-correlation between the received signal and transmitted

signal can be expressed as follows.

$$\begin{aligned} \boldsymbol{y}^{\dagger}\boldsymbol{a}(\phi_i) &= (\sqrt{\rho N}\boldsymbol{a}(\phi_i)+\boldsymbol{n})^{\dagger}\boldsymbol{a}(\phi_i) && (7.53)\\ &= \sqrt{\rho N}+\boldsymbol{n}^{\dagger}\boldsymbol{a}(\phi_i) && (7.54)\end{aligned}$$

$$\begin{aligned} \Rightarrow \mathbb{E}\left[\boldsymbol{y}^{\dagger}\boldsymbol{a}(\phi_i)|\mathcal{H}_i\right] &= \sqrt{\rho N} && (7.55)\\ \mathrm{Var}[\boldsymbol{y}^{\dagger}\boldsymbol{a}(\phi_i)|\mathcal{H}_i] &= \mathrm{Var}[\boldsymbol{n}^{\dagger}\boldsymbol{a}(\phi_i)] && (7.56)\\ &= \mathbb{E}[\boldsymbol{a}^{\dagger}(\phi_i)\boldsymbol{n}\boldsymbol{n}^{\dagger}\boldsymbol{a}(\phi_i)] && (7.57)\\ &= 1 && (7.58)\end{aligned}$$

$$\Rightarrow \mathbb{T}(\boldsymbol{y}|\mathcal{H}_i)\sim\mathcal{N}\left(\boldsymbol{y};\sqrt{\rho N},\frac{1}{2}\right) \quad (7.59)$$

Under $\mathcal{H}_j$, the cross-correlation between the received signal and transmitted signal can be expressed as follows.

$$\begin{aligned} \Rightarrow \boldsymbol{y}^{\dagger}\boldsymbol{a}(\phi_i) &= (\sqrt{\rho N}\boldsymbol{a}(\phi_j)+\boldsymbol{n})^{\dagger}\boldsymbol{a}(\phi_i) && (7.60)\\ &= \boldsymbol{n}^{\dagger}\boldsymbol{a}(\phi_i) && (7.61)\\ \text{provided } \boldsymbol{a}^{\dagger}(\phi_j)\boldsymbol{a}(\phi_i) &= 0 \qquad \forall j\neq i && (7.62)\end{aligned}$$

$$\begin{aligned} \Rightarrow \mathbb{E}\left[\boldsymbol{y}^{\dagger}\boldsymbol{a}(\phi_i)\middle|\mathcal{H}_j\right] &= 0 && (7.63)\\ \mathrm{Var}\left[\boldsymbol{y}^{\dagger}\boldsymbol{a}(\phi_i)\middle|\mathcal{H}_i\right] &= \mathrm{Var}[\boldsymbol{n}^{\dagger}\boldsymbol{a}(\phi_i)] && (7.64)\\ &= 1 && (7.65)\end{aligned}$$

$$\Rightarrow \mathbb{T}(\boldsymbol{y}|\mathcal{H}_j) \sim \mathcal{N}\left(\boldsymbol{y};0,\frac{1}{2}\right) \quad (7.66)$$

Theorem 5. *For a spatial frequency resolution of $\frac{2}{N}$, the BTS succeeds in detecting the beam direction under Bayesian detection criterion with the probability of error P_e where,*

$$P_e = 1-\Phi^{N-1}\left(\sqrt{\rho N}\right) \quad (7.67)$$

where $\Phi(\cdot)$ is the CDF of unit normal random variable and ρ is the received SNR.

Proof An error occurs when any of the $N-1$ test statistics becomes greater than the test statistics associated with the true hypothesis. Now the probability of error can be expressed as follows.

$$\mathrm{P}_e = \sum_{i=0}^{N-1} \mathrm{Prob}\left\{\mathbb{T}_i < \max(\mathbb{T}_1, \cdots, \mathbb{T}_{i-1}, \mathbb{T}_{i+1}, \cdots, \mathbb{T}_N) \middle| \mathcal{H}_i\right\} \mathrm{Prob}\left\{\mathcal{H}_i\right\} \tag{7.68}$$

Owing to symmetry, all of the conditional error probabilities in the above sum are equal due to underlying orthogonal structure of transmit signals and therefore following simplification can be made.

$$\begin{aligned}
\mathrm{P}_e &= \mathrm{Prob}\left\{\mathbb{T}_i < \max(\mathbb{T}_1, \mathbb{T}_2, \cdots, \mathbb{T}_{i-1}, \mathbb{T}_{i+1}, \cdots, \mathbb{T}_N) \middle| \mathcal{H}_i\right\} && (7.69)\\
&= 1 - \mathrm{Prob}\left\{\mathbb{T}_i > \max(\mathbb{T}_1, \mathbb{T}_2, \cdots, \mathbb{T}_{i-1}, \mathbb{T}_{i+1}, \cdots, \mathbb{T}_N) \middle| \mathcal{H}_i\right\} && (7.70)\\
&= 1 - \mathrm{Prob}\left\{\mathbb{T}_1 < \mathbb{T}_i, \cdots, \mathbb{T}_{i-1} < \mathbb{T}_i, \mathbb{T}_{i+1} < \mathbb{T}_i, \cdots, \mathbb{T}_N < \mathbb{T}_i\right\} && (7.71)\\
&= 1 - \int_{-\infty}^{+\infty} \mathrm{Prob}\left\{\mathbb{T}_1 < t, \cdots, \mathbb{T}_{i-1} < t, \mathbb{T}_{i+1} < t, \cdots \mathbb{T}_N < t\right\} f_{\mathbb{T}_i}(t) dt && (7.72)
\end{aligned}$$

The covariance of any two test statistics can be calculated as follows.

$$\begin{aligned}
\mathsf{Cov}(\mathbb{T}_\mathsf{i}, \mathbb{T}_\mathsf{j}) &= \mathbb{E}[\mathbb{T}_i^\dagger \mathbb{T}_j] - \mathbb{E}^\dagger[\mathbb{T}_i]\mathbb{E}[\mathbb{T}_j] && (7.73)\\
&= \mathbb{E}\left[\left(\boldsymbol{n}^\dagger \boldsymbol{a}(\phi_i)\right)^\dagger \left(\boldsymbol{n}^\dagger \boldsymbol{a}(\phi_j)\right)\right] && (7.74)\\
&= \boldsymbol{a}(\phi_i)^\dagger \boldsymbol{a}(\phi_j) && (7.75)\\
&= 0 \qquad \forall j \neq i && (7.76)
\end{aligned}$$

Since $\{\mathbb{T}_j\}_{j=1}^N$ are jointly Gaussian and uncorrelated random variables, so they are independent random variables. Therefore, the events $\{\mathbb{T}_j < t\}_{\forall j \neq i}$ will become statistically independent. It, therefore, follows from Eq. (7.72) that

$$\mathrm{P}_e = 1 - \int_{-\infty}^{+\infty} \Phi^{N-1}\left(t\sqrt{2}\right) \mathcal{N}\left(t; \sqrt{\rho N}, \frac{1}{2}\right) dt \tag{7.77}$$

Let $Y \sim \mathcal{N}(t; 0, 1)$ be a standard normal random variable, then Eq. (7.77) can be simpli-

fied as follows.

$$\begin{aligned} \mathrm{P}_e &= 1 - \left[\mathrm{Prob}\left\{Y < \mathbb{T}_i\sqrt{2}\right\}\right]^{N-1} && (7.78) \\ &= 1 - \left[\mathrm{Prob}\left\{\frac{Y}{\sqrt{2}} - \mathbb{T}_i < 0\right\}\right]^{N-1} && (7.79) \end{aligned}$$

Let $Z = \frac{Y}{\sqrt{2}} - \mathbb{T}_i$, then using the property that the difference of two Gaussian-distributed random variables exhibits a Gaussian distribution we end up with a random variable having probability distribution $Z \sim \mathcal{N}(z; -\sqrt{\rho N}, 1)$. It follows that

$$\mathrm{P}_e = 1 - \Phi^{N-1}\left(\sqrt{\rho N}\right) \tag{7.80}$$

where $\Phi(\cdot)$ is the CDF of unit normal random variable which completes the proof.

7.5.3 Asymptotic Analysis for Bayesian detector

Let $\mathbb{T}_i^{(N)}$ denote the test statistic under true hypothesis $\mathcal{H}_i$ with number of directions tested equal to N and let $\mathbb{M}^{(N)} = \max\left(\mathbb{T}_1^{(N)}, \mathbb{T}_2^{(N)}, \cdots, \mathbb{T}_{i-1}^{(N)}, \mathbb{T}_{i+1}^{(N)}, \cdots, \mathbb{T}_N^{(N)}\right)$ denote the maximum of a sample whose components are test statistics under false hypotheses $\{\mathcal{H}_j\}_{j\neq i}$. The maximum of i.i.d. zero mean Gaussian random variables is $\mathcal{O}(\log N)$ and $G := \left(\mathbb{M}^{(N)} - b_N\right)/a_N$ admits Gumbel distribution with location paramter $b_N = \sqrt{2\log N}$ and scaling parameter to be roughly $a_N = b_N^{-1}$ [111]. Since $\mathbb{T}_i^{(N)}$ is $\mathcal{O}(\sqrt{N})$ so it follows that

$$\left[\mathbb{T}_i^{(N)} > M^{(N)}\right] \supseteq \left[\mathbb{T}_i^{(N)} > \frac{\sqrt{\rho N}}{2} \cap M^{(N)} < \frac{\sqrt{\rho N}}{2}\right] \tag{7.81}$$

Since $\mathbb{T}_i^{(N)}$ and $N_T^{(N)}$ are statistically independent so the probability of the subset event can be expressed as follows.

$$\begin{aligned} &\mathrm{Prob}\left[\mathbb{T}_i^{(N)} > \tfrac{\sqrt{\rho N}}{2} \cap M^{(N)} < \tfrac{\sqrt{\rho N}}{2}\right] \\ &= \mathrm{Prob}\left[\mathbb{T}_i^{(N)} > \tfrac{\sqrt{\rho N}}{2}\right] \mathrm{Prob}\left[M^{(N)} < \tfrac{\sqrt{\rho N}}{2}\right] && (7.82) \end{aligned}$$

Clearly, since $\mathbb{T}_i^{(N)}$ admits Gaussian distribution with mean $\sqrt{\rho N}$ and variance $\frac{1}{2}$,

$$\text{Prob}\left[\mathbb{T}_i^{(N)} > \frac{\sqrt{\rho N}}{2}\right] \uparrow 1 \quad as \quad N \uparrow \infty \tag{7.83}$$

On the other hand,

$$\begin{aligned}
\liminf_{N\uparrow\infty} \text{Prob}\left[M^{(N)} < \frac{\sqrt{\rho N}}{2}\right] &= \liminf_{n\uparrow\infty} \text{Prob}\left[\frac{M^{(N)} - b_N}{a_N} < \frac{\frac{\sqrt{\rho N}}{2} - b_N}{a_N}\right] && (7.84)\\
&\geq \lim_{n\uparrow\infty} \text{Prob}\left(\frac{M^{(N)} - b_N}{a_N} < k\right) && (7.85)\\
&\stackrel{d}{\Rightarrow} \text{Prob}(G < k) \quad \forall k && (7.86)
\end{aligned}$$

where Eq. (7.86) follows from

$$\text{Prob}\left(\frac{M^{(N)} - b_N}{a_N} < k\right) \stackrel{d}{\Rightarrow} \text{Prob}\,(G < k) \tag{7.87}$$

Choosing k to be large enough $\text{Prob}\,(G < k)$ goes to 1 and to satisfy the lower bound in Eq. (7.85), we get

$$\lim_{N\uparrow\infty} \text{Prob}\left(M^{(N)} < \frac{\sqrt{\rho N}}{2}\right) = 1 \tag{7.88}$$

Combining Eq. (7.5.3) with Eq. (7.5.3), we obtain

$$\text{Prob}\left(\mathbb{T}_i^{(N)} > M^{(N)}\right) \to 1 \quad as \quad N \uparrow \infty \tag{7.89}$$

Since $\text{P}_e = 1 - \text{Prob}\left(\mathbb{T}_i^{(N)} > M^{(N)}\right)$ so as $N \uparrow \infty$, $\text{P}_e^{(N)} \to 0$.

7.6 Numerical Experiments and Simulation

This section is devoted towards numerical experiments to verify the performance of proposed algorithms in terms of probability of beam misalignment and mean-square error. Moreover, the analytical expressions for probability of beam misalignment under various estimators are verified via simulation results. All the simulation results are averaged over

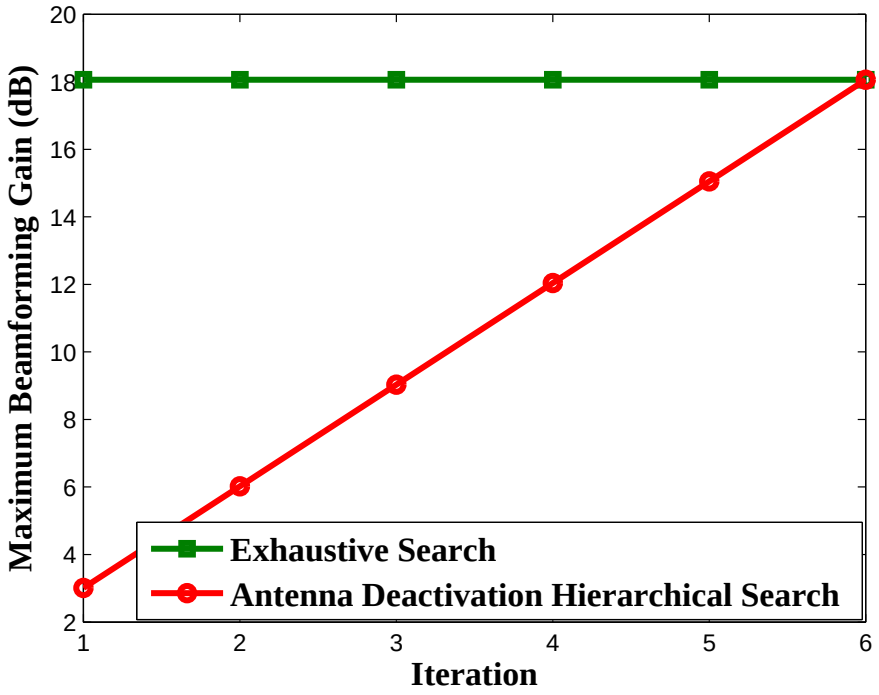

Figure 7.10: Beamforming Gain Comparison of Hierarchical Search and Exhaustive Search at N = 64

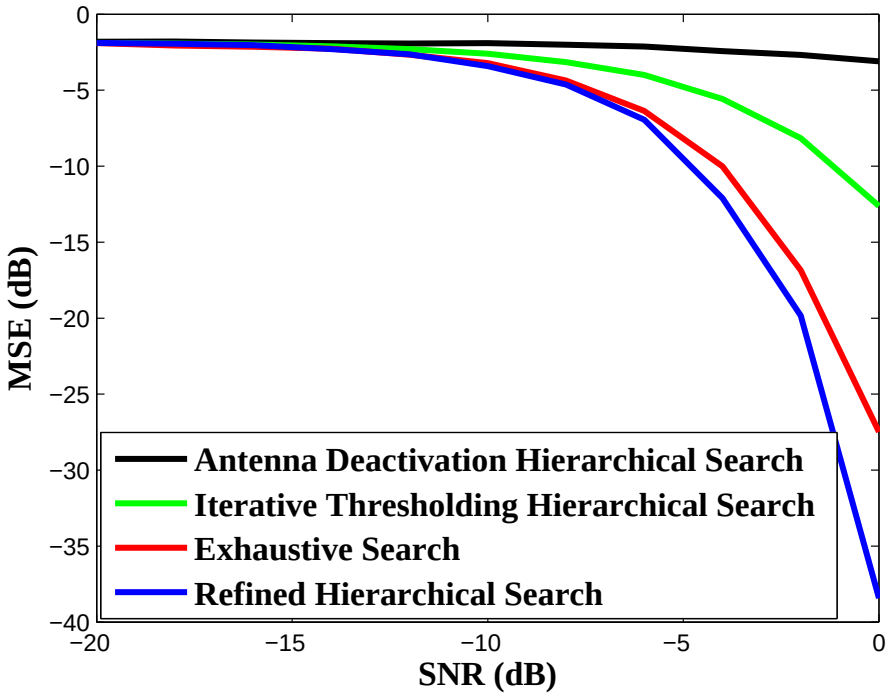

Figure 7.11: Mean-Square Error Comparisons of Proposed Algorithms with Existing Schemes for N = 16

10, 000 Monte Carlo runs. In all the experiments, the numbers of antennas is assumed to be equal to number of directions tested, i.e., $N_T = N$. In order to do fair comparison, the energy budget is assumed to be same for all the algorithms in one figure. We take SNR in dB to be in negative range as mmWave systems are noise-limited in general. Suppose our mmWave system is operating at 73 GHz with a coherence bandwidth of 100 MHz.

Consider a high-mobility user moving at the high speed of 4m/s, then the coherence time is equal to 1ms which is very small. Now, if we have 100 pilot symbols which will span $1\mu s$, then approximately 10% of our resources will be wasted into beam-training phase thereby resulting in throughput loss. As a result, we do performance evaluation of our algorithms with existing schemes at number of training symbols equal to 16, 32. Furthermore, consider that the MS transmits at peak power of 20 dBm [112,113] and BTS

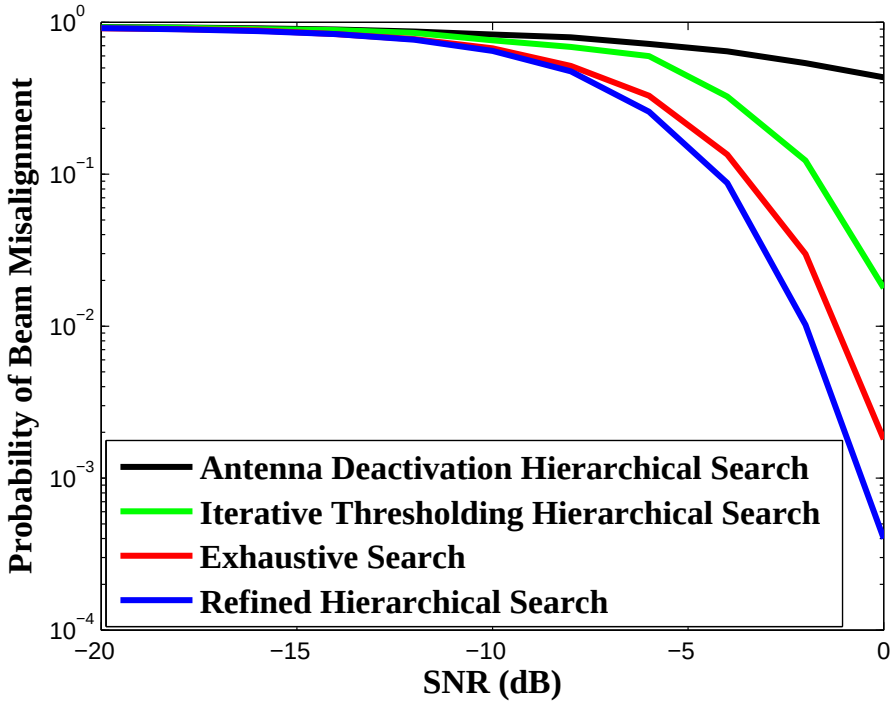

Figure 7.12: Beam Misalignment Probability Comparisons of Proposed Algorithms with Existing Schemes for N = 16

noise figure is 5 dB, then following the path-loss parameters ($\alpha = 69.8, \beta = 2$) of [81], we achieve a receive SNR before beamforming of -16.8 dB and -20.3 dB at distance of 20 metres and 30 metres from the BTS respectively. Thus, it is imperative to align the beams at the BTS for such high-speed users with poor SNR in few training slots in order to conserve energy resources while maintaining reasonable throughput.

Fig. 7.10 demonstrates the beamforming gain achieved by the hierarchical search in different stages and is compared with the beamforming gain of exhaustive search which is flat because it keeps all the antennas activated whereas the antenna deactivation approach sequentially attains higher beamforming gains in later stages due to more antennas activated in higher stages. For $N = 64$, exhaustive search achieves a beamforming gain of 18 dB which antenna deactivation approach achieves in 6-th iteration.

Fig. 7.11 graphs the MSE (in dBs) versus receive SNR per antenna in dBs for iterative-thresholding-hierarchical search (ITHS), antenna-deactivation-hierarchical search (ADHS), exhaustive search (ES), and refined-hierarchical search (RHS) for $N = 16$. Fig. reveals that ITHS beats the performance of ADHS after -12 dB and ES outperforms the ADHS after -13 dB. Additionally, RHS offers superior performance in comparison to ES beyond -6 dB. At SNR of 0 dB, ITHS offers an MSE of -13 dB which is 10 dB less than that offered by ADHS. Similarly, RHS offers 11 dB improvement over ES. Thus, in general, ITHS outperforms ADHS and RHS offers superior performance over ES. This is happening because in ADHS, initial stages use wide beams which have low beamforming gain but ITHS uses narrow beams in initial stages as well. Hence, ITHS becomes able to track the user in true region in initial stages due to usage of narrow beams in all steps of hierarchical search. On the other hand, RHS spends one half of training time in searching a user and then based on a threshold it refines its search via selecting the one with highest gain in the second stage. In contrast, conventional ES uses full training time for searching the best direction and due to lack of threshold selects the beam direction with the maximum gain.

Fig. 7.12 plots the probability of beam misalignment versus receive SNR per antenna in dBs for ITHS, ADHS, ES and RHS for $N = 16$. At 0 dB, ITHS beats the performance of ADHS by offering an error rate of 2×10^{-2}. However, ES offers error rates as low as 2×10^{-3} at 0 dB whereas RHS offers error rate of 4×10^{-4} at receive SNR of 0 dB. Beyond -10 dB, RHS offers better performance than ES and ITHS outperforms ADHS. After -10 dB, RHS outperforms ES and ITHS outperforms ADHS. Thus, in terms of both performance metrics, MSE and Error Rate, RHS outperforms all the competing schemes with same amount of training and energy resources.

Fig. 7.13 delineates the beam misalignment probability versus receive SNR in dBs for energy and bayesian estimators for $N = 16,32$. The plot of analytical probability

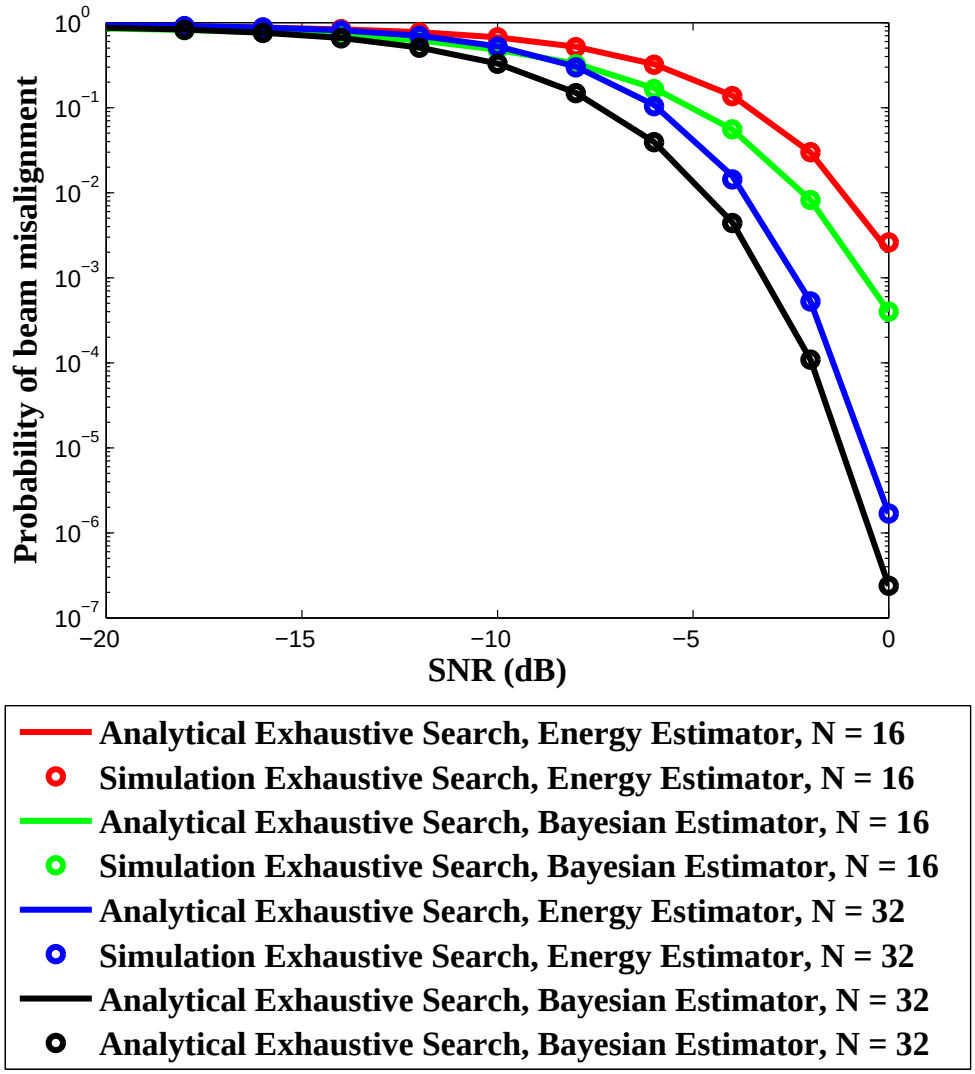

Figure 7.13: Beam Misalignment Probability Comparisons of Exhaustive Search under Energy and Bayesian Estimators for N = 16,32

expressions are compared with experimentals results from Monte Carlo simulations and derived results fit in well with simulated outcomes. Additionally, for both $N = 16,32$ the Bayesian estimator offers better performance than energy estimator beyond -12 dB. In particular at 0 dB the Bayesian estimator offers error rate of 3×10^{-4} whereas energy estimator shows error probability of 2×10^{-3} for $N = 16$. For $N = 32$, bayesian estimator offers error rates as low as 10^{-7} whereas energy estimator gives error rate of 2×10^{-6}. Thus, bayesian estimator is a viable design choice instead of conventional energy estimators.

7.7 Conclusion

In this chapter, we dealt with the issue of beam alignment which arises in mmWave massive MIMO systems under an RF chains constraint. We proposed two novel hierarchical search algorithms for beam alignment which offer superior performance to existing hierarchical search based beam alignment. Furthermore, we proposed a Bayesian approach of detecting a beam instead of using energy based detection. We derived closed-form expressions for probability of beam-misalignment under exhaustive search for Bayesian and energy based detections. Numerical results corroborate the validity of our derived results.

Chapter 8

Conclusions

This thesis addresses the challenge of limited RF chains in massive MIMO operating in TDD mode.

We began the thesis in Chapter 3 with the pilot contamination problem which had been addressed earlier by [25] by using coordination among BTSs for scheduling of training sequences. We proposed a non-coordinated approach in which random training sequences are employed across cells which are orthogonal within a cell. The proposed random training sequences become orthogonal with out-of-cell sequences asymptotically as their length increases. The random training sequences offer superior performance in terms of network capacity in comparison to reuse of same set of training sequences across different cells.

Spatial modulation format can be used to tackle the problem of limited RF chains in massive MIMO. In Chapter 4, we proposed a novel CS aided linear detection algorithm exploiting the sparse structure of transmit data in GSM for the MIMO ISI channel. Our proposed algorithm offers superior performance in comparison to existing CS based techniques in terms of MSE and BER. We extended single-user GSM system to multi-user GSM system and investigated the sparse recovery of transmit data which achieved the

performance of interference free point-to-point systems.

In Chapter 5, we showed using achievable rates that a GSM system can offer same achievable rate as a SM system but using less transmit antennas and with a lower channel estimation burden. In GSM system, CSI is required at MS to do data detection which can be sent from BTS through a feedback link. This causes a huge overhead because all the channel link gains need to be sent to MS through backhaul or control channel as channel estimation is done at BTS in massive MIMO operating in TDD mode.

Another solution to mitigate the spectral efficiency loss occurring due to limited RF chains is antenna selection. In antenna selection, the MS just needs to know the channel power gain which being a scalar can be reported to MS from BTS through feedback link with low overhead. In Chapter 6, we provided a large system analysis of antenna selection massive MIMO. The deterministic equivalent of capacity is shown to be a deterministic function of number of RF chains and transmit antenna elements in Rayleigh fading environment. Our proposed expression can be used to design and optimize a system without the requirement of extensive Monte Carlo runs. A design insight from large system analysis is that we can calculate the required number of RF chains to achieve the target capacity for a given number of transmit antenna elements using our asymptotic limit.

MmWave massive MIMO systems offer huge bandwidths but the RF chains constraint becomes significant at mmWave frequencies. A key problem in mmWave massive MIMO is beam alignment which arises due to narrow beams of high-gain antennas at mm-Wave frequencies. In Chapter 7, our key contributions are two novel algorithms for beam alignment in mmWave massive MIMO operating in uplink. The proposed algorithms are premised on iterative thresholding hierarchical search and refined hierarchical search in which all the antenna elements are activated in all the training slots to reap the benefits of huge beamforming gain. Our proposed refined hierarchical search outperforms the optimal

exhaustive search in terms of MSE and probability of beam misalignment. Furthermore, we proposed Bayesian approach for beam detection which offers superior performance in comparison to conventional energy based detection.

Appendix A

List of Acronyms

ADC	Analogue to Digital Converter
AWGN	Additive White Gaussian Noise
BER	Bit Error Rate
BPSK	Binary Phase Shift Keying
CDF	Cumulative Distribution Function
CWGN	Complex White Gaussian Noise
CS	Compressive Sensing
DAC	Digital to Analogue Converter
ES	Exhaustive Search
GSM	Generalized Spatial Modulation
IBI	Inter-Block Interference
ISI	Inter-Symbol Interference
ITHS	Iterative thresholding hierarchical search
LNA	Low Noise Amplifier
MAP	Maximum-A-Posteriori
MGF	Moment Generating Function

MIMO	Multiple-Input Multiple-Output
MISO	Multiple-Input Single-Output
ML	Maximum Likelihood
mmWave	Millimetre Wave
MSE	Mean Square Error
NMSE	Normalized Mean Square Error
OFDM	Orthogonal Frequency Division Multiplexing
PDF	Probability Density Function
QAM	Quadrature Amplitude Modulation
RHS	Refined Hierarchical Search
SIMO	Single-Input Multiple-Output
SISO	Single-Output Single-Output
SM	Spatial Modulaion
SNR	Signal-to-Noise Ratio
TLS	Total Least Squares

Appendix B

List of Notations

$\mathbb{A}$	Set of antenna indices
$\lvert\cdot\rvert$	Absolute Value
$\lVert\cdot\rVert^2$	L_2 or Eucledian Norm
$\mathbb{C}$	Set of complex numbers
$\mathbb{C}^N$	Set of $N \times 1$ complex vectors
$\mathbb{C}^{N\times N}$	Set of $N \times N$ complex matrices
$\mathcal{C}(\boldsymbol{A})$	Column space of matrix $\boldsymbol{A}$
$\mathrm{Cov}(X, Y)$	Covariance of random variables X and Y
$\mathcal{CN}(\mathbf{0}, \boldsymbol{R})$	Complex Gaussian with mean $\mathbf{0}$ and Covariance $\boldsymbol{R}$
$\mathsf{diag}[a_i]_{i=1\cdots N}$	Diagonal matrix with diagonal entries $a_1, \cdots, a_N$
$\lfloor\rfloor$	Floor function
$()^H$	Complex Conjugate Transpose
$\langle \boldsymbol{X}, \boldsymbol{Y}\rangle$	Inner product $\mathsf{Trace}(\boldsymbol{X}^H\boldsymbol{Y})$
$\langle \boldsymbol{x}, \boldsymbol{y}\rangle$	Inner product $\boldsymbol{x}^H\boldsymbol{y}$
$()^\dagger$	Pseudo-Inverse of Matrix
$\in$	Is an element of

$\cup$	Union
$\cap$	Intersection
$\subseteq$	is subset of
$\supseteq$	is superset of
$\mathbb{E}[\cdot]$	Statistical Expectation Operator
$f_X(x)$	Probability density function of random variable X
$F_X(x)$	Cumulative distribution function of random variable X
$\aleph(\boldsymbol{A})$	Null space of matrix $\boldsymbol{A}$
$p_X(x)$	Probability mass function
P_e	Probability of error
$\mathbf{I}$	Identity matrix
$\Im$	Imaginary part of complex number
$\limsup_n x_n$	limit superior of $(x_n)_{n\geq 1}$, i.e., for every $\epsilon > 0$,
	there exists $n0(\epsilon)$, such that $x_n \leq \limsup_n x_n + \epsilon \forall n > n_0(\epsilon)$
$\liminf_n x_n$	limit inferior, i.e., $\liminf_n x_n = \limsup_n x_n$
$\mathbf{1}$	Vector of ones
$\boldsymbol{P}$	Antenna activation pattern matrix
P_e	Probability of error
$\mathbb{R}$	Set of real numbers
$\mathbb{R}^N$	Set of $N \times 1$ real-valued vectors
$\mathcal{R}(\boldsymbol{A})$	Row space of matrix $\boldsymbol{A}$
$\Re$	Real part of complex number
var	Variance of random variable
$\boldsymbol{W}$	Precoding Matrix
x	Scalar x
$\boldsymbol{x}$	Vector $\boldsymbol{x}$

$\boldsymbol{X}$	Matrix $\boldsymbol{X}$
$\boldsymbol{x}(i)$	i-th component of vector $\boldsymbol{x}$
$\mathbb{Z}$	Set of integers
$\mathbb{Z}_+$	Set of positive integers
$\mathbf{0}$	Vector of zeros
$\stackrel{d}{\Rightarrow}$	Converges in distribution to

Appendix C

List of Publications

The following conference papers related to this thesis were published during the course of this PhD.

1. Z. A. Shaikh, S. V. Hanly, and I. B. Collings, "Analysis of adaptive least squares filtering in massive MIMO", in *Proc.* AusCTW, 2014, Sydney, Australia.

2. Z. A. Shaikh, I. B. Collings, S. V. Hanly, and P. Whiting, "Compressive Sensing Aided Data Detection for GSM Systems in MIMO ISI wireless channels," in *Proc.* IEEE ICC, 2015, London, UK.

3. S. V. Hanly, I. B. Collings, Z. A. Shaikh and P. Whiting, "Law of large numbers analysis of antenna selection aided downlink beamforming in massive MISO under RF chains constraint", in *Proc.* AusCTW, 2016, Melbourne, Australia.

The following conference paper not related to this thesis was published during the course of this PhD.

1. Z. Azmat and H. D. Tuan, "Power allocation for Gaussian Mixture model prior knowledge in wirless sensor networks", in *Proc.* IEEE ICASSP, 2013, Vancouver, Canada.

Appendix D

Derivation of Conditional Entropy

To obtain Eq. (5.23) from Eq. (5.22), it is required to average the above expression with respect to marginal pdf of output ,i.e., $p_{\boldsymbol{Z}}(\boldsymbol{z})$ to calculate the conditional entropy $H(U|\boldsymbol{Z})$.

$$
\begin{aligned}
H(U|\boldsymbol{Z}) &= \int_{D_{\boldsymbol{z}}} f_{\boldsymbol{Z}}(\boldsymbol{z}) H(U|\boldsymbol{Z}=\boldsymbol{z}) d\boldsymbol{z} \\
&= \int_{D_{\boldsymbol{z}}} \frac{1}{N_a S} \sum_{\gamma=1}^{N_a} \sum_{\nu=1}^{S} \frac{1}{\det\left(\pi N_o \mathbf{I}\right)} \exp\left(-\beta \|\boldsymbol{z} - \mathbf{h}_{[\gamma]} u_\nu\|^2\right) \\
&\times \frac{\displaystyle\sum_{\nu=1}^{S}\sum_{\gamma=1}^{N_a} \exp\left(-\beta \|\boldsymbol{z} - \mathbf{h}_{[\gamma]} u_\nu\|^2\right) \log_2 \left[\frac{\displaystyle\sum_{\mu=1}^{S}\sum_{\alpha=1}^{N_a} \exp\left(-\beta \|\boldsymbol{z} - \mathbf{h}_{[\alpha]} u_\mu\|^2\right)}{\displaystyle\sum_{\gamma=1}^{N_a} \exp\left(-\beta \|\boldsymbol{z} - \mathbf{h}_{[\gamma]} u_\nu\|^2\right)} \right]}{\displaystyle\sum_{\alpha=1}^{N_a}\sum_{\mu=1}^{S} \exp\left(-\beta \|\boldsymbol{z} - \mathbf{h}_{[\alpha]} u_\mu\|^2\right)} d\boldsymbol{z}
\end{aligned}
$$

$$= \tfrac{1}{N_a S} \sum_{\nu=1}^{S} \sum_{\gamma=1}^{N_a} \int_{D_{\boldsymbol{z}}} \frac{d\boldsymbol{z}}{\det\left(\pi N_o \mathbf{I}\right)} \exp\left(-\beta \|\boldsymbol{z} - \mathbf{h}_{[\gamma]} u_\nu\|^2\right) \log_2 \left[\frac{\sum_{\mu=1}^{S} \sum_{\alpha=1}^{N_a} \exp\left(-\beta \|\boldsymbol{z} - \mathbf{h}_{[\alpha]} u_\mu\|^2\right)}{\sum_{\gamma=1}^{N_a} \exp\left(-\beta \|\boldsymbol{z} - \mathbf{h}_{[\gamma]} u_\nu\|^2\right)} \right]$$

$$= \tfrac{1}{N_a S} \sum_{\nu=1}^{S} \sum_{\gamma=1}^{N_a} \int_{D_{\mathbf{n}}} \frac{\exp\left(-\beta \|\mathbf{n}\|^2\right)}{\det\left(\pi N_o \mathbf{I}\right)} \log_2 \left[\frac{\sum_{\mu=1}^{S} \sum_{\alpha=1}^{N_a} \exp\left(-\beta \|u_\nu \mathbf{h}_{[\gamma]} - u_\mu \mathbf{h}_{[\alpha]} + \mathbf{N}\|^2\right)}{\sum_{\gamma=1}^{N_a} \exp\left(-\beta \|u_\mu \left(\mathbf{h}_{[\gamma]} - \mathbf{h}_{[\alpha]}\right) + \mathbf{N}\|^2\right)} \right] d\mathbf{n} \quad \text{(D.1)}$$

where the last equality follows from the substitution $\boldsymbol{z} = \mathbf{h}_{[\gamma]} u_\nu + \mathbf{n}$. It is well-known that the expected value of a function of random variable can be expressed as follows

$$\mathbb{E}\left[g(X)\right] = \int_{D_x} g(x) f_X(x) dx \quad \text{(D.2)}$$

In light of above expression, Eq. (D.1) can be modified to get compact expression for conditional entropy as follows

$$H(U|\boldsymbol{Z}) = \frac{1}{N_a S} \sum_{\nu=1}^{S} \sum_{\gamma=1}^{N_a} \mathbb{E}_{\mathbf{N}} \log_2 \left[\frac{\sum_{\mu=1}^{S} \sum_{\alpha=1}^{N_a} \exp\left(-\beta \|u_\nu \mathbf{h}_{[\gamma]} - u_\mu \mathbf{h}_{[\alpha]} + \mathbf{N}\|^2\right)}{\sum_{\gamma=1}^{N_a} \exp\left(-\beta \left\| u_\mu \left(\mathbf{h}_{[\gamma]} - \mathbf{h}_{[\alpha]}\right) + \mathbf{N} \right\|^2\right)} \right] \quad \text{(D.3)}$$

Bibliography

[1] Cisco, "Cisco visual networking index: Global mobile data traffic forecast update: 2013- 2018," *Cisco*, Feb. 2014. [Online]. Available: http://www.cisco.com/c/en/us/solutions/collateral/service-provider/visual-networking-index-vni/mobile-white-paper-c11-520862.html

[2] A. Goldsmith, S. A. Jafar, N. Jindal, and S. Vishwanath, "Capacity limits of MIMO channels," *IEEE J. Sel. Area. Commun.*, vol. 21, no. 5, pp. 684–702, June 2003.

[3] E. T. Ar and I. E. Telatar, "Capacity of multi-antenna Gaussian channels," *Eur. Trans. Telecommun.*, vol. 10, pp. 585–595, 1999.

[4] H. Weingarten, Y. Steinberg, and S. Shamai, "The capacity region of the Gaussian MIMO broadcast channel," in *Proc. IEEE ISIT*, 2004, p. 174.

[5] E. Dahlam, S. Parkvall, J. Skold, and P. Beming, *3G Evolution HSPA and LTE for Mobile Broadband*. New York: Academic, 2008.

[6] G. Caire and S. Shamai, "On the achievable throughput of a multiantenna Gaussian broadcast channel," *IEEE Trans. Inf. Theory*, vol. 49, no. 7, pp. 1691–1706, July 2003.

[7] H. Weingarten, Y. Steinberg, and S. S. Shamai, "The capacity region of the Gaussian Multiple-Input Multiple-Output broadcast channel," *IEEE Trans. Inf. Theory*, vol. 52, no. 9, pp. 3936–3964, Sept 2006.

[8] G. Caire, N. Jindal, M. Kobayashi, and N. Ravindran, "Multiuser MIMO achievable rates with downlink training and channel state feedback," *IEEE Trans. Inf. Theory*, vol. 56, no. 6, pp. 2845–2866, June 2010.

[9] M. Kobayashi, N. Jindal, and G. Caire, "Training and feedback optimization for multiuser MIMO downlink," *IEEE Trans. Commun.*, vol. 59, no. 8, pp. 2228–2240, August 2011.

[10] H. Huh, A. M. Tulino, and G. Caire, "Network MIMO with linear zero-forcing beamforming: Large system analysis, impact of channel estimation, and reduced-complexity scheduling," *IEEE Trans. Inf. Theory*, vol. 58, no. 5, pp. 2911–2934, May 2012.

[11] R. Zakhour and S. V. Hanly, "Base station cooperation on the downlink: Large system analysis," *IEEE Trans. Inf. Theory*, vol. 58, no. 4, pp. 2079–2106, April 2012.

[12] D. Gesbert, S. Hanly, H. Huang, S. S. Shitz, O. Simeone, and W. Yu, "Multi-cell MIMO cooperative networks: A new look at interference," *IEEE J. Sel. Area. Commun.*, vol. 28, no. 9, pp. 1380–1408, December 2010.

[13] D. Aktas, M. N. Bacha, J. S. Evans, and S. V. Hanly, "Scaling results on the sum capacity of cellular networks with MIMO links," *IEEE Trans. Inf. Theory*, vol. 52, no. 7, pp. 3264–3274, July 2006.

[14] E. G. Larsson, O. Edfors, F. Tufvesson, and T. L. Marzetta, "Massive MIMO for next generation wireless systems," *IEEE Commun. Mag.*, vol. 52, no. 2, pp. 186–195, February 2014.

[15] T. L. Marzetta, "Noncooperative cellular wireless with unlimited numbers of base station antennas," *IEEE Trans. Wireless Commun.*, vol. 9, no. 11, pp. 3590–3600, November 2010.

[16] J. Nam, J. Y. Ahn, A. Adhikary, and G. Caire, "Joint spatial division and multiplexing: Realizing massive MIMO gains with limited channel state information," in *Proc. CISS*, 2012, pp. 1–6.

[17] L. Lu, G. Y. Li, A. L. Swindlehurst, A. Ashikhmin, and R. Zhang, "An overview of massive MIMO: Benefits and challenges," *IEEE J. Sel. Top. Signal Process.*, vol. 8, no. 5, pp. 742–758, Oct 2014.

[18] D. Tse and P. Viswanath, *Fundamentals of Wireless Communication.* New York, USA: Cambridge University Press.

[19] V. Venkateswaran and A. J. V. D. Veen, "Analog beamforming in MIMO communications with phase shift networks and online channel estimation," *IEEE Trans. Signal Process.*, vol. 58, no. 8, pp. 4131–4143, Aug 2010.

[20] X. Zhang, A. F. Molisch, and S.-Y. Kung, "Variable-phase-shift-based RF-baseband codesign for MIMO antenna selection," *IEEE Trans Sig. Process.*, vol. 53, no. 11, pp. 4091–4103, Nov 2005.

[21] R. W. Heath, N. Gonzalez-Prelcic, S. Rangan, W. Roh, and A. M. Sayeed, "An overview of signal processing techniques for millimeterwave MIMO systems," *IEEE J. Sel. Topics Signal Process.*, vol. 10, no. 3, pp. 436–453, 2016.

[22] S. Hur, T. Kim, D. J. Love, J. V. Krogmeier, T. A. Thomas, and A. Ghosh, "Millimeter wave beamforming for wireless backhaul and access in small cell networks," *IEEE Trans. on Commun.*, vol. 61, no. 10, pp. 4391–4403, 2013.

[23] Z. Xiao, T. He, P. Xia, and X.-G. Xia, "Practical antenna training for millimeter wave MIMO communication," *IEEE Trans. Wireless Commun.*, vol. 15, no. 5, pp. 3380–3392, 2016.

[24] T. S. Rappaport, *Wireless Communications: Principles and Practice*, 2nd ed. Prentice Hall, 2002.

[25] H. Yin, D. Gesbert, M. Filippou, and Y. Liu, "A coordinated approach to channel estimation in large-scale multiple-antenna systems," *IEEE J. Sel. Area. Commun.*, vol. 31, no. 2, pp. 264–273, February 2013.

[26] C. Shi, R. A. Berry, and M. L. Honig, "Adaptive beamforming in interference networks via bi-directional training," in *Proc. CISS*, Princeton, NJ, 2010, pp. 17–19.

[27] ——, "Bi-directional training for adaptive beamforming and power control in interference networks," *IEEE Trans. Signal Process.*, vol. 62, no. 3, pp. 607–618, Feb 2014.

[28] A. Younis, N. Serafimovski, R. Mesleh, and H. Haas, "Generalised spatial modulation," in *Proc. IEEE ACSSC*, 2010, pp. 1498–1502.

[29] H. Crámer, *Random Variables and Probability Distributions.* Cambridge, UK: Cambridge University Press, 1970.

[30] T. Cover and J. Thomas, *Elements of Information Theory.* Wiley-Interscience, 2006.

[31] A. Goldsmith, *Wireless Communications.* Cambridge University Press, 2004.

[32] H. Nyquist, "Certain topics in telegraph transmission theory," *Trans. AIEEE*, vol. 47, no. 2, pp. 617–644, 1928.

[33] C. E. Shannon, "Communication in the presence of noise," *Proc. IRE*, vol. 32, no. 1, pp. 623–656, 1949.

[34] D. Donoho, "Compressed sesning," *IEEE Trans. Inf. Theory*, vol. 52, no. 4, pp. 1289–1306, 2006.

[35] E. J. Candes, J. Romberg, and T. Tao, "Robust uncertainty principles: exact signal reconstruction from highly incomplete frequency information," *IEEE Trans. Inf. Theory*, vol. 52, no. 2, pp. 489–509, Feb 2006.

[36] S. Chen, D. Donoho, and M. Saunders, "Atomic decomposition by basis pursuit denoising," *SIAM J. on Scientific Computing*, vol. 20, no. 1, pp. 33–61, 1998.

[37] E. J. Candes and T. Tao, "Decoding by linear programming," *IEEE Trans. Inf. Theory*, vol. 51, no. 12, pp. 4203–4215, Dec 2005.

[38] R. Baraniuk, M. Davenport, R. DeVore, and M. Wakin, "A simple proof of the restricted isometry property for random matrices," *Constructive Approximation*, vol. 28, no. 3, pp. 253–263, 2008.

[39] E. J. Candes, J. Romberg, and T. Tao, "Stable signal recovery from incomplete and inaccurate measurements," *Communications on Pure and Applied Mathematics*, vol. 59, no. 8, pp. 1207–1223, 2006.

[40] S. M. Kay, *Fundamentals of Statistical Signal Processsing.* Englewodd Cliffs, NJ USA : Prentice Hall, 1993.

[41] Golub and V. Loan, "An analysis of the total least squares problem," *SIAM J. Numer. Anal.*, vol. 17, no. 6, 1980.

[42] V. Huffel and J. Vanderwalle, *The Total Least Squares Problem: Computational Aspects and Analysis.* Philadelphia, PA: SIAM, 1991.

[43] B. L. Ng, J. S. Evans, S. V. Hanly, and D. Aktas, "Distributed downlink beamforming with cooperative base stations," *IEEE Trans. Inf. Theory*, vol. 54, no. 12, pp. 5491–5499, Dec 2008.

[44] J. Zhang, B. Zhang, S. Chen, and L. Hanzo, "Pilot contamination elimination for large-scale multiple antenna aided OFDM systems," *IEEE J. Sel. Topics Signal Process.*, vol. 8, no. 5, pp. 759–772, 2014.

[45] V. R. Cadambe and S. A. Jafar, "Interference alignment and degrees of freedom of the K-user interference channel," *IEEE Trans. Inf. Theory*, vol. 54, no. 8, pp. 3425–3441, Aug 2008.

[46] S. W. Peters and R. W. Heath, "Cooperative Algorithms for MIMO interference channels," *IEEE Trans. Veh. Technol.*, vol. 60, no. 1, pp. 206–218, Jan 2011.

[47] X. Zhou, T. A. Lamahewa, P. Sadeghi, and S. Durrani, "Two-way training: optimal power allocation for pilot and data transmission," *IEEE Trans. Wirel. Commun.*, vol. 9, no. 2, pp. 564–569, February 2010.

[48] M. L. Honig, *Advances in Muliuser Detection.* Wiley-IEEE press, 2009.

[49] R. Y. Mesleh, H. Haas, S. Sinanovic, C. W. Ahn, and S. Yun, "Spatial modulation," *IEEE Trans. Veh. Technol.*, vol. 57, no. 4, pp. 2228–2241, July 2008.

[50] A. Younis, D. A. Basnayaka, and H. Haas, "Performance analysis for generalised spatial modulation," in *Proc. European Wireless Conf.*, 2014, pp. 1–6.

[51] W. Liu, M. J. N. Wang, and H. Xu, "Denoising detection for the generalized spatial modulation using sparse property," *IEEE Commun. Lett.*, vol. 18, no. 1, pp. 22–25, 2014.

[52] E. J. Candes and M. B. Waking, "An introduction to compressive sampling," *IEEE Signal Process. Mag.*, vol. 25, no. 2, pp. 21–30, 2008.

[53] P. Tune, S. R. Bhaskaran, and S. V. Hanly, "Number of measurements in sparse signal recovery," in *Proc. IEEE ISIT*, 2009, pp. 16–20.

[54] L. Davis, S. Hanly, P. Tune, and S. R. Bhaskaran, "Channel estimation and user selection in the MIMO broadcast channel," *Elsevier Digital Signal Processing*, vol. 21, no. 5, pp. 608–618, 2011.

[55] D. Gesbert, S. Hanly, H. Huang, S. S. Shitz, O. Simeone, and W. Yu, "Multi-cell MIMO cooperative networks: A new look at interference," *IEEE J. Sel. Area. Commun.*, vol. 28, no. 9, pp. 1380–1408, December 2010.

[56] S. R. Bhaskaran, L. Davis, A. Grant, S. Hanly, and P. Tune, "Downlink scheduling using compressed sensing," in *Proc. IEEE ITW*, 2009, pp. 201–205.

[57] C. M. Yu, S. H. Hsieh, H. W. Liang, C. S. Lu, W. H. Chung, S. Y. Kuo, and S. C. Pei, "Compressed sensing detector design for space shift keying in MIMO systems," *IEEE Commun. Lett.*, vol. 16, no. 10, pp. 1556–1559, October 2012.

[58] X. Li, Y. Zhang, L. Xiao, X. Xu, and J. Wang, "A novel precoding scheme for downlink multi-user spatial modulation system," in *Proc. IEEE PIMRC*, 2013, pp. 1361–1365.

[59] S. Narayanan, M. J. Chaudhry, A. Stavridis, M. D. Renzo, F. Graziosi, and H. Haas, "Multi-user spatial modulation MIMO," in *Proc. IEEE WCNC*, 2014, pp. 671–676.

[60] R. Hunger, "Floating point operations in matrix-vector calculus," Techneische universitat Munchen associate institute for signal processing, Tech. Rep., 2007.

[61] C.-S. Park, Y.-S. Byun, A. M. Bokiye, and Y.-H. Lee, "Complexity reduced zero-forcing beamforming in massive mimo systems," in *Proc. ITA'14*, 2014, pp. 1–5.

[62] J. Wang, S. Jia, and J. Song, "Generalised spatial modulation system with multiple active transmit antennas and low complexity detection scheme," *IEEE Trans. Wireless Commun.*, vol. 11, no. 4, pp. 1605–1615, April 2012.

[63] Y. Xiao, Z. Yang, L. Dan, P. Yang, L. Yin, and W. Xiang, "Low-complexity signal detection for generalized spatial modulation," *IEEE Commun. Lett.*, vol. 18, no. 3, pp. 403–406, March 2014.

[64] W. Liu, N. Wang, M. Jin, and H. Xu, "Denoising detection for the generalized spatial modulation system using sparse property," *IEEE Commun. Lett.*, vol. 18, no. 1, pp. 22–25, 2014.

[65] X. Guan, Y. Cai, and W. Yang, "On the mutual information and precoding for spatial modulation with finite alphabet," *IEEE Wireless Commun. Lett.*, vol. 2, no. 4, pp. 383–386, August 2013.

[66] Z. Yang, C. Liang, X. Xu, and X. Ma, "Block markov superposition transmission with spatial modulation," *IEEE Wireless Commun. Lett.*, vol. 3, no. 6, pp. 565–568, Dec 2014.

[67] A. A. I. Ibrahim, T. Kim, and D. J. Love, "On the achievable rate of generalized spatial modulation using multiplexing under a Gaussian mixture model," *IEEE Trans. Commun.*, vol. 64, no. 4, pp. 1588–1599, April 2016.

[68] R. W. Heath, S. Sandhu, and A. Paulraj, "Antenna selection for spatial multiplexing systems with linear receivers," *IEEE Commun. Lett.*, vol. 5, no. 4, pp. 142–144, April 2001.

[69] X. Gao, O. Edfors, F. Tufvesson, and E. G. Larsson, "Massive MIMO in real propagation environments: Do all antennas contribute equally?" *IEEE Trans. Commun.*, vol. 63, no. 11, pp. 3917–3928, Nov 2015.

[70] X. Gao, O. Edfors, J. Liu, and F. Tufvesson, "Antenna selection in measured massive MIMO channels using convex optimization," in *IEEE GLOBECOM Workshop*, 2013, pp. 129–134.

[71] J. Pan and W. K. Ma, "Antenna subset selection optimization for large-scale MISO constant envelope precoding," in *Proc. IEEE ICASSP*, 2014, pp. 3137–3141.

[72] M. Benmimoune, E. Driouch, W. Ajib, and D. Massicotte, "Joint transmit antenna selection and user scheduling for Massive MIMO systems," in *Proc. IEEE WCNC*, 2015, pp. 381–386.

[73] D. Mi, M. Dianati, S. Muhaidat, and Y. Chen, "A novel antenna selection scheme for spatially correlated massive MIMO uplinks with imperfect channel estimation," in *Proc. VTC-Spring*, 2015, pp. 1–6.

[74] S. Sanayei and A. Nosratinia, "Antenna selection in MIMO systems," *IEEE Commun. Mag.*, vol. 42, no. 10, pp. 68–73, Oct 2004.

[75] T. Rappaport, "Millimeter wave mobile communications for 5G cellular: It will work!" *IEEE Access*, vol. 1, no. 1, pp. 335–349, 2013.

[76] P. B. Papazian, G. A. Hufford, R. J. Achatz, and R. Hoffman, "Study of the local multipoint distribution service radio channel," *IEEE Trans. Broadcasting*, vol. 43, no. 2, pp. 175–184, 1997.

[77] S. Yong and C. Chong, "An overview of multigigabit wireless through millimeter wave technology: potentials and technical challenges," *EURASIP J. Wireless Commun. Netw.*, vol. 23, no. 2, pp. 50–60, 2007.

[78] R. Daniels and R. W. Heath, "60 GHz wireless communications: emerging requirements and design recommendations," *IEEE Trans. Veh. Technol. Mag.*, vol. 2, no. 3, pp. 41–50, 2007.

[79] G. Hendrantoro, R. Bultitude, and D. Falconer, "Use of cell-site diversity in millimetre-wave fixed cellular systems to combat the effects of rain attenuation," *IEEE J. Sel. Area. Commun.*, vol. 20, no. 3, pp. 602–614, 2002.

[80] Z. Pi and F. Khan, "An introduction to millimeter-wave mobile broadband systems," *IEEE Commun. Mag.*, vol. 49, no. 6, pp. 101–107, 2011.

[81] T. S. Rappaport, R. W. Heath, R. C. Daniels, and J. N. Murdock, *Millimeter Wave Wireless Communications*. Prentice Hall, 2014.

[82] S. K. Yong, P. Xia, and A. Valdes-Garcia, *60GHz Technology for Gbps WLAN and WPAN: from Theory to Practice*. West Sussex, UK: Wiley.

[83] J. O. P. Xia, H. Niu and C. Ngo, "Practical antenna training for millimeter wave MIMO communication," in *Proc. IEEE VTC-Fall*, 2008, pp. 1–5.

[84] J. Wang, Z. Lan, C. Pyo, T. Baykas, C. Sum, M. Rahman, J. Gao, R. Funada, F. Kojima, and H. Harada, "Beam codebook based beamforming protocol for multi-

Gbps millimeter-wave WPAN systems," *IEEE J. Sel. Area. Commun.*, vol. 27, no. 8, pp. 1390–1399, 2009.

[85] J. Wang, Z. Lan, C. Sum, C. Pyo, J. Gao, T. Baykas, A. Rahman, R. Funada, F. Kojima, and I. Lakkis, "Beamforming codebook design and performance evaluation for 60GHz wideband WPANs," in *Proc. IEEE VTC-Fall*, no. 1-6, 2009.

[86] S. Sun, T. S. Rappaport, R. W. Heath, A. Nix, and S. Rangan, "MIMO for millimeter-wave wireless communications: beamforming, spatial multiplexing, or both?" *IEEE Commun. Mag.*, vol. 52, no. 12, pp. 110–121, 2014.

[87] N. G.-P. A. Alkhateeb, J. Mo and R. Heath, "MIMO precoding and combining solutions for millimeter-wave systems," *IEEE Commun. Mag.*, vol. 52, no. 12, pp. 122–131, 2014.

[88] W. R. amd J-Y. Seol, J. Park, B. Lee, J. Lee, Y. Kim, J. Cho, K. Cheun, and F. Aryanfar, "Millimeter-wave beamforming as an enabling technology for 5G cellular communications: theoretical feasibility and prototype results," *IEEE Commun. Mag.*, vol. 52, no. 2, pp. 106–113, 2014.

[89] P. Wang, Y. Li, L. Song, and B. Vucetic, "Multi-gigabit millimeter wave wireless communications for 5G: from fixed access to cellular networks," *IEEE Commun. Mag.*, vol. 53, no. 1, pp. 168–178, 2015.

[90] A. Alkhateeb, O. E. Ayach, G. Leus, and R. W. Heath, "Channel estimation and hybrid precoding for millimeter wave cellular systems," *IEEE J. Sel. Top. Signal Process.*, vol. 8, no. 5, pp. 831–846, 2014.

[91] A. Alkhateeb, G. Leus, and R. W. Heath, "Compressed sensing based multi-user millimeter wave systems: How many measurements are needed?" in *Proc. IEEE ICASSP*, 2015, pp. 2909–2913.

[92] Y. Peng, Y. Li, and P. Wang, "An enhanced channel estimation method for millimeter wave systems with massive antenna arrays," *IEEE Commun. Lett.*, vol. 19, no. 9, pp. 1592–1595, 2015.

[93] P. Xia, S. K. Yong, J. Oh, and C. Ngo, "Multi-stage iterative antenna training for millimeter wave communications," in *Proc. IEEE GLOBECOM*, 2008, pp. 1–6.

[94] Z. Xiao, L. Bai, and J. Choi, "Iterative joint beamforming training with constant-amplitude phased arrays in millimetre-wave communications," *IEEE Commun. Lett.*, vol. 18, no. 5, pp. 829–832, 2014.

[95] J. Wang, Z. Lan, C. Sum, C. Pyo, J. Gao, T. Baykas, A. Rahman, R. Funada, F. Kojima, and I. Lakkis, "Beamforming codebook design and performance evaluation for 60ghz wideband WPANs," in *Proc. IEEE VTC-Fall*, 2009, pp. 1–6.

[96] L. Chen, Y. Yang, X. Chen, and W. Wang, "Multi-stage beamforming codebook for 60 GHz WPAN," in *Proc. CHINACOM*, 2011, pp. 36–365.

[97] T. He and Z. Xiao, "Suboptimal beam search algorithm and codebook design for millimeter-wave communications," *Mobile Networks and Applications*, pp. 86–97, 2015.

[98] T. S. Rappaport, E. B. Dor, J. N. Murdock, and Y.Qiao, "38 GHz and 60 GHz angle-dependent propagation for cellular and peer-to-peer wireless communications," in *Proc. IEEE ICC*, 2012.

[99] A. Sayeed and J. Brady, "Beamspace MIMO for high-dimensional multiuser communication at millimetre-wave frequencies," in *Proc. IEEE GLOBECOM*, 2013, pp. 3679–3684.

[100] H. Q. Ngo, E. G. Larsson, and T. L. Marzetta, "Aspects of favorable propagation in massive MIMO," in *Proc. IEEE EUSIPCO*, 2014, pp. 76–80.

[101] A. Alkhateeb, G. Leus, and R. W. Heath, "Limited feedback hybrid precoding for multi-user millimeter wave systems," *IEEE Trans. Wireless Commun.*, vol. 14, no. 11, pp. 6481–6494, 2015.

[102] A. Alkhateeb, R. W. Heath, and G. Leus, "Achievable rates of multi-user millimetre-wave systems with hybrid precoding," in *IEEE ICC Workshop*, 2015, pp. 1232–237.

[103] S. Hur, T. Kim, D. J. Love, J. V. Krogmeier, T. A. Thomas, and A. Ghosh, "Millimeter wave beamforming for wireless backhaul and access in small cell networks," *IEEE Trans. Commun.*, vol. 61, no. 10, pp. 4391–4403, 2013.

[104] C. N. Barati, S. A. Hosseini, S. Rangan, P. Liu, T. Korakis, and S. S. Panwar, "Directional cell search for millimeter wave cellular systems," in *Proc. IEEE SPAWC*, 2014.

[105] A. Alkhateeb, G. Leus, and R. W. Heath, "Compressed sensing based multi-user millimeter wave systems: How many measurements are needed?" in *Proc. IEEE ICASSP*, 2015, pp. 2909–2913.

[106] T. Bai, V. Desai, and R. W. Heath, "Millimeter wave cellular channel models for system evaluation," in *Proc. IEEE ICNC*, 2014.

[107] Z. Xiao, T. He, P. Xia, and X. G. Xia, "Hierarchical codebook design for beamforming training in millimeter-wave communication," *IEEE Trans. Wireless Commun.*, vol. 15, no. 5, pp. 3380–3392, May 2016.

[108] A. M. Sayeed, "Deconstructing multiantenna fading channels," *IEEE Trans. Signal Process.*, vol. 50, no. 10, pp. 2563–2579, Oct 2002.

[109] H. Zhu, G. Leus, and G. B. Giannakis, "Sparse regularized total least squares for sensing applications," in *Proc IEEE SPAWC*, 2010, pp. 1–5.

[110] C. Ekanadham, D. Tranchina, and E. P. Simoncelli, "Recovery of sparse translation-invariant signals with continuous basis pursuit," *IEEE Trans. Signal Process.*, vol. 59, no. 10, pp. 4735–4744, Oct 2011.

[111] P. Hall, "On the rate of convergence of normal extremes," *Journal of Applied Probability*, vol. 16, no. 2, pp. 433–439, 1979.

[112] Z. Pi and F. Khan, "An introduction to millimeter-wave mobile broadband systems," *IEEE Commun. Mag.*, vol. 49, no. 6, pp. 101–107, June 2011.

[113] F. Khan and Z. Pi, "mmWave mobile broadband (MMB): Unleashing the 3-300 GHz spectrum," in *Proc. IEEE Sarnoff Symposium*, 2011, pp. 1–6.